Engineered Silk Hydrogels for the Delivery of Mesenchymal Stem Cells to the Stroked Brain

Suttinee Phuagkhaopong

Institute of Pharmacy and Biomedical Sciences

University of Strathclyde

A thesis submitted in fulfilment of the requirements for the degree of

Doctor of Philosophy

November 2021

Declaration of Authenticity and Author's Rights

'This thesis is the result of the author's original research. It has been composed by the author and has not been previously submitted for examination which has led to the award of a degree.'

'The copyright of this thesis belongs to the author under the terms of the United Kingdom Copyright Acts as qualified by University of Strathclyde Regulation 3.50. Due acknowledgement must always be made of the use of any material contained in, or derived from, this thesis.'

Signed: 
(Suttinee Phuagkhaopong)
Date: 5 November 2021

ACKNOWLEDGEMENTS

It is my great pleasure to express my gratitude to all those people who have supported me throughout my study over the past three years. I am especially grateful to my supervisor, Dr. Philipp Seib, for his passion, guidance, and discipline throughout my PhD project. The thesis would not have been possible without his support and patience. I will always remember one sentence that he keep saying to me since we first met "If you need a hand, you know where I am". The fact that his office door always open and his in-depth knowledge in silk applications extremely assisted me to resolve all of questions and issues. Nevertheless, he was and remains my best role model for a mentor and scientist. His constant encouragement and insightful to pursue a career in academia is an immense inspiration to me. Moreover, I would like to extend my sincere thanks to my co-supervisor, Dr. Hilary Carswell, who provides me invaluable contribution and animal experimental advices to animal study presented in this thesis. In addition, I would like to thank Dr. Iola Duarte for her valuable comments on the results and supports in metabolomic profiling work and input as a collaborator on my manuscript submissions.

Apart from my supervisors, I thank Dr. Natalia Gorenkova for her enormous help to set up animal experiments and her wealth of experience when starting my PhD. I also thank Linda Horan and BPU staffs for helping me look after my experimental animals. I would like to thank Dr. Thomas McGlone and Dr. Deborah Bowering for providing me an excellent training of advance machines in CMAC and enormous technical supports, and Mr Graeme MacKenzie for training in confocal and epifluorescence microscopy.

It is my pleasure to acknowledge all my former and current colleagues in the Seib lab, Dr. Thidarat Wongpinyochit (P'Tar), Dr John Totten, Gemma Egan, Saphia Matthew, Kimia Witte, and Jirada Kaewchuchuen who always being a good friend and providing me with valuable motivation and intensive discussions. I also thank my lovely friends in SIPBS; Lina Akil for her friendship and supports. Special thanks to my Thai friends in SIPBS; Kanidta Niwasabutra, Jitkasem Meewan, Panicha Aruvornlop, in Glasgow and in Thailand for their friendship, help and encouragement.

I would like to gratefully acknowledge the financial support from Development and Promotion of Science and Technology talents project (DPST) scholarship, The Institute for the Promotion of Teaching Science and Technology (IPST), Royal Thai Government for funding my PhD. I also would like to thank the

EPSRC Future CMAC Research Hub and SIPBS to facilitate and support all equipments and resources throughout my research.

Finally, the biggest thanks go to my parents and my entire family members for all their love and support over the past years. Last but not least, thank you to my partner who always support me during the good times and the struggles and always unwaveringly believed in me. I truly would have not been able to complete this thesis without their supports.

ABSTRACT

Bombyx mori silk has the potential to be deployed as a delivery matrix in advanced cell-based therapies (Chapter 1). My principle hypothesis is that silk can be engineered into hydrogels to mimic the structure and function of the native extracellular matrix [ECM], ultimately influencing cellular biology. The aim of this thesis was to assess self-assembling silk hydrogels that serve as ECM mimetics to support mesenchymal stem cell [MSCs] function, and to assess silk hydrogel performance in the context of strokes. Viscoelasticity is a key mechanical property of the ECM. Therefore, the mechanics of silk hydrogels were engineered, and the impact in two-dimensional MSC cultures was assessed (Chapter 2; Phuagkhaopong *et al.* 2021). Elastic and viscoelastic silk hydrogels with identical stiffness (~1 kPa) were generated from equal silk concentrations by chemical and physical crosslinking, respectively. Physically crosslinked silk hydrogels showed stress relaxation ($\tau 1/2 = 250$ s) when exposed to 15% compressive stress, covering the stress relaxation range observed in soft tissues (60–3,600 s). The viscoelastic and elastic silk hydrogels induced differential patterns of gene expression, protein secretion, and extracellular metabolome that were linked to substrate mechanics. For example, strong activation of IL-1β signaling was observed in MSCs grown on elastic silk hydrogels. In Chapter 3, viscoelastic silk hydrogels were tuned to match native brain tissue. These self-assembling silk hydrogels were stereotactically injected into the stroke epicenter to assess their 6- and 12-month performance in rats.. Histological assessment showed excellent host-tissue integration, cell ingrowth, and M2-like phenotype macrophages. Also, neuronal progenitor cells remodeled the chronic stroke. This thesis drew on both *in vitro* and *in vivo* studies to assess the potential of tissue-mimetic silk hydrogels intended for cell therapy. The reported findings will expand the use of silk hydrogels as an engineered ECM mimetic in advanced therapy products (Chapter 4).

TABLE OF CONTENTS

LIST OF FIGURES

LIST OF TABLES

LIST OF ABBREVIATIONS

BDNF	Brain-derived neurotrophic factor
BSA	Bovine serum albumin
DMEM	Dulbecco's modified eagle medium
DCX	Doublecortin
ECM	Extracellular matrix
FN	Fibronectin
FDA	U.S. Food and Drug Administration
FTIR	Fourier transform infrared spectroscopy
GFAP	Glial fibrillary acid protein
HA	Hyaluronic acid
H_2O_2	Hydrogen peroxide
hMSCs	Human mesenchymal stem cells
HRP	Horseradish peroxidase
MMPs	Matrix metalloproteinase
MSCs	Mesenchymal stem cells
MCAo	Middle cerebral artery occlusion
NPC	neural progenitor cell
NMR	Nuclear magnetic resonance
PEG	Polyethylene glycol
PBS	Phosphate buffer saline
RGD	Arginine-glycine-aspartic acid peptide motifs
SEM	Scanning electron microscopy
SDF-1	Stromal cell-derived factor 1
$\tau_{1/2}$	Half-stress relaxation time
tPA	Tissue plasminogen activator
TGF-β1	Transforming growth factor beta 1
VEGF	Vascular endothelial growth factor
YAP/TAZ	Yes-associated protein/transcriptional co-activator

CHAPTER 1
INTRODUCTION

Chapter summary:

This chapter provides a general introduction to silk, including its structure and properties. This chapter also describes hydrogels, their advantages, their role in cell-based therapies, and their clinical applications. The importance of substrate stress relaxation on MSC response is highlighted, and hydrogel-based materials are explored as a potential supportive matrix for cell-based therapy. This chapter also describes the general methodology used to engineer silk hydrogels. This information is relevant for all experimental thesis chapters, describing both (i) horseradish peroxidase [HRP]/ hydrogen peroxide [H_2O_2]-induced chemical crosslinking silk hydrogels and (ii) sonication-induced physical crosslinking of silk hydrogels. Finally, the overall hypothesis of the thesis is introduced, along with accompanying aims and objectives.

1.1 Silk

Silk is a natural fibrous protein spun by many insects and spiders for use outside their bodies. The most widely studied silks are *Bombyx mori* from silkworms and dragline silk from *Nephila clavipes* spiders. Both are extremely light and strong for their size and thickness. Spidroins, made by spiders, are much stronger than fibroins, made by *B. mori* silkworms[1]. One hypothesis claims that poly-GA repeat proteins, present in the repetitive part of fibroins—as opposed to poly-A blocks, present in spidroins—reduces the binding strength of the β-sheets, which likely also affects their tensility. In biomedical applications, *B. mori* silk is more popular than spider silk because *B. mori* silk has a robust and established supply chain. Unlike spider silk, *B. mori* silk can be farmed. *B. mori* silk has many desirable properties, including tunable biocompatibility, controllable biodegradation, and toughness—all of which are often superior to current synthetic polymers. In addition, *B. mori* silk is thermally stable up to 250°C[2]. It can be processed into a range of biomaterial formats, such as nanofibers, nanoparticles, films, hydrogels, and scaffolds[3].

1.1.1 *B. mori* silk cocoon

B. mori cocoon silk can be obtained either directly from the silk gland of the silkworm or reverse-engineered from their cocoons (Figure 1.1A). Silk fibroins consist of two main parts: a heavy chain (MW: 350 kDa) and a light chain (MW: 25 kDa), which are connected by a single disulfide bond at the C-terminal of the heavy chain (Figure 1.1B). The heavy chain contains hydrophobic blocks that account for 94% of the heavy chain sequence. These blocks are made of repeating sequences of glycine (G; 46%),

alanine (A; 29%), and serine (S; 12%)—forming the well-known GAGAGS silk sequence (Figure 1.1C). These hydrophobic blocks are interspersed with hydrophilic blocks, which account for 6% of the sequence. These hydrophilic blocks contain polar amino acids, mainly tyrosine (Y; 4.8%), glutamic acid (E; 0.6%), and lysine (K; 0.6%)[3]. Data from X-ray crystallography and solid-state nuclear magnetic resonance [NMR] revealed that poly(alanine) sequences in hydrophobic blocks can form β-sheet structures or crystallize through hydrogen bonding and hydrophobic interactions which cause the excellent tensile strength of silk fibroin. In nature, silk fibroin aqueous solution is produced in silkworm glands in a protein concentration of up to 30% [w/v] and contains many random coils and features an α-helical structure. During fiber spinning, shear forces and elongation flow–induced self-assembly and transform the amorphous protein into a β-sheet structure, leading to the formation of solid fibers[4]. In the gland, silk fibroins are thought to adopt a spherical micellar conformation (100–200 nm in diameter), which is composed of a hydrophobic core surrounded by the C- and N-terminals of the heavy chain[5]. During the natural spinning process, silk fibroins will be covered with sericin. Sericin (MW: 27 kDa) is a glycoprotein, acting as a glue and thus combining fibroin filaments through hydrophobic interactions. The role of sericin in the conversion of the silk I structure (soluble) into the silk II structure (insoluble) is currently not fully understood[6]. The majority of the silk I structure comprises random coils and α-helices, whereas β-sheets constitute the majority of the silk II structure. The silk II structure can be triggered by low pH, high temperature, and antisolvents[7]. Notably, the silk II structure contributes to the excellent mechanical properties of silk.

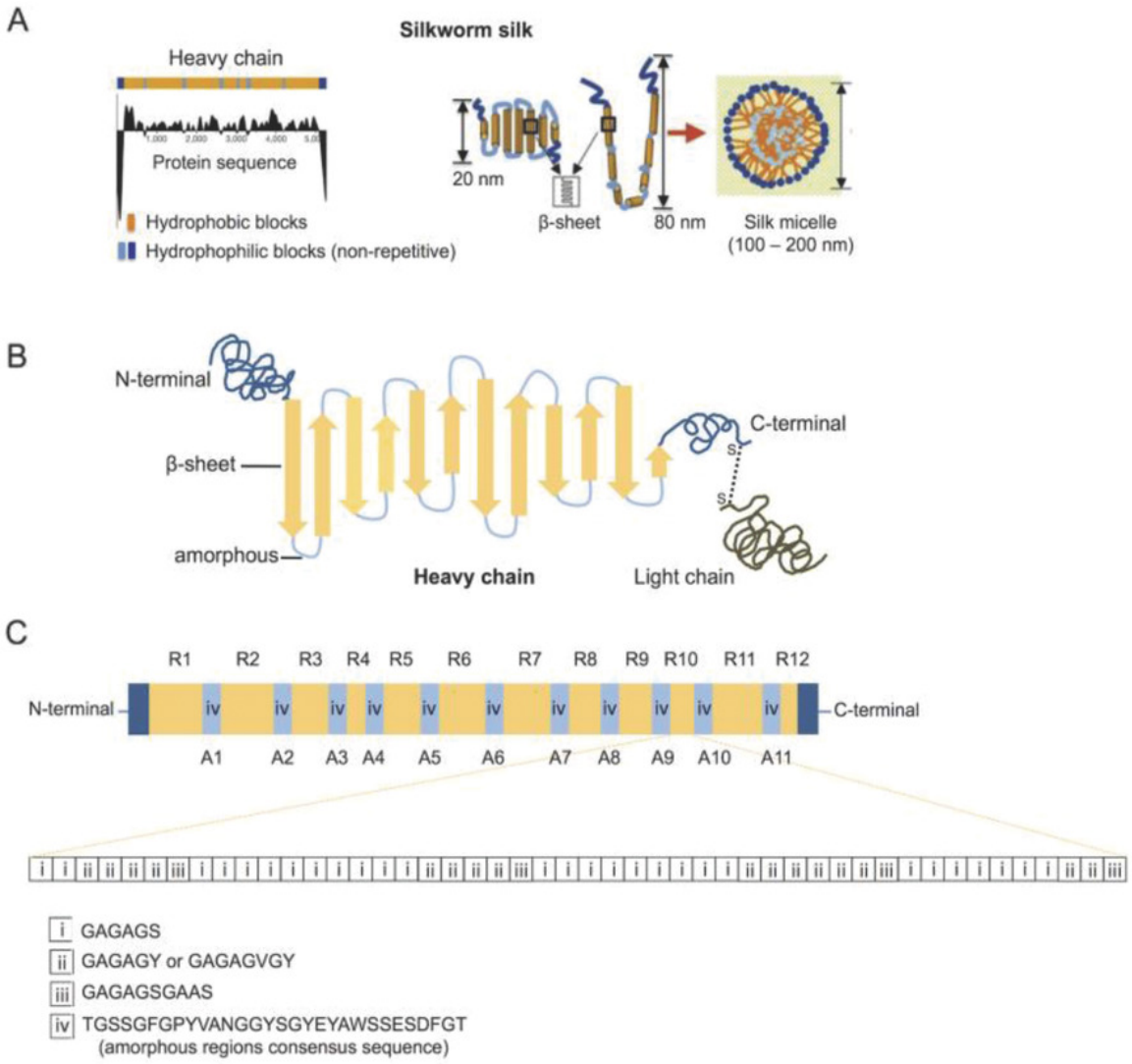

Figure 1.1 Schematic representation of *B. mori* silk fibroin conformation.

(A) Silk fibroin primary, secondary and micelle assembly structure (B) silk heavy chain consists of N-terminus, C-terminus, amorphous regions, and crystalline domains linking to silk light chain by a single disulfide bond (C) primary structure of silk heavy chain including repetitive GAGAGS sequence regions. A – C adapted from[3].

1.1.2 Properties of *B. mori* silk

1.1.2.1 Biocompatibility

Silk is considered a biocompatible material because it is a natural protein and has been used as sutures for several thousands of years[8]. However, it has been shown that the native silk fibers containing sericin can activate an innate immune response, resulting in a severe allergic reaction[9]. Recent studies have demonstrated that this immune response is triggered by virgin silk (i.e., silk that still contains sericin and other constituents) but not by either fibroin or sericin on their own[10,11]. The degree of biocompatibility depends on many factors, including material format, route of application, application site, and the foreign body immune response. For example, intravenous administration of silk fibroin protein can induce an immunogenic/inflammatory response more readily than introducing the same material subcutaneously because intravenously administered material directly confronts immune cells in the bloodstream. Numerous *in vivo* studies show that silk can induce a transient and mild immune response by the recruitment and activation of macrophages. However, this response diminishes within 14 days after exposure[9]. There is currently no evidence that silk induces an adaptive immune response. The absence of this response is a key point that now supports the development of silk-based materials for clinical applications. In recent years, there has been increased interest in using cytokine-loaded silk hydrogels in clinical applications (e.g., IFN-γ and IL-4)[12,13]. These cytokines might be able to activate macrophage polarization. Therefore, balancing macrophage functioning (e.g., M1 inflammatory vs. M2 anti-inflammatory) remains an untapped opportunity when working with cytokine-loaded silk hydrogels.

1.1.2.2 Biodegradability

Silk can be degraded by mammalian proteolytic enzymes (e.g., α-chymotrypsin, proteinase K, matrix metalloproteinases [MMPs], and collagenase) and nonmammalian proteinase enzymes (e.g., proteinase XIV and papain)—the latter are often being used in *in vitro* studies. The silk II (β-sheets) structure cannot be degraded in water or biological salt solutions[14]. The type of proteolytic enzyme is specific to the application site and the material form. Silk will be degraded by proteolytic enzymes in order to form hydrophilic blocks, the C- and N-terminals of heavy chains, light chains, and hydrophobic blocks (silk II structure). The duration of degradation depends on many factors, including the application site, the material form (porosity), the material size, the degree of the silk II structure, and the amount of silk content[15]. For example, an open silk structure (i.e., silk hydrogels) degrades faster than tightly packed silk (e.g., silk film) because proteases have better access to cleavage sites in a more open structure[16]. *In vivo*

studies demonstrated that silk degradation involved immune cell invasion into the silk material which triggered the release of factors such as MMP-1 and MMP-2, primarily from macrophages. Degraded/leached silk products can also induce immune cell recruitment, promoting phagocytosis[9].

1.2 Hydrogels

A hydrogel is a highly hydrated material (>30% water by weight)[17], which maintains structural integrity by either physical or chemical crosslinking between the polymeric chains. Hydrogel-based materials have become an attractive cell support substrate because of their unique properties[18]. They can mimic the native extracellular matrix (ECM), including its physical and mechanical properties. In addition, hydrogels can be tuned, promoting the release of signaling molecules from resident host cells to regulate cellular proliferation and differentiation. Alternatively, cells can be added to the hydrogel first. Cells can be embedded in a hydrogel by mixing cells during the solution-gel transition. This encapsulates cells inside the hydrogel. Hydrogels can be generated from biological polymers (e.g., collagen, hyaluronic acid [HA], and alginate) and synthetic polymers (e.g., polyethylene glycol [PEG] and polyacrylamide)[19]. Fully synthetic hydrogels have the advantage of being manmade and are endowed with many advantages (e.g., reproducibility and good controllability with regard to their structure and properties)[20]. However, biopolymer-based hydrogels are rivaling synthetic systems. One example is the biopolymer silk. Silk-based hydrogels are becoming more commonly used in tissue engineering because they mimic many features of the native ECM and often support tissue ingrowth[21] and vascularization[22]. Hydrogels can be fabricated and tuned to meet the required application-oriented specifics. This in turn makes them ideal for use in regenerative medicine applications (e.g., neurogenesis following stroke and glioblastoma).

1.2.1 Hydrogels as extracellular matrix mimetics

1.2.1.1 Physical properties of hydrogels

1.2.1.1.1 Stiffness

The matrix stiffness of ECM differs between tissues and these are not necessarily static. Stiffness can change both during development and stages of disease. Cell-deposited native tissues range in stiffness from 0.1 kPa to 1000 kPa[23]. A hydrogel with the desired mechanical properties (in terms of stiffness and tensile strength) can be developed by adjusting parameters such as the type of polymers used, their concentrations, and the crosslinking type and density. Target stiffnesses are 0.1–1 kPa for brain tissue, 1–10 kPa for adipose tissue, and 11–50 kPa for bone tissue. Whitehead *et al.* reported that MSC cultured on

PEG hydrogels developed soft hydrogels (8–10 kPa) that mimicked adipose tissue stiffness and promoted adipocyte-like morphology and increased expression of adipogenic-specific markers (e.g., *Ppar-γ* and *Srebp-1c*), whereas stiff hydrogels (50–60 kPa) mimicked bone tissue and promoted osteocyte-like morphology and increased expression of osteogenic-specific markers (e.g., *Runx2* and *ALP*). However, there was no difference in cell proliferation between these hydrogels[24]. Floren *et al*. generated 2D silk fibroin hydrogels with varying silk concentrations 1–4% [w/v] using high-pressure CO_2. Here, the stiffness and pore size of the resulting hydrogels were 16–64 kPa and 3.5–5 μm, respectively. However, 1.5% [w/v] silk fibroin hydrogel (16 kPa) enableed less cell spreading compared with 4% [w/v] silk fibroin hydrogel (64 kPa). Only 3% [w/v] silk fibroin hydrogel (33 kPa) increased vascular marker expression (e.g., *MYH11*). Floren *et al.* further examined transforming growth factor beta-1 [TGF-β1]-loaded 3% [w/v] silk fibroin hydrogels and found a twofold increase in the vascular-specific protein markers *calponin* and *MHC*[25].

1.2.1.1.2 Elasticity

Stress relaxation is a key characteristic of natural ECM. The vast majority of hydrogels used as cell culture ECM mimetics are elastic. Classic covalently crosslinked hydrogels (e.g., PEG and polyacrylamide) are elastic. Typically, chemical crosslinking generates covalent bonds, resulting in an irreversible and thus purely elastic network. Thus, stress applied to such a matrix will result in these forces being stored within the hydrogel network, indicating that there is no remodeling of the matrix. Therefore, there is no time-independent stress relaxation. This in turn is known to regulate adherent cell behavior [26,27,28]. Degradation of covalently crosslinked hydrogels is required for the cells to undergo these processes, but the extent and kinetics of degradation can be difficult to control. In the body, purely elastic tissues do exist (e.g., blood vessels, cartilage, and ligaments)[27]. However, in nature, many tissues (e.g., brain[26], fat[28], breast[29], and liver tissue[30]) are viscoelastic due to their ECM composition. Therefore, these tissue-derived hydrogels are typically not purely elastic but viscoelastic. Viscoelastic means that these systems are somewhat rigid but with dissipation. Physical crosslinking relies on noncovalent bonds such as ionic or hydrogen bonds. These bonds are typically reversible and thus can exhibit viscoelastic behavior when sufficient stress is applied (e.g., the hydrogel begins to flow). This is important when exposing cells to such viscoelastic hydrogel systems. When cells attach to the matrix, they apply a force to the hydrogel substrate. At the same time, the matrix will initially resist and exhibit a certain initial strength (e.g., initial elastic modulus). These cell forces can dissipate over time through increased matrix deformation by two main mechanisms:

matrix crosslinker unbinding and matrix flow. This physical phenomenon is referred to as time-dependent stress relaxation or creep. A simple way to determine the rate of relaxation is via the half-stress relaxation time [$\tau_{1/2}$], which is the time corresponding to half of the initial value of the modulus. Several studies highlight that the time scale of the stress relaxation of viscoelastic hydrogels plays a major role in cell behaviors such as cell spreading, cell proliferation, and MSC lineage-specific differentiation (rather than substrate stiffness)[31,32].

1.2.1.1.3 Porosity

Another important feature in natural ECM is the pore architecture (i.e., pore size, porosity, and pore interconnectivity) required for the hydrogel to support nutrient and waste flux, oxygen exchange, homogeneous cell distribution, integration with the surrounding native tissue, angiogenesis, and mechanotransduction pathways such as focal adhesion formation. Macroporous hydrogels are often advantageous over nanoporous hydrogels for clinical translation. Scanning electron microscopy showed that the optimum pore size of hydrogels for tissue regeneration in different tissue types was 5 μm for blood vessels, 20 μm for hepatocytes, 40 μm for neurons, 20–125 μm for skin, and 100–350 μm for bone. Oliviero *et al.* reported that human mesenchymal stem cells [hMSCs] cultured on vascular endothelial growth factor [VEGF]-loaded PEG and heparin hydrogels with a pore size range of 35–100 μm optimally promoted neovascularization, determined via *in vivo* chick chorioallantoic membrane assay[33]. Dziubla *et al.* reported that human microvascular endothelial cells cultured on poly 2-hydroxyethylmethacrylate-based hydrogels with pore sizes ranging from 5 to 16 μm revealed that pore sizes above 9 μm promoted maximal cell infiltration and tubule formation[34]. Porcine chondrocytes cultured on 3D microcavity alginate hydrogels with 80–300 μm pores revealed optimal cell proliferation and chondrocyte differentiation in smaller pores (80–120 μm)[35]. By contrast, hMSCs cultured on 3D collagen and HA hydrogels with a pore size of 300 μm promoted chondrogenic differentiation, which was not observed in hydrogels with 94 and 130 μm pores[36]. However, pore shape is also important. For example, hMSCs cultured on spongy (50–60 μm) and columnar (100–150 μm) hydrogels showed that the spongy structure elicited more spreading and a higher osteogenic differentiation by upregulation of osteogenic markers[37]. Overall, several studies demonstrated that both the pore size and pore shape of hydrogels induce cell-specific lineage differentiation.

1.2.1.2 Biochemical property of hydrogels

The mechanical and biochemical microenvironment of cell culture matrix substrates is responsible for paracine release profiles from cells. For example, MSCs cultured on stiffer hydrogels (20–40 kPa) secreted more VEGF than did those cultured on softer hydrogels (0.5–2 kPa)[38]. Mechanical stiffness promoted the release of many trophic factors and cytokines. Human dermal microvascular endothelial cells cultured in conditioned media from mechanically loaded MSCs exhibited angiogenic formation through increased levels of MMP-2, TGF-β, and FGF[39]. However, 2D and 3D culture conditions have a profound impact on MSC secretome; 2D conditions induced cell polarity, which was absent in the 3D system. The 3D system promoted cellular interaction more than the 2D system. Seib *et al.* reported that hMSCs cultured on 2D PEG/HA/gelatin hydrogels at 20 kPa promoted paracrine release, including VEGF, μPA, and IL-8, but this was not observed in the equivalent hydrogel system with a 2 kPa elasticity[40]. Chaudhuri *et al.* reported that cultured bovine chondrocytes in 3D alginate hydrogels (3 kPa) with fast-stress relaxation promoted cell differentiation as indicated by enhanced matrix-forming genes (e.g., *COL2* and *AGGRECAN*), while elastic hydrogels induced cell death via enhanced matrix degradation (e.g., IL-1β, MMP-13, and ADAMTS4)[41].

1.2.2 Hydrogel elasticity in stem cell biology

1.2.2.1 Hydrogel viscoelasticity in cell attachment, cell spreading, and cell morphology

The impact of matrix elasticity extends beyond cell spreading. Based on the mechanotransduction theory, a viscoelastic matrix is expected to increase stress relaxation or creep. This in turn would reduce resistance to cell adhesion over time, thus reducing cell spreading. There has been some confusion over the relevant time scales with regard to the impact of viscoelasticity on cell spreading. Some studies revealed that viscoelastic hydrogels enhanced cell spreading, which contradicts the theory. For example, Tang *et al.* reported that hMSCs cultured on 2D PEG hydrogels (14–60 kPa, $\tau 1/2$ = 0.5–1s) with reversible coronate bonds (viscoelastic hydrogels) rather than irreversible azide-alkyne cycloaddition bonds (elastic hydrogel) increased cell volume and cell shape. This triggered the translocation of the Yes-associated protein [YAP], a key transcriptional regulator, from the nucleus to the cytoplasm and promoted cell proliferation and differentiation[42]. McKinnon *et al.* reported that myoblasts (C2C12) cultured on 3D PEG hydrogels generated by two hydrazine based bonds with faster stress relaxation ($\tau 1/2$ = 10 s) extended cell spreading, whereas slower stress relaxation ($\tau 1/2$ = 6,000 s) resulted in a rounded cell shape[43]. In stress-relaxing PEG hydrogels, embryonic stem cell–derived motor neurons promoted neuron ingrowth into the hydrogel[44].

Similarly, Lou *et al.* reported that hMSCs cultured on 3D viscoelastic HA and collagen hydrogels exhibited great cell spreading and enhanced focal adhesion protein expression[45]. Hydrogel-based substrate should contain cell-matrix adhesion sites to provide the physical link to enable the interaction between the cell and matrix substrate (e.g., arginine-glycine-aspartic acid [RGD] peptide motifs). RGD enables integrin-mediated cell adhesion, which promotes cell-ECM substrate adhesion, cell spreading, and cell morphology. Previous studies have suggested that fast stress relaxation hydrogels reduce mechanical confinement and enhance ligand clustering, leading to greater cell spreading. Chaudhuri *et al.* reported that cultured human osteosarcoma cells (U2OS) on 2D RGD-coupled alginate hydrogels with ionically-crosslinked viscoelastic substrates enhanced cell spreading compared with covalent-crosslinked elastic substrates with an equivalent stiffness (3.4 kPa). Integrin – matrix unbinding and matrix flow for viscoelastic substrates resulted in faster stress relaxation, ultimately supporting cell spreading[46]. Similarly, Chaudhuri *et al.* reported that human fibroblast cells (3T3) cultured on 2D RGD-coupled alginate hydrogels with greater stress relaxation (9 kPa, $\tau 1/2 = 70$ s) enhanced cell spreading and cell proliferation compared with those cultured following a $\tau 1/2$ range from 1 min to 1 h[26]. Many studies have revealed that substrate stiffness is responsible for cell spreading, the organization of the cytoskeleton, and focal adhesion. Seib *et al.* cultured hMSCs on 2D PEG/HA/galatin hydrogels, finding that the cells grown on hydrogels with a medium stiffness (20 kPa) exhibited less cell spreading and enhanced paracrine secretion (e.g., VEGF, μPA, and IL-8) than the cells cultured on softer hydrogels (2 kPa)[40]. Kuboki *et al.* cultured hMSCs on 2D gelatin hydrogels and showed that cells grown on 52 kPa hydrogels increased the expression of the cytoskeleton protein vimentin compared with those grown on softer hydrogels (3 kPa)[47]. Yeung *et al.* cultured hMSCs on 2D collagen-coated acrylamide, demonstrating that increased stiffness leads to greater cell spreading[48].

1.2.2.2 Hydrogel viscoelasticity in cell proliferation

The impact of matrix elasticity extends beyond cell proliferation. For example, mouse myoblasts cultured on stiffer 2D alginate hydrogels (0.25 kPa) exhibited greater cell proliferation by regulating the expression of the retinoblastoma protein. This in turn promoted cell proliferation into the G1/S cell cycle stage. In addition to substrate stiffness, time-dependent deformation is known to regulate cell proliferation. Bauer *et al.* reported that mouse myoblasts cultured on 2D alginate hydrogels with faster stress relaxation showed greater cell spreading and cell proliferation than those cultured on similar hydrogels with slower stress relaxation[49]. Cameron *et al.* generated viscoelastic collagen-coated polyacrylamide hydrogels by varying

the concentrations of acrylamide and bis-acrylamide crosslinkers. High acrylamide and low bis-acrylamide concentrations generated the highest loss modulus (4.7 kPa) through the movement of the loose ends of the polyacrylamide polymer chain. hMSCs cultured on 2D collagen-coated polyacrylamide hydrogels with the fastest stress relaxation exhibited greater cell spreading via increased *Rac1* and *N-cadherin* expression and enhanced release of smooth muscle cell induction factors. By contrast, cell size and maturity of focal adhesion was decreased among cells cultured on viscoelastic hydrogels[49,50].

1.2.2.3 Hydrogel viscoelasticity in cell differentiation

Cell differentiation is highly influenced by substrate elasticity. Mechanical stiffness affects cell-generated forces, the interaction of the ligand presented by the material, and the subsequent material–receptor cell interaction. This in turn affects intracellular cytoskeleton organization, activating downstream cell signaling pathways and transcription factors. These effects are now known to direct manipulate stem cell fate and lineage commitment. Engler *et al.* reported that human bone marrow–derived MSCs cultured on soft (0.1–10 kPa) and purely elastic 2D polyacrylamide hydrogels in the absence of differential media promoted neuron-like morphology and neuron-specific marker expression (e.g., β3 tubulin and nestin). Soft-hard hydrogels (8–17 kPa), mimicking muscle stiffness, promoted myoblastic morphology and muscle-specific marker expression. Stiff hydrogels (25–40 kPa), mimicking bone stiffness, promoted osteogenic morphology marker expression (e.g., CBF α1)[51]. The Engler lab reported that at equivalent stiffness but varying substrate, pore size did not alter cell lineage commitment. Besides substrate stiffness, MSC differentiation into specific lineages depends also on the rate of stress relaxation, which was not examined in these seminal studies). Subsequent studies from the Mooney lab reported that murine MSCs cultured on 2D RGD-coupled alginate hydrogels with an initial elastic modulus of 17 kPa (mimicking bone) and half stress relaxation of 60 s promoted osteogenic differentiation, evidenced by increased matrix mineralization and type I collagen deposition[26]. These differentiation results complemented previous work. An elastic modulus of 18 kPa in fast-relaxing ionically crosslinked alginate hydrogels optimally promoted osteogenic differentiation of hMSCs[52]. The Mooney lab also reported that an elastic modulus of 3 kPa with a fast relaxation time optimally promoted cartilage production[52].

1.2.3 Preclinical use of silk hydrogels

1.2.3.1 Silk hydrogels in drug delivery

Silk hydrogels show promise for delivering drugs of varying payloads[53,54]. The highly porous structure of

silk hydrogels enables the introduction of a large load of drugs, and the porosity can be adjusted to facilitate drug release[55]. Seib *et al.* evaluated the ability of physically crosslinked silk hydrogels to load and release the anticancer drug doxorubicin. They found that 2% silk hydrogels exhibited faster drug release than 6% silk hydrogels. *In vivo* studies showed that drug-loaded hydrogels reduced tumor size and metastasis more than a freely diffusible drug. However, varying the size of silk protein fragments by varying degumming time did not alter the amount of drug released from silk hydrogels[56].

1.2.3.2 Silk hydrogels in tissue regeneration

Silk fibroin–based hydrogels have been widely used in engineering both soft and hard tissues (e.g., bone[57], cartilage[58], and fat). Silk hydrogels allow stem cells to be encapsulated before gelation and can thus deliver large quantities of cells. Silk hydrogels exhibit tuned properties based on the method used to effect sol-gel transition. For example, electric field–induced silk hydrogels are dominated by a silk I conformation[59], whereas sonicate-induced silk hydrogels are dominated by a silk II conformation. High β-sheet concentrations result in opaque[60], brittle, and inelastic hydrogels[61]. Therefore, sonicated silk hydrogels are more appropriate for engineering bone, cartilage, and brain tissue than for engineering fat. Previous studies concerning the fitness of MSCs over silk materials have shown that the attachment and survival of MSCs positively correlate with matrix stiffness due to their favorable mechanical stability for cell adhesion and growth. Fernańdez-Garciáa *et al.* reported that the implantation of silk fibroin hydrogels into the mouse brain was safe and tolerable[62]. Mice that had suffered acute strokes and were injected with silk hydrogels (2% w/v, 5 μl) plus MSCs recovered more fully (i.e., no inflammation or neural death) than those treated with MSCs or silk hydrogels alone. The total volume of implanted silk hydrogels also reduced by 50% after four weeks[63]. In a subsequent study, Fernańdez-Garciáa *et al.* cultured MSCs on 3D silk hydrogels (2% w/v) pretreated with TNFα for 48 h to induce inflammation. TGF-β1 release increased in cell culture media 12 h posttreatment. They suggested that silk hydrogels induced functional recovery in a mouse stroke model, probably due to the significant release of TGF-β1 from MSCs after encapsulation[64]. Similarly, my research group reported that MSC-encapsulated silk hydrogels have the potential to be used in delivering MSCs into small lesion cavities in the brain. The *in vitro* study by Osama *et al.* reported that sonication-induced silk hydrogels exhibited no swelling after being incubated in phosphate buffer saline [PBS] overnight. MSCs encapsulated in silk hydrogels (2–4% w/v silk fibroin) promoted cell proliferation over 14 days, and MSC growth in the hydrogels followed a consistent distribution. In a later *in vivo* study, intracerebral injection of sol-gel sonicates induced silk hydrogels (4% w/v silk fibroin) filled the cavity

without damaging the surrounding tissue in a rat ischemic stroke model induced by Middle cerebral artery occlusion [MCAo][65]. Natalie *et al.* later investigated the impact of the intracerebral injection of sonicate-induced silk hydrogels on morbidity, mortality, space conforming, and biocompatibility after MCAo-induced ischemic stroke in rats. They found that silk hydrogels spread in stroke cavities without tissue swelling and promoted tissue repair, indicated by reduced glia scarring and endogenous cell proliferation. In addition, there was no increase in microglial and macrophagic activation, indicating that silk hydrogels did not promote an innate immune response[66].

1.3 Stroke

Stroke is the second-most common cause of death worldwide and the main cause of severe and long-term disability in adults67. Most tissues and organs can repair themselves when damage occurs, but the brain cannot. It has a limited capacity to repair damaged tissue and regenerate lost tissue. Brain tissue injury thus can involve severe impacts. About 40% of stroke patients suffer permanent disabilities. A stroke occurs when blood supply to the brain is interrupted or blocked by a blood clot. There are two types of stroke, based on the cause: ischaemic stroke and hemorrhagic stroke. Ischaemic stroke, which represents 90% of strokes, results from brain cell death and loss of brain tissue volume due to lack of oxygen. Hemorrhagic stroke, accounting for 10% of strokes, is caused by blood vessels bursting and bleeding inside the brain. Following injuries, cells and extracellular matrix (ECM) are phagocytosed and removed from the lesion core to produce a cavity filled with extracellular fluid. Typically, this stroke cavity is fully formed by 2 weeks post-injury and is surrounded by glial scarring that delineates this lesion core from the peri-infarct tissue[68]. One common drug is used in treating strokes: tissue plasminogen activator [tPA][69]. tPA is used to break blood clots, but the damaged brain tissue still remains. Additionally, tPA has a narrow time window (4.5 h) for administration after the onset of symptoms, so few stroke patients can really derive benefits from these treatments[70].

1.3.1 Clinical translational considerations in implantation of biomaterials for stroke therapy

1.3.1.1 Timing to inject hydrogels

Many therapeutic materials for ischemic stroke have failed in translating for clinical trial because it presents a complex and dynamic cascade of mechanisms implicated in stroke pathophysiology. These mechanisms are time-dependent. Therefore specific therapeutic strategies need to be matched to coincide with the best timing for therapeutic intervention. The timeline for administrating a hydrogels after stroke

depends on the extent of damage and thus a cavity to accommodate the therapy. This cavity develops naturally in the subacute and chronic phase following a substantial stroke (Figure 1.2). By 90 days post-stroke, up to 94% of patients will have tissue cavitation, dependent on the location and extent of stroke[71]. The tissue cavity is typically fully formed by 2 weeks post-injury and surrounded by glial scarring that delineates the lesion core from surrounding damaged tissue[68].

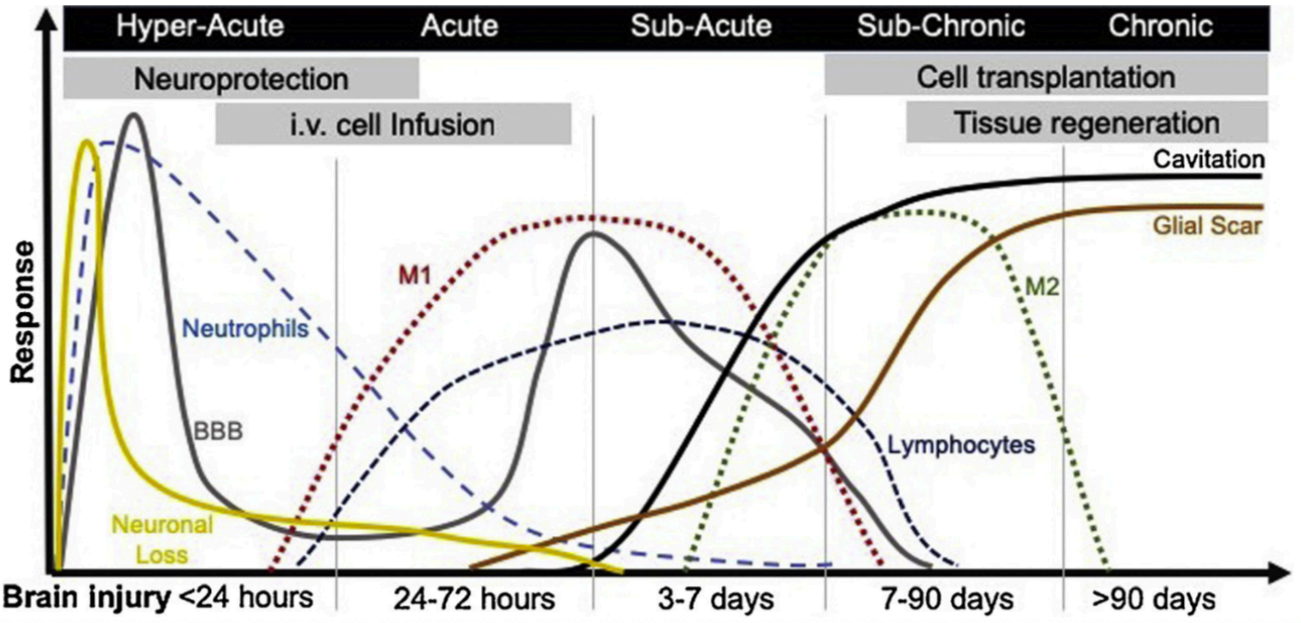

Figure 1.2 Timeline of activated pathophysiological processes following brain injury.
Ischemic stroke presents a complex and dynamic cascade of mechanisms implicated in its physiopathology. These mechanisms are time-dependent beginning shortly after the ischemic event and continue presenting for a months and years. An ischemic stroke leads to rapid loss of neurons at the core of the infarct. This area will cavitate and be surrounded by a glial scar. Acute inflammation promotes immune response that recruits neutrophils into brain tissue and produce a disruption in the blood brain barrier. Most infiltrating cells into infarct are M1- like phenotype macrophages. During cell death clearance phase,macrophages tend to polarize towards an M2- like phenotype macrophages. Figure adapted from[72].

Therefore, the likely timing of a biomaterial-based therapy would be in the subacute (7–90 day post-injury) -to-chronic (>90 day post-injury) phase to replace apoptotic cells and stimulate new compensatory connections. Most studies that used ischemic stroke models have selected the poststroke injection time point at 2 weeks or less[73]. The optimal window for neurogenesis, angiogenesis, change of macrophage

and microglia phenotype, and spontaneous recovery can be also used to guide the timing of the injection (Figure 1.3). Additionally, imaging and histology can be used to locate lesion characteristics and predict the optimal timing of the administration.

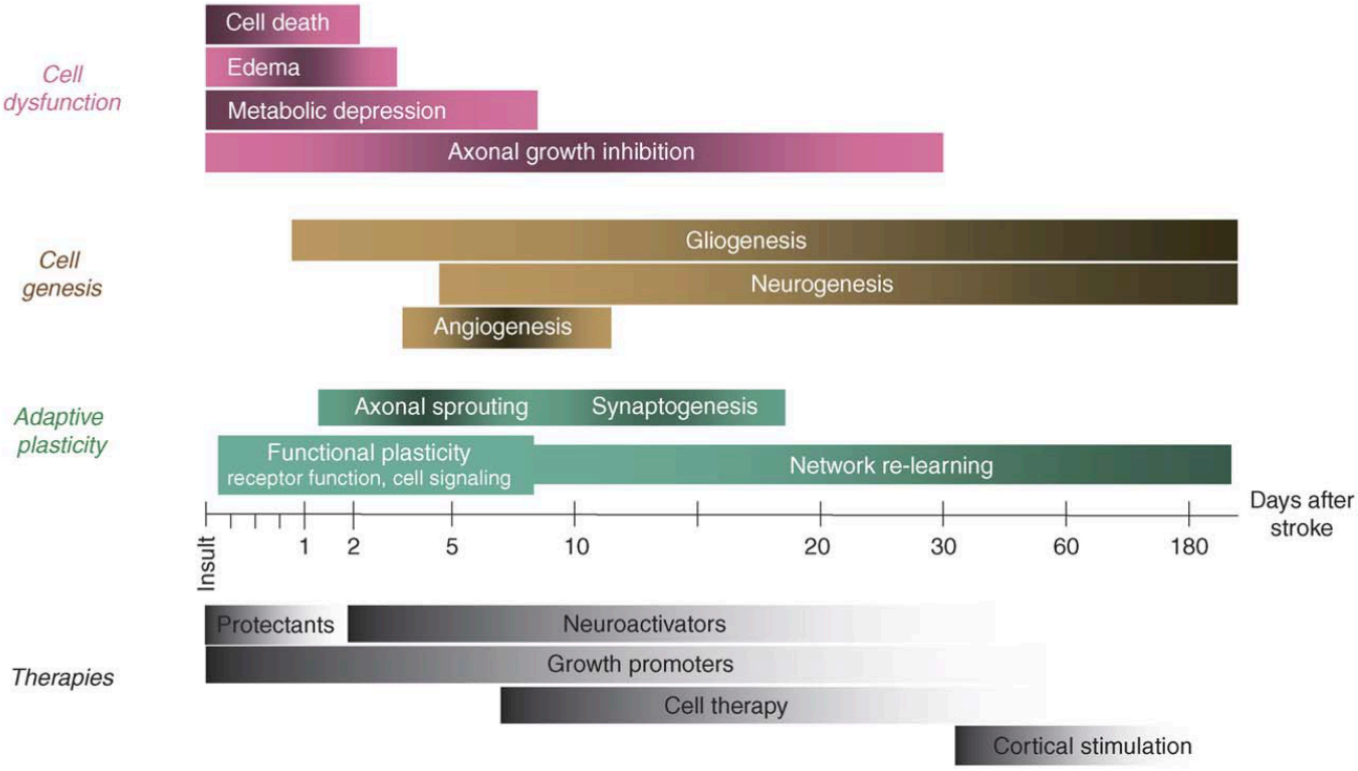

Figure 1.3 Therapeutic strategies focusing on selective mechanism depends on their respective therapeutic windows.

The implantation of biomaterial to promote in situ tissue engineering needs to be considered based on relevant pathophysiological events and the context of other therapeutics (i.e. promote neuronal survival, neovascularization) and their time window. Figure adapted from[74].

1.3.1.2 Imaging to locate implanted hydrogels

To increase both the success of the treatment and its relevance to clinical applications, a starting point could be the imaging of the biomaterial over time, ensuring conformal filling of the stroke lesion, sufficient stability, and adequate degradation for newly formed tissue[75]. Preclinical studies often assume a fixed infarct volume and use a fixed volume of implanted hydrogel; however, stroke lesion size and location in human vary. To address this, the Modo group used magnetic resonance imaging [MRI] to measure the individual infarct volume in each animal, in order to adjust the volume of hydrogel delivered and to guide injections to the precise site of injury[76]. Imagining can assist to examine the connection between functional

recovery and observed changes at the stroke lesion and also the morphology and composition of residual lesions in post-mortem individuals.

1.3.1.3 Efficacy of implanted hydrogels

Acute brain injury might not be a good model to study the post stroke therapeutic effect of implanted hydrogels in terms of efficacy of the therapeutic materials or behavioral outcomes. Some materials have been found to improve post-stroke neurogenesis in *in vivo* models (e.g. increase the presence of neural progenitor cells in damaged tissue and promote a functional tissue regeneration) but they fail in clinical studies because those outcomes are not enough to improve significantly the disabilities induced by stroke. To get better clinical relevant outcomes, long term study in a subacute and chronic models and standard behavioral measurement are needed[77].

1.3.2 Preclinical use of hydrogels as a supportive matrix to promote endogenous repair response in a stroke model

Some studies have posited that hydrogels are a promising supportive matrix for tissue repair after stroke in *in vivo* models[78,79,80,72]. Nih *et al.* reported that injection of microporous annealing particle hydrogels in the stroke cavity for 10 days reduced gliosis (glial fibrillary acid protein; GFAP+) and inflammation (Ionized calcium binding adaptor molecule -1+) while increasing the peri-infarct vasculature and promoting neural progenitor cell (doublecortin; DCX/Ki67) infiltration into the hydrogels[81]. Similarly, the Modo lab intracerebrally introduced porcine-derived urinary bladder matrix-ECM hydrogels with three different concentrations (i.e., 3, 4, and 8 mg/ml) into the subacute stroke cavity for three months, and the remaining volume of implanted hydrogels was determined by MRI. The 3 and 4 mg/ml hydrogel concentrations exhibited fast degradation: 80% after 14 days with promoting neuronal cell (NeuN+) infiltration and neovascular formation (RECA+). Only 32% of the 8 mg/ml hydrogels were resorbed after 90 days. These findings suggest that degradation of hydrogels, represented by an increased M1-to-M2 transition of macrophages, is responsible for tissue remodeling and *de novo* tissue formation[82,83]. A subsequent study by Jian *et al.* reported that implanting encapsulated glycosaminoglycan-based hybrid hydrogels with SDF-1α and bFGF into acute stroke lesions for one month elevated neural progenitor cell signaling (DCX+/Nestin+/Ki67+), which in turn promoted stroke repair, as determined by the restoration of forelimb movements[84].

1.4 Clinical use of MSCs in tissue regeneration

MSCs have attracted widespread interest as safe and effective candidates in cell-based therapies to repair damaged tissue. One reason for the widespread use of MSCs is their easy access via harvesting from adult donors. MSCs also appear to be immune privileged with no adverse reaction in the allogenic transplantation setting[85]. MSCs are multipotent nonhematopoietic progenitor cells and can be easily isolated from various tissues, including bone marrow, human amniotic fluid, placenta[86], fat and umbilical cord blood[87]. All these MSCs can differentiate into several distinct mesenchymal lineages, especially those derived from bone, cartilage, and fat. Additionally, controversial data suggest that MSCs may give rise to myogenic cells such as cardiomyocytes, endothelial cells, and even neural cells of nonmesodermal origin. An intriguing characteristic of MSCs is their ability to secrete a wide range of bioactive cytokines and growth factors that can influence nearby cells via paracrine signaling. Key factors include VEGF, FGF, HGF, IGF, PDGF, interleukin, and MMP. These secreted factors are involved in biological processes such as angiogenesis, immune modulation, and cell recruitment and differentiation[88]. In the vast majority of preclinical and clinical studies, MSCs are administered as a bolus injection either systemically (via the circulatory system) or locally at the site of injury[89]. Previous clinical trials showed that MSC transplantation into stroke injury sites in human patients had no adverse effect[90]. Stem cells have been studied for use in many therapeutic applications. However, a major challenge is the low cell retention at the application site because of rapid cell death (due to the absence of supporting signals). One way to overcome this limitation is by using a biomaterial carrier, which can encapsulate the cells before transplantation and thus enhance stem cell viability, proliferation, and retention at the target site. Hydrogels are becoming key candidates in this process because they (i) have the potential to support cell behavior by presenting cues (e.g., RGD), (ii) may provide a fibrillary structure to support cells, and (iii) possess tunable mechanical and biochemical properties[91]. Hydrogels used for stem cell delivery must be biocompatible and often biodegradable. The degradation of the hydrogel matrix plays a key role in determining *de novo* tissue formation (e.g., space for new cells and tissue formation). Often, the hydrogel is expected to degrade at the same rate as tissue is replaced, thus accommodating cell-secreted ECMs and ultimately tissue regeneration[55].

1.4.1 Clinical use of MSCs and biomaterials to promote endogenous brain tissue repair

Bone marrow MSCs derived from autologous or allogeneic donors are the most common cellular material used in cell-based therapy[92]. Phase I/II clinical studies demonstrated that hMSCs have a low chance to

develop into cancer cells[93]. A phase I/II study involving stroke patients following the National Institutes of Health Stroke Scale (NIHSS) revealed that 92% of patients experienced complete recovery after receiving autologous bone marrow mononuclear cells[94]. Preclinical studies have evaluated new strategies to improve cell-based therapies, such as using genetically modified bone marrow–derived MSCs or a biomaterial coadministered with the MSC stem cells[95,90]. A collaboration between NIH and the Chinese Academy of Sciences studied the impact of an Injectable Collagen Scaffold™ combined with MSCs on functional recovery in patients with traumatic brain injury and stroke (ClinicalTrials.gov identifier: NCT02767817).

1.5 General methodology

1.5.1 HRP/H_2O_2-induced chemical crosslinking silk hydrogels

In 1964, Anderson *et al.* found that in the presence of H_2O_2, HRP can be used to generate silk hydrogels that are elastic, highly stable in water, and transparent. In 1976, Aeschbach *et al.* identified a mechanism underlying HRP/H_2O_2-induced silk hydrogels: the formation of a dityrosine crosslink by oxidation of the amino acid tyrosine in silk fibroin[96]. The proposed mechanism to generate silk hydrogels via HRP enzymatic crossing involves HRP becoming activated in the presence of H_2O_2 and then acting as a powerful reducing agent that can oxidize 4-hydroxyphenyl group amino acids (specifically tyrosine)—but not natural aromatic group amino acids (phenylalanine and tryptophan). This reaction creates two single free radicals (Figure 1.4). One free radical reacts with the other to create either dityrosine or isodityrosine, and this reaction produces two water molecules. Lack of rigid crystalline or β-sheet structure results in excellent elasticity and resilience.

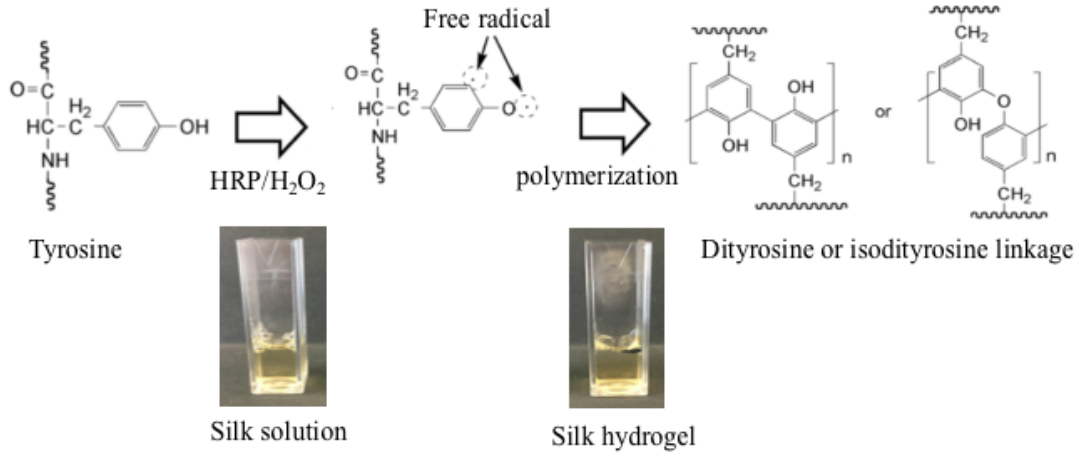

Figure 1.4 Proposed reaction pathway for HRP/H_2O_2-mediated chemical crosslinking

The optimum reaction condition facilitating the fastest gelation depends on the concentration of HRP, H_2O_2, and silk fibroin as well as the molecular weight of the silk fibroin (by varying degumming time) (Table 1.1). In 2014, Partlow *et al.* investigated the gelation condition to develop elastic silk hydrogels with stiffnesses between 0.2 and 10 kPa[97]. To assess the mechanical properties and the cytocompatibility of the hydrogels, HRP/H_2O_2-induced silk hydrogels 1–5% [w/v] were developed by fixing a concentration of 10 units of HRP per 1 ml of silk fibroin when presenting 0.5% H_2O_2. They found that the stiffnesses of 1%, 3%, and 5% HRP/H_2O_2-induced silk hydrogels after 60 min of degumming were 1, 3, and 4 kPa, respectively. At the same percentage of silk fibroin, silk hydrogels made in a shorter degumming time, which contained larger silk fiber chains, were stiffer than those made in a longer degumming time (10 kPa in 10 min vs. 4 kPa in 60 min). hMSCs cultured on 2D and 3D HRP/H_2O_2-induced silk hydrogels (3% w/v silk fibroin at 60 min degumming time) promoted cell attachment similar to cells cultured on tissue culture plastic controls. Cell proliferation increased with time and plateaued after 24 days in 2D culture and after 30 days in 3D culture. In addition, an *in vivo* study involving the subcutaneous implantation of HRP/H_2O_2 silk hydrogels into a mouse model showed that cells can infiltrate the hydrogels within two weeks. The degraded hydrogel fragments were initially found at two weeks. In 2017, Chirila *et al.* generated 5% silk hydrogels using three fabricated methods—genipin-induced chemical crosslinking, HRP/H_2O_2-induced enzymatic crosslinking, and physical crosslinking—to compare mechanical properties and cytocompatibility of these hydrogels. HRP/H_2O_2-induced enzymatic crosslinking silk hydrogels were highly elastic and had less β-sheet structure content. Human corneal epithelial cells (HCE-Ts) cultured on these hydrogels exhibited enhanced cell attachment and cell proliferation during seven days of culturing[98].

Table 1.1 Composition of the chemical crosslinking mixtures in 1 ml silk solution

Silk fibroin concentration (%)	HRP concentration (Unit/ml)	H_2O_2 concentration (%)	Unit of HRP/ml of total mixture	Unit of HRP/mg of silk fibroin	Stiffness (kPa)	Main conformation	Reference
1–6	1000	0.5	10	0.2	0.2–10	random coil	[97]
1–3	150	0.3	1.2–5	0.12–0.5	0.01–1	random coil	[99]
4, 10	900	0.5	17.3	0.18–0.45	10–100	random coil	[100]
16	210	0.36	18	0.13	1–1000	β-sheet	[101]
5	150	0.3	2.5–26	0.05-0.8	10–30	β-sheet	[98]

1.5.2 Sonication-induced physical crosslinking silk hydrogels

The proposed mechanism for generating silk hydrogels via ultrasonication comprises two main kinetic steps. Sonication energy activates silk fibroin mobility, which in turn promotes hydrogen bond formation between hydrophobic blocks, resulting in the conformational transition from the random coil to the antiparallel β-sheet structure with some interchain physical crosslinks. Then, the β-sheet structure is extended and many interchain β-sheet crosslinks form, resulting in a silk hydrogel network (Figure 1.5)[102]. β-sheet conformation is thermodynamically stable. The β-sheet structure can function as a physical crosslink. Gelation time can be controlled from minutes to hours based on the sonication parameters used (e.g., power output and time) and silk solution concentrations, as well as the effects of strong ions (e.g., potassium ions), high temperature, and low pH[103]. Ultrasonication is a promising method for achieving cell encapsulation in silk hydrogels[25,99,104]. Wang *et al.* developed sonicate-induced silk hydrogels with 4%, 8%, and 12% [w/v] silk fibroin, and hMSCs were encapsulated in the solution 0.5–2 h before the hydrogels completely formed. The results showed that cell survival was lower in the hydrogels with higher concentrations of silk fibroin. hMSCs encapsulated in 4% silk hydrogels exhibited significant cell growth for 21 days, whereas those encapsulated in 8% and 12% silk hydrogels exhibited increased cell death at 6 days and 1 day, respectively[105].

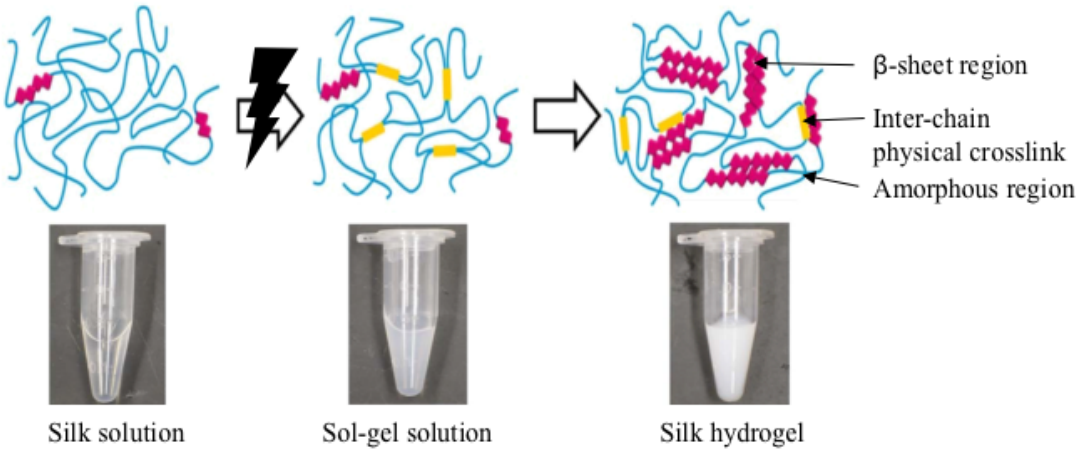

Figure 1.5 Schematic illustration of the mechanism of sonicate-induced silk gelation

1.6 Hypothesis and specific aims

The main hypothesis of this thesis is that silk hydrogels can be used as a supportive substrate in cell-based therapies. I expect that viscoelastic silk hydrogels (rather than elastic silk hydrogels) can mimic native ECM, particularly brain tissue. I tested this hypothesis by conducting *in vitro* (Chapter 2) and *in vivo* studies (Chapter 3). The specific thesis aims are:

(i) To determine the mechanical properties of elastic and viscoelastic silk hydrogels

(1) To determine the conditions required for fabricating elastic and viscoelastic silk hydrogels with equivalent silk concentrations and stiffness

(2) To compare structural characteristics between elastic and viscoelastic silk hydrogels

(ii) To investigate the impact of viscoelasticity of silk hydrogels on human MSC behavior

(1) To determine cell morphology and the cytoskeleton structure of hMSCs on elastic and viscoelastic silk hydrogels

(2) To determine the cell survival and cell proliferation of hMSCs on elastic and viscoelastic silk hydrogels

(3) To determine the cell signaling gene and protein expression of hMSCs cultured on elastic and viscoelastic silk hydrogels

(4) To determine the metabolic profiles of hMSCs cultured on elastic and viscoelastic silk hydrogels

(iii) To assess the long-term performance of implantated silk hydrogels in an experimental stroke model using rats

(1) To visualize the gelation, retention, and biodegradation of implanted silk hydrogels

(2) To determine the phenotypes of invading cells in relation to tissue repair

(2.1) To establish phenotypic macrophagic ingrowth in relation to tissue remodeling

(2.2) To visualize neuronal cell infiltration and survival in implanted areas in relation to tissue regeneration

CHAPTER 2

SILK HYDROGEL SUBSTRATE STRESS RELAXATION PRIMES MESENCHYMAL STEM CELL BEHAVIOR IN 2D

Chapter summary:

This chapter was published as an original article (Phuagkhaopong *et al.* 2021. ACS Appl. Mater. Interfaces. 13(26): 30420–30433)[106] and has been adapted accordingly for this thesis. Data acquisition and analysis for Figures 2.12 was conducted in collaboration with Dr. Iola Duarte. This included metabolomic profiling works. Data acquision and analysis for all other figures were conducted by myself. As the first author of the study, I wrote the manuscript with input from the other authors.

This chapter stressed the role silk hydrogel stress relaxation on MSC performance. Silk hydrogels were fabricated to serve as ECM mimetic culture substrate for hMSCs by either chemical or physical cross-linking, generating elastic and viscoelastic hydrogels, respectively. Properties of the hydrogels were determined by scanning electron microscopy [SEM], Fourier Transform Infrared Spectroscopy [FTIR], and rheology. Following by determine the impact of these hydrogels on hMSC behavior in 3 main aspects (i.e. gene expression, extracellular protein secretion, and extracellular metabolome). Viscoelasticity is one mechanical cue of ECM which plays a substantial role in responsibility for cellular mechanotransduction, leading to regulation of cell fate including cell proliferation, cellular gene expression, and paracrine secretion.

2.1 Abstract

Tissue-mimetic silk hydrogels are being explored for diverse healthcare applications, including stem cell delivery. However, the impact of stress relaxation of silk hydrogels on hMSC biology is poorly defined. The aim of this study was to fabricate silk hydrogels with tuned mechanical properties that allowed the regulation of MSC biology in two dimensions. The silk content and stiffness of both elastic and viscoelastic silk hydrogels were kept constant to permit direct comparisons. Gene expression of IL-1β, IL-6, LIF, BMP-6, BMP-7, and protein tyrosine phosphatase receptor type C were substantially higher in MSCs cultured on elastic hydrogels than those on viscoelastic hydrogels, whereas this pattern was reversed for insulin, HNF-1A, and SOX-2. Protein expression was also mechanosensitive and the elastic cultures showed strong activation of IL-1β signaling in response to hydrogel mechanics. An elastic substrate also induced higher consumption of glucose and aspartate, coupled with a higher secretion of

lactate, than was observed in MSCs grown on viscoelastic substrate. However, both silk hydrogels changed the magnitude of consumption of glucose, pyruvate, glutamine, and aspartate, and also metabolite secretion, resulting in an overall lower metabolic activity than that found in control cells. Together, these findings describe how stress relaxation impacts the overall biology of MSCs cultured on silk hydrogels.

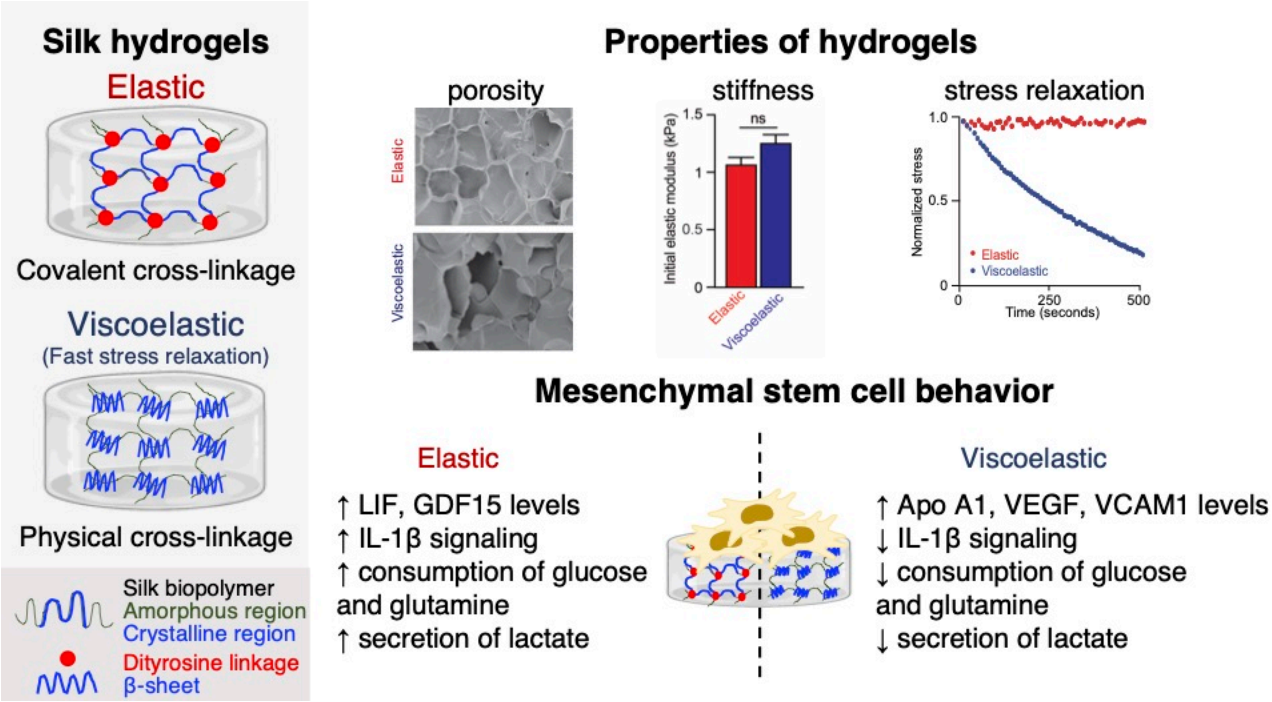

Figure 2.1 Graphical abstract

2.2 Introduction

hMSCs are widely explored in the clinic because they can differentiate into mesenchymal linages of bone, cartilage, or fat for the repair of injured tissues.[107] However, MSCs also produce a myriad of paracrine and trophic factors that increase their therapeutic versatility as potent immunosuppressive and anti-inflammatory mediators. One example is the clinical use of MSCs to treat Graft-versus-Host disease.[108] However, MSCs delivered by simple intravenous injection rapidly undergo perforin-dependent apoptosis within cytotoxic recipient tissues.[109] Therefore, preclinical studies are now exploring delivery strategies that include bioengineered scaffolds in an effort to improve MSC function. For example, encapsulating MSCs into alginate hydrogels prior to intravenous dosing in mice can change the pharmacokinetic parameters and increase the elimination half-life, extend MSC survival, and improve allogenic bone marrow engraftment.[110]

MSCs are responsive to many different cues, including physical features such as niche geometry and mechanics.[111] For example, substrate stiffness is a key regulator of MSC linage commitment both in two[51] and three dimensions.[26] However, the wider mechanical space also impacts cell behavior,[112] including MSC biology.[26] Therefore, the stiffness and the substrate stress-relaxation are key physical parameters that dictate MSC biology. Both fundamental and applied studies have used a range of materials, including Matrigel®, alginate, polyethylene glycol, and polyacrylamide-based hydrogels, to tune the mechanics of transplanted MSCs. However, many of these materials are not suited for clinical applications.

The use of materials with potential for clinical translation is particularly timely. One promising contender for MSC application is silk.[113] Silk fiber is clinically approved for use in humans and has a robust track record.[3] *Bombyx mori* silk fibers have been used for millennia as a suture material that is renowned for its availability, mechanical robustness, knot strength, ease of handling, and biocompatibility. However, silk has wider potential extending far beyond sutures. Over the past 2 decades, interest has been renewed in biomedical applications of silk, both in its spun fiber format and in a fully reverse-engineered liquid format.[3] For example, knitted silk surgical meshes (SERI® Surgical Scaffold, Sofregen Inc., MA, USA) fabricated from naturally spun silk fibers or from silk hydrogels (e.g., a bulking agent for vocal fold insufficiency, Silk Voice®, Sofregen Inc.) derived from liquid silk have recently been approved for use in humans.[114] Silk fibers, films, scaffolds, and hydrogels have been combined with MSCs to explore potential tissue engineering applications in two, three, and four dimensions.[113] This includes the use of silk-based materials for use as scaffolds to deploy tumor-homing MSCs armed with genetically introduced therapeutic genes.[115] Emerging evidence currently supports the use of silk hydrogels for MSC applications.[116] Therefore, controlling silk hydrogel function is now a key research area.

Silk hydrogels can be readily tuned by tailoring the silk protein concentration and composition, in addition to manipulating the crosslinking mechanism and density.[105,98,117,118] The resulting silk hydrogels have been explored in a broad spectrum of tissues and applications (e.g., skin,[119] bone,[120] cartilage,[121] muscle,[25] pancreas,[122] and brain.[63, 123] For example, embedding MSCs within a physically cross-linked 4% [w/v] silk hydrogel provided the best cell proliferation, whereas a higher silk content (8 and 12%, w/v) impaired cell proliferation.[105]

The ability to trigger the solution-gel transition was explored as a benefit for stereotactic injections.[65] MSCs retained their viability in the solution phase, allowing minimally invasive administration deep into the target site, where the administrated dose completed the solution-gel transition in situ. Seminal work by González-Nieto and co-workers[63] subsequently demonstrated the suitability of this delivery technology

for the administration of MSCs into the epicenter of a cortical stroke region in mouse brains. Mice treated with MSCs showed reduced cortical tissue loss, improved MSC survival, and cortical rewiring with partial functional recovery. *In vitro* studies have shown that MSCs exposed to silk hydrogels respond by downregulation of stromal cell-derived factor 1 [SDF-1], brain-derived neurotrophic factor [BDNF], and VEGF, while increasing TGF-β1 secretion.[64]

Despite the increasing popularity of silk for tissue engineering applications,[3] the proposed use of silk hydrogels as carriers for cell therapies (i.e., advanced therapy medicinal products)[116] and the fundamental understanding of silk hydrogel performance[124] and its impact on MSC biology remain limited. This also includes the performance of MSCs in two dimensions. In particular, the impact of silk hydrogel stress relaxation on human MSC gene expression and the composition of the secretome and metabolome is unknown. Therefore, the aim of the present study was to exploit chemical and physically crosslinking to fabricate elastic and viscoelastic silk hydrogels, respectively, that had equivalent silk content and stiffness. These hydrogels were used to form two-dimensional cell culture substrates. The cell choice for this study was primary human MSCs obtained from four different healthy donors to minimize source variability.

2.3 Materials and Methods

2.3.1 Silk hydrogel manufacture.

The silk fibroin solution was prepared from *Bombyx mori* cocoons. Briefly, dried cocoons were cut into 5 × 5 mm pieces and 5 g samples were degummed with 2 L of 25 mM Na_2CO_3 for 60 min (degumming time). The degummed fibers were then rinsed with 1L of Milli-Q water for 20 min; this process was repeated twice more. The extracted silk fibroin was air dried in a fume hood overnight, then dissolved in 9.3 M LiBr [silk/LiBr ratio of 1:4 (g/mL)], and heated in an oven at 60˚C for up to 4 h. The dissolved silk fibroin was then transferred to a dialysis cassette (molecular weight cutoff 3500 Da; Thermo Fisher Scientific Inc., Waltham, MA, USA) and dialyzed against Milli-Q water, with six water changes over 48 h. The dialyzed silk fibroin solution was then collected, centrifuged twice at 9500 × g for 20 min to remove any aggregates, and stored at 4˚C until use. The silk fibroin concentration was calculated gravimetrically.[125]

Silk hydrogels denoted as viscoelastic were manufactured by sonication using a digitally controlled probe sonicator (Sonoplus HD 2070, Bandelin, Berlin, Germany) fitted with a 23 cm long sonication tip (0.3 cm diameter tip and tapered over 8 cm). A total volume of 4 mL of 4% [w/v] silk fibroin solution was added to 15 mL Falcon tubes (1.4 cm diameter and 11 cm long) (Greiner Bio-One GmbH, Kremsmünster,

Austria) and exposed to a 30% amplitude for two or three sonication cycles on ice (one cycle consisted of 30 s on and 30 s off) to induce the solution-gel transition.

Silk hydrogels denoted as elastic were generated by dityrosine cross-linking[97] using HRP (Sigma-Aldrich). Unless stated otherwise, chemical cross-linking was performed with 2.25 U of freshly prepared HRP for every 1 mg of silk fibroin protein. Briefly, 1 mL of 4% [w/v] silk fibroin solution was added to a 1.5 mL Eppendorf tube (Fisher Scientific), followed by 150 µL of HRP (600 U/mL) and 150 µL of fresh 0.3% H_2O_2, followed by gentle mixing. The mixtures were then stored at 37°C until gels were formed.

2.3.2 Dityrosine bond monitoring.

Elastic silk hydrogel samples were prepared as described above. The tyrosine fluorescence signal was monitored using an excitation wavelength of 310 nm ± 20 nm and emission wavelength of 410 nm ± 20 nm (FP-6500 spectrofluorometer, Jasco international CO., Ltd., Japan). Dityrosine fluorescence emission was monitored between 350 and 550 nm. The scan rate was set at 200 nm/min, with 2 nm data intervals. The photomultiplier tube detector voltage was fixed. A silk solution without HRP and H_2O_2 was used as a control.

2.3.3 Mechanical properties analysis by rheology.

Samples were prepared in silicone molds forming a 20 mm diameter with an average thickness of 4 mm. The hydrogels were then subjected to rheological characterization at 25°C (HAAKE™ MARS™ rheometer, Thermo Fisher Scientific, UK) using stainless steel parallel plates with a 20 mm diameter and appropriate gap size. The storage modulus (G') was recorded continuously using a time sweep over a strain of 0.01–100% at a frequency of 1.0 Hz. Subsequently, the rate of stress relaxation (loss modulus G'') was determined at a fixed gap width and a 15% strain to mimic the human extracellular matrix.[26] The resulting stress was monitored every 10 s for a total of 500 s. Stress was normalized by the initial stress, and $\tau_{1/2}$, which is the time corresponding to half of the initial stress, was then calculated (as detailed previously[26]). Before measurement, all samples were equilibriated for 20 min and shielded to minimize water evaporation and drying.

2.3.4 Secondary conformation analysis by FTIR.

Samples were frozen overnight at -20°C and lyophilized (Epsilon 2-4 LSCplus, Christ, Germany). The secondary structure of the dried samples was assessed using a TENSOR II FTIR spectrometer (Bruker

Optik GmbH, Ettlingen, Germany) with 128 scans at a 4 cm^{-1} resolution over the wavenumber range of 400 to 4000 cm^{-1}, and the secondary structures were assigned. Briefly, the amide I region (1595–1705 cm^{-1}) was identified and deconvoluted: 1605–1615 cm^{-1} as side chains, 1616–1637 cm^{-1} and 1697–1703 cm^{-1} as β-sheet structures, 1638–1655 cm^{-1} as random coil structures, 1656–1662 cm^{-1} as α-helical bands, and 1663–1696 cm^{-1} as β-turns.[126]. All spectra were normalized and corrected for water signals. OriginPro 9.0 software was used to peak fit the amide I region of all spectra. The peak full-width at half-maximum was maintained at a fixed value to avoid overfitting the data. Air-dried and 70% ethanol-treated silk films were used as reference samples for low and high β-sheet content, respectively.

2.3.5 Scanning electron microscopy.

Silk hydrogels were attached to an electrically conducting sticky carbon patch (Agar Scientific, UK), mounted on aluminum stubs, and freeze-dried overnight. Samples were sputter coated with 15 nm of gold using an ACE200 low-vacuum sputter coater (Leica Microsystems, Wetzlar, Germany). The morphology of the silk hydrogels were imaged by SEM using a FE-SEM SU6600 instrument (Hitachi High Technologies, Krefeld, Germany) with a 5 kV accelerating voltage.

2.3.6 Immunodetection of adsorbed protein.

Human fibronectin [FN] (Sigma-Aldrich, St. Louis, MO, USA) was reconstituted to a final concentration of 10 and 100 ng/mL in PBS (pH 7.4). Prior to protein adsorption, the hydrogel surfaces were rinsed twice with PBS for 10 min. The prepared FN solutions (400 μl) were applied to the hydrogel surface, and the samples were sealed to minimize evaporation and incubated at 37°C for 1, 3, 6, and 24 h. A 250 kDa fluorescein isothiocyanate–labeled dextran (2 mg/ml, Sigma-Aldrich) was used as a reference control to account for possible differences between the hydrogels. After the indicated incubation time, the remaining solution was collected and centrifuged at 5,000 × g for 5 min. The surface density of adsorbed fibronectin was calculated by measuring the depletion of FN from solution using a human FN ELISA kit (R&D Systems, USA), according to the manufacturer's protocol. The data were normalized using the dextran control. The concentration of dextran was determined using a fluorescence plate reader (excitation: 485 nm; emission: 528 nm).

2.3.7 Cell culture and viability.

Human primary MSCs were isolated from bone marrow aspirates of healthy donors after I obtained their informed consent. The institutional review board of the Medical Faculty at the University Hospital Dresden approved the study. Human MSCs were expanded and characterized[127]. For all silk hydrogel studies, MSCs were used for up to three passages. Elastic and viscoelastic silk hydrogels were prepared as described above but using filter-sterilized stocks (prepared with a 33 mm Millex-GP syringe filter fitted with a polyethersulfone membrane with 0.22 μm pores). A 50 μL sample undergoing the solution-gel transition was pipetted into each well of a tissue culture-treated polystyrene 96-well plate (well surface area 0.32 cm^2) (Corning Inc., New York, USA). Plates were transferred to a cell incubator (humidified atmosphere of 5% CO_2 at 37°C) for 3 h to allow completion of the silk solution-gel transition. A 200 μL volume of low glucose Dulbecco's modified Eagle medium [DMEM] (Thermo Fisher Scientific) supplemented with 10% v/v fetal bovine serum (Stem Cell Technologies, France), 1% GlutaMAX (Thermo Fisher Scientific), 50 U/mL penicillin, and 50 μg/mL streptomycin (Thermo Fisher Scientific) was carefully added onto the top of the silk hydrogels. The medium was changed twice and the silk hydrogels were allowed to equilibrate overnight in the cell incubator. The next day, the medium was removed and human MSCs in complete DMEM were seeded on top of the hydrogels at a density of 5000 cells/cm^2 in 200 μL of medium (i.e., two dimensional culture). The medium was changed at days 3 and 7. Cell viability was measured at days 1-14. In brief, the medium was removed, replaced with fresh DMEM medium, and 25 μL of resazurin was added (440 μM stock in PBS, Thermo Fisher Scientific). The cells were allowed to metabolize the substrate for 4 h, and then 100 μL of the supernatant was transferred into a black 96-well plate (Sigma-Aldrich, St. Louis, MO, USA). The fluorescence was measured with a fluorescence plate reader (POLARstar Omega BMG LABTECH GmbH, Ortenburg, Germany) by fixing the photo multiplier tube and setting the excitation and emission filters at 560 nm and 590 nm, respectively. Blank hydrogels from the same time points were used as controls to subtract background fluorescence.

2.3.8 Cell proliferation.

DNA concentration was measured at days 1-14 using the Quant-iTTM PicoGreen® kit (Invitrogen-Life Technologies, Grand Island, NY, USA). In brief, culture medium was removed and replaced with 200 μL PBS for 3 h. The samples were homogenized and digested with 200 μL papain buffer solution (5 mg/mL papain, 2 mM cysteine, 50 mM sodium phosphate, and 2 mM ethylenediaminetetraacetic acid, pH 6.5, in

nuclease-free water) at 60°C for 16 h. The papain-digested samples were collected and centrifuged for 5 min at 13,000 × g to eliminate cellular debris. The supernatants were collected and dDNA was quantified with the Quant-iTTM PicoGreen® kit, following the manufacturer's protocol. Blank hydrogels from the same time points were used as controls to account for background fluorescence.

2.3.9 Cell staining.

hMSCs were cultured on silk hydrogel substrates in four-chamber slides for 3 days. Cell-seeded hydrogels were fixed in 4% v/v methanol-free formaldehyde, permeabilized in 0.1% v/v Triton-X 100 for 15 min, and blocked in 1% [w/v] bovine serum albumin (BSA; Sigma-Aldrich) for 1 h at room temperature. Hydrogels were then incubated overnight at 4°C with primary antibodies against YAP (rabbit polyclonal anti-YAP1 antibody, 1:50 dilution in PBS/BSA 1% [w/v], Abcam, UK). The hydrogels were given three 10 min washes with PBS and then incubated in the dark at room temperature for 2 h with secondary antibodies (AlexaFluor 555 goat anti-rabbit IgG, 1:500 dilution in PBS/BSA 1% [w/v], Abcam). The hydrogels were then rinsed three times with PBS and stained with a Hoechst 33342 nuclear stain (1:1000 dilution in PBS, Cayman Chemicals, USA) for 10 min, followed by two rinses with PBS. For actin filament visualization cells were stained with a phalloidin-Alexa488 dye, according to the manufacturer's instructions (Thermo Fisher Scientific Inc., Waltham, MA, USA). In brief, cells were washed and fixed as detailed above. Next, cells were incubated at room temperature with phalloidin-Alexa 488 at a final concentration 0.165 μM in PBS for 1 h to stain the β-actin cytoskeleton. Stained hydrogels were stored in the dark at 4°C until imaging (Epifluorescence upright microscope, Nikon Eclipse E600). Exposure time and other image settings for each respective channel were held constant during imaging. Images were adjusted, processed and analyzed in ImageJ 1.51s (National Institutes of Health, Bethesda, USA).

2.3.10. Image analyses.

For investigate of the cytoskeletal organization of the cells, single cells were manually traced from fluorescent actin images. Area, perimeter, fit ellipse, and shape descriptors were quantified by image J[128]. Shape descriptor values were then used to calculate four metrics; namely, cell area (π x radius^2), circularity ((4 x π x area)/(perimeter^2)), roundness ((4 x area)/(π x major axis length^2)), and aspect ratio (major axis length/minor axis length) (Figure 2.2)[129]:With these metrics, a line and a circle have values of 0 and 1, respectively. For YAP/TAZ staining, the nuclear to cytoplasmic ratio was calculated with the formula:

nuclear YAP = (nuclear YAP intensity/ area of nucleus)/(cytosolic YAP intensity/ area of cytosol) (detailed previously[130]).

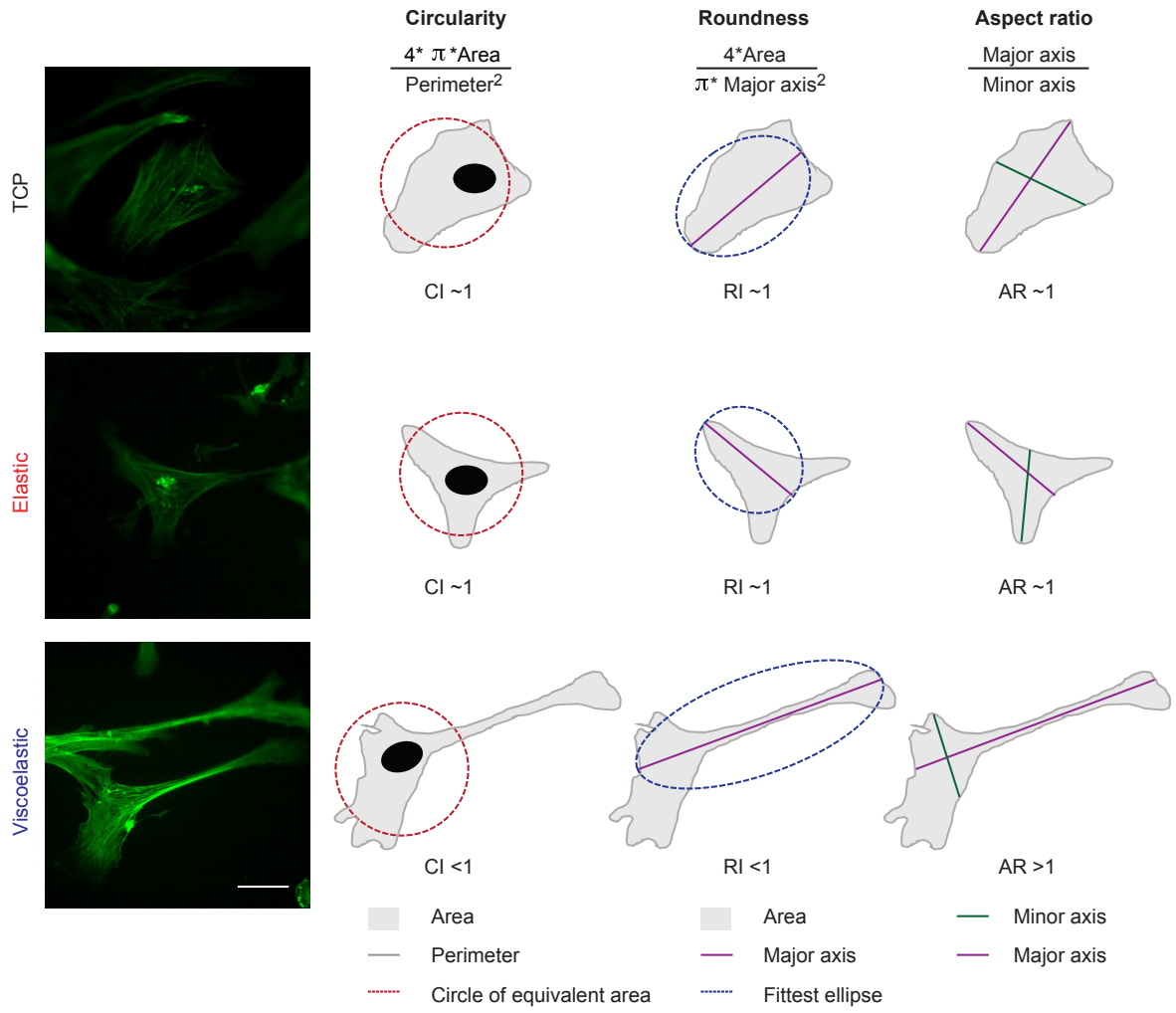

Figure 2.2 Schematic representation of morphological metrics used to quantify cell area, circularity, roundness, and aspect ratio, using ImageJ software.

CI, circularity; RI, roundness; AR, aspect ratio. Scale bar = 10 µm. Figure adapted from reference. [129]

2.3.11 Quantitative real-time polymerase chain reaction (qRT-PCR).

Gene expression of hMSC cultured on different elastic hydrogels was assessed using a similar cell culture approach as detailed above. Briefly, medium was removed, followed by washing with PBS twice and then cells were harvested with Accutase (Thermo Fisher Scientific). Total RNA was extracted from hMSCs using MicroRNeasy Kit (Qiagen), according to the manufacturer's instructions. Quantification of RNA

was performed on a Nanodrop 2000 spectrophotometer (Thermo Scientific). RNA samples from each donor were used to determine the expression of nine selected target genes. The cDNA was synthesized from 1 μg of total RNA using the QuantiTect reverse transcription kit (Qiagen, USA). Quantitative RT-PCR was performed using the QuantiTect SYBR Green PCR kit (Qiagen) on an Applied Biosystems 7500 Real-time PCR system (ABI 7500, Applied Biosystems). The targets, which included human *IL-1B, IL-6, ITGB1, ITGV, LIF, MMP2, RhoA, VEGFA,* and *VCAM1*, were determined according to the Qiagen guidelines. *GAPDH* and *RPL30* were used as reference genes. The threshold cycle (C_t) value of each target gene was normalized to the expression of two different housekeeping genes (*GAPDH* and *actin-beta*) for the RT^{2}Profiler PCR Array and *GAPDH* and *RPL30* for single target primer assays. The difference between the C_t value of a target gene and the housekeeping genes of cells cultured on hydrogels was subtracted from the difference between the C_t value of the target gene and housekeeping genes of cells cultured on plasma-treated tissue culture plastic, and it was then expressed as a relative fold change according to the $2^{-\Delta\Delta Ct}$ method. The relative fold change value of plasma-treated tissue culture plastic was defined as 1. For RT^{2}Profiler PCR Array experiments, extracted RNA from MSCs of the four healthy donors were pooled. Single-stranded complementary DNA (cDNA) was synthesized from 500 ng of total RNA and amplified with RT^2 PreAMP cDNA synthesis with RT^2 PreAMP cDNA Synthesis Primer Mix for hMSCs. The RT^{2}Profiler PCR Array (PAHS-082Z, Qiagen) was used for transcriptome profiler expression analysis according to the manufacturer's instructions.

Table 2.1 Table of primer sequences.

Gene name	Gene bank number	Primer sequence (5'-3')	Product size (bp)
IL-1B	NM_008361	QuantiTect Primer Assay (Qiagen) Hs_IL1B_1_SG	117
IL-6	NM_031168	QuantiTect Primer Assay (Qiagen) Hs_IL6_1_SG	120
ITGB1	NM_004763	QuantiTect Primer Assay (Qiagen) Hs_ITGB1_1_SG	152
ITGV	NM_001144999	QuantiTect Primer Assay (Qiagen) Hs_ITGAV_1_SG	125
LIF	NM_002309	QuantiTect Primer Assay (Qiagen) Hs_LIF_1_SG	97
MMP2	NM_004530	QuantiTect Primer Assay (Qiagen) Hs_MMP2_1_SG	95
RhoA	NM_001664	QuantiTect Primer Assay (Qiagen) Hs_RHOA_1_SG	92
VEGFA	NM_001025366	QuantiTect Primer Assay (Qiagen) Hs_VEGFA_1_SG	273
VCAM1	NM_001078	QuantiTect Primer Assay (Qiagen) Hs_VCAM1_1_SG	106
GAPDH	NM_001256799	QuantiTect Primer Assay (Qiagen) Hs_GAPDH_1_SG	95
RPL30	NM_000989	QuantiTect Primer Assay (Qiagen) Hs_RPL30_1_SG	100

2.3.12 Gene network and pathway analysis.

A short list of differentially expressed genes was generated based on the following criteria: mRNAs with p-value < 0.05 and log 2 fold change > 2. The transcriptome data set in response to MSC culture was visualized by comparing the MSCs on silk hydrogels to those on a tissue culture plastic. A normalized z-score was calculated and a heat map was generated using the R package software (R Studio 3.5.2 version; The R Foundation, Boston, MA; available at r-project.org). Similarly, the short-listed differentially expressed genes were used to perform a core analysis with the IPA software (Qiagen) to identify the upstream regulators of the differentially expressed genes and related canonical pathways that were altered by culture on silk hydrogels. The IPA core analyses were based on previous knowledge of the associations of upstream regulators and their downstream target genes archived in the Ingenuity Knowledge Base. When mapped to canonical pathways, the pathway that had the highest IPA score was considered the most differentiated from the others. The p-values were calculated by Fisher's exact test for the upstream regulator analysis.

2.3.13 Proteome profiler analysis.

Protein expression patterns were determined from pooled conditioned culture medium from the four MSC donors. The conditioned medium was collected and centrifuged at 5,000 × g for 5 min to remove any cells or cell debris. The supernatant was transferred to new tubes and stored at −80°C until use. Human cytokine proteome profiler (Panel A, R&D Systems, Minneapolis, MN, USA) was used, according to the manufacturer's instructions. For the analysis of arrays, blots were threshold adjusted and analyzed using Image J. The intensity for a specific cytokine was then computed by averaging over duplicated spots.

2.3.14 Sample preparation for metabolomics and NMR spectroscopy.

The culture medium was collected, clarified by centrifugation at 5,000 × g for 5 min, lyophilized, and stored at −80 °C until use. NMR analyses were conducted after reconstituting freeze-dried medium in 600 µL deuterated phosphate buffer (100 mM, pH 7.4) containing 0.1 mM 3-(trimethylsilyl)propionate sodium salt, (TSP)-d4. A 550 µL volume of each sample was transferred into 5 mm NMR tubes, and NMR spectra were acquired on a Bruker Avance III HD 500 spectrometer (University of Aveiro, Portuguese NMR Network) operating at 298 K and 500.13 MHz for ^{1}H observation. Standard 1D ^{1}H spectra with water presaturation (pulse program "noesypr1d" in the Bruker library) were recorded with a 7002.801 Hz spectral width, 32768 data points, a 2 s relaxation delay, and 512 scans. The spectral processing comprised

cosine multiplication (ssb 2), zero-filling to 65536 data points, manual phasing, baseline correction, and chemical shift calibration to the TSP-d_4 signal at δ 0 ppm. Each spectrum was multiplied by a correction factor to account for the different volumes of medium lyophilized and the different cell numbers, which were associated with DNA content.

Metabolites were identified by matching our spectral data to reference spectra in the reference libraries in the Human Metabolome Data Base (HMDB), BBIOREFCODE-2-0-0 (Bruker Biospin, Rheinstetten, Germany), and Chenomx (Edmonton, AB, Canada). Quantitative variations were assessed through spectral integration of selected signals using Amix-Viewer 3.9.15 (Bruker Biospin, Rheinstetten, Germany). For each metabolite, fold changes were calculated relative to respective acellular medium controls. Metabolite variations with an absolute fold change ≥ 1.05 were classified as consumed or secreted and plotted as a heat map.

2.3.15 Data and statistical analyses.

Data were analyzed using GraphPad Prism 8.0@ (GraphPad Software, La Jolla, CA). Student's t-tests were used to analyze sample pairs. One-way analysis of variance (ANOVA) between controls and elastic and viscoelastic silk hydrogels were conducted, followed by Tukey's multiple comparison post hoc test for multiple samples. For the short list of differentially expressed genes between elastic and viscoelastic silk hydrogels and upstream regulator analysis, the p-values were calculated by Fisher's exact test. Statistical significance was indicated by asterisks in each figure legend and assigned as follows: *($p \leq 0.05$) and **($p \leq 0.01$). All data were plotted as mean ± standard deviation (SD) and, unless otherwise stated, refer to a minimum of three independent biological repeats. The number of independent experiments (n) is noted in each figure legend.

2.4 Results

2.4.1 Fabrication and Characterization of Silk Hydrogels with Tuned Stress Relaxation.

Elastic silk hydrogels were formed using enzymatic cross-linking to yield dityrosine or isodityrosine linkages within the amorphous regions of the silk fibroin heavy chain (Figure 2.3A). The solution-gel transition was confirmed to be due to covalent cross-linking by analyzing the dityrosine and isodityrosine emission peak spectra by fluorescence spectrophotometry. Dityrosine cross-links were confirmed by a spectral shift from 310 nm to 410 nm. Linker concentration directly correlated with increased fluorescence intensity and thus cross-link density and ultimately mechanics (Figure 2.4A). Viscoelastic silk hydrogels

were manufactured using sonication energy to induce physical cross-linking, coordinated by hydrogen bond formation between the crystalline regions of the silk fibroin heavy chain (Figure 2.3A). This change in secondary structure resulted in a conformational transition from random coil to an anti-parallel β-sheet structure (detailed below). Macroscopic examination of both silk hydrogel types indicated that both could be easily manipulated for cell culture while retaining their overall integrity. Elastic silk hydrogels were transparent to visible light, whereas viscoelastic silk hydrogels were opaque because of the abundant β-sheets (detailed below) that caused light scattering. The hydrogels were qualitatively assessed by SEM. Both hydrogel types showed a smooth surface and a similar pore structure (Figure 2.3A).

The secondary structure of the silk hydrogels was characterized by FTIR. The amide I region (1595–1705 cm^{-1}) was identified and deconvoluted. Hydrogel samples were compared to untreated and 70% (v/v) ethanol-treated silk films that served as controls for low (38.78±0.64%) and high (49.27±0.24%) crystallinity, respectively. Spectra of viscoelastic silk hydrogels showed a high β-sheet content (47.05±0.14%) and significantly fewer α-helix and random coil structures when compared to the untreated, water-soluble, amorphous silk films. By contrast, the elastic hydrogels had a comparatively small amount of β-sheet structures (21.90%) and side chains (6.44%), but higher percentages of α-helix (8.08%), random coil (38.12%), and turn (25.43%) structures. Importantly, attempts to change the secondary structure of the elastic hydrogels (i.e., by treatment with 70% [v/v] ethanol) only slightly increased the β-sheet content but substantially enhanced the percentage of random coil structures when compared to untreated elastic hydrogels (Figure 2.4B).

Hydrogel assembly was tuned to generate hydrogels that had an identical silk fibroin content and an identical initial elastic modulus (G') but a different loss modulus (G"), thereby resulting in hydrogels with more elastic or more viscoelastic behaviors. This fine-tuning included titration of the enzymatic cross-linker concentration (2.25 to 6.75 unit/mg) to generate elastic hydrogels that had an initial modulus of 1 kPa (Figure 2.5B). Under higher strain levels, the storage modulus (G') of the viscoelastic hydrogels showed a sharp decline, while only a very slight drop was observed with the elastic hydrogels. The loss modulus of elastic hydrogels (G") was very low compared to that of the viscoelastic hydrogels because of their stable covalently crosslinking network, indicating that the formed hydrogels were predominately elastic (Figure 2.3D and Figure 2.5A). Stress relaxation tests were performed to quantify the viscoelastic properties. The physically crosslinking silk fibroin displayed fast stress relaxation ($\tau_{1/2}$ = ~250 seconds), whereas covalently crosslinking hydrogels exhibiting a steady response with no stress relaxation over time, as expected for elasticity performance. Overall, these mechanical characteristics justified the

selected nomenclature of the respective silk hydrogel. The impact of time and cells on hydrogel mechanics was also characterized. The changes in the mechanical properties and dry masses of these hydrogels were not significant over a timescale of at least 14 days (Figure 2.3B and 2.3C). In the absence of cells, the elastic moduli for both hydrogel types remained statistically the same over 14 days. In the presence of cells, the elastic hydrogels were always stiffer than the control hydrogels (e.g., 0.98 kPA vs 1.12 kPA at day 14). By contrast, the viscoelastic hydrogels became progressively softer, showing a significant drop from 1.24 to 1.05 kPA at day 14 (Figure 2.5C). Viscoelastic hydrogels with cells also showed progressively faster stress relaxation in culture, with a 25% reduction at day 14 compared to that at day 1 (Figure 2.3D and 2.3E).

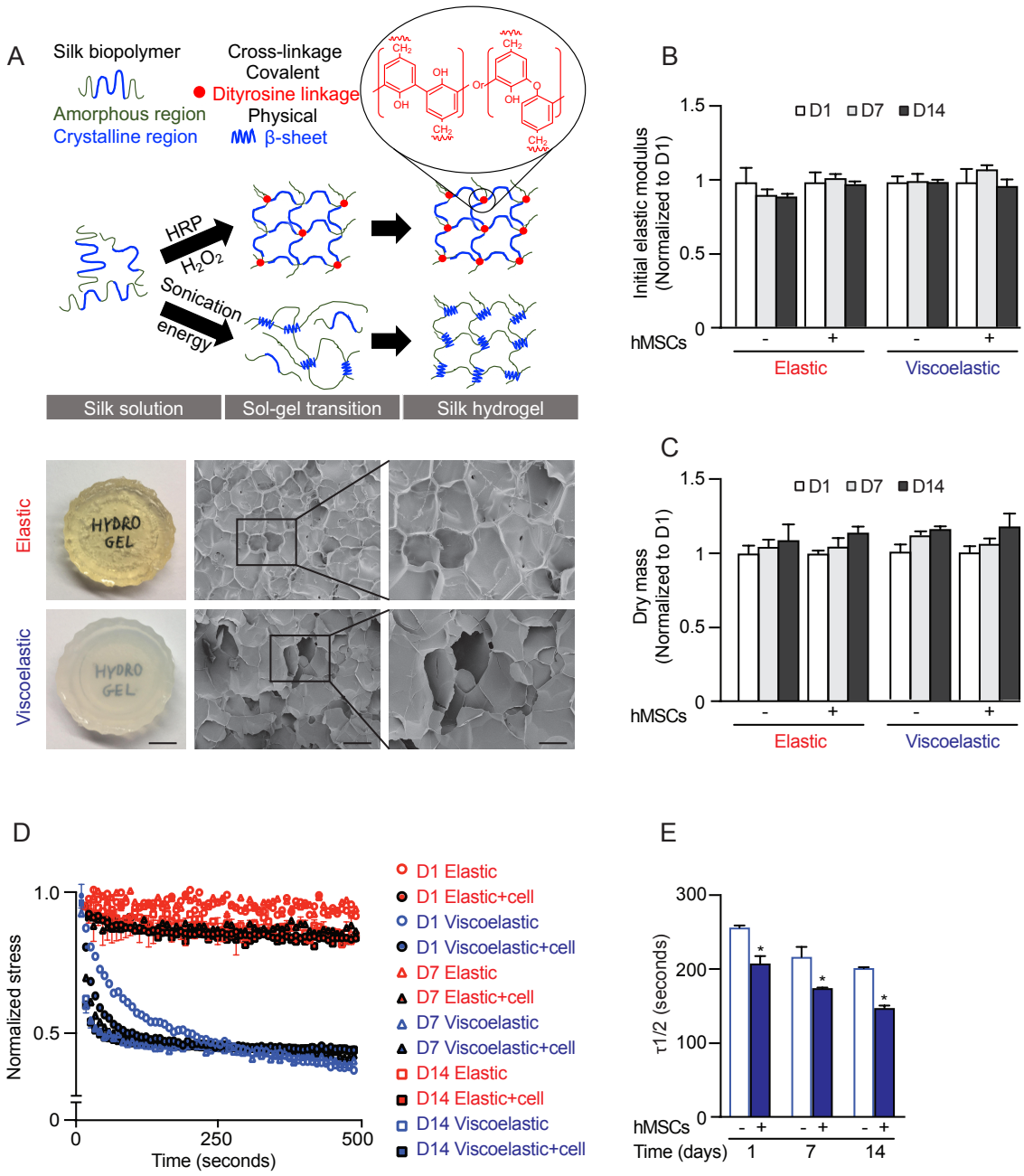

Figure 2.3 Silk hydrogels used for cell culture studies.

(A) Schematic depiction of elastic and viscoelastic silk hydrogel preparation and corresponding macroscopic (scale bar 0.5 cm) and scanning electron microscopic images (scale bar, 200 μm; zoom, 100 μm) of silk hydrogels. (B) Initial elastic modulus (~1 kPa) and (C) dry mass after 7 and 14 days in the presence and absence of cells, normalized to the value of day 1. (D, E) Stress relaxation under a compressional strain of 15% of the hydrogels in the presence and absence of cells for up to 14 days. Data

are presented as mean ± SD, n = 5 independent experiments. Error bars are hidden in the plot symbols when not visible. For *p ≤ 0.05, a comparison of silk hydrogel with and without cell culture at the respective time point.

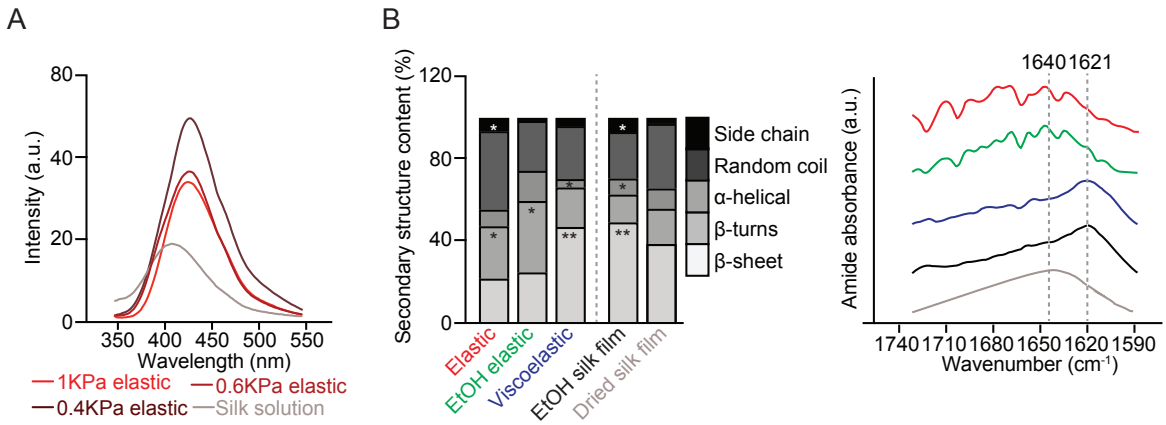

Figure 2.4 Structural analyses of elastic and viscoelastic silk hydrogels.

(A) Monitoring the dityrosine bond peak at 425 nm of elastic silk hydrogels of various stiffnesses (0.4-1 KPa). (B) Secondary structure contents of silk hydrogels. The amide I region was converted from FTIR spectra. Lines indicate the β- sheet peak (1621 cm-1) and α-helix peak (1640 cm-1). Statistical significances were assigned as *(p≤0.05) and **(p≤0.01) for secondary structure analyses between hydrogel samples and dried silk film (i.e. low β- sheet content). The ethanol treated silk film served as a positive control (i.e. high β-sheet content). n=3 independent experiments.

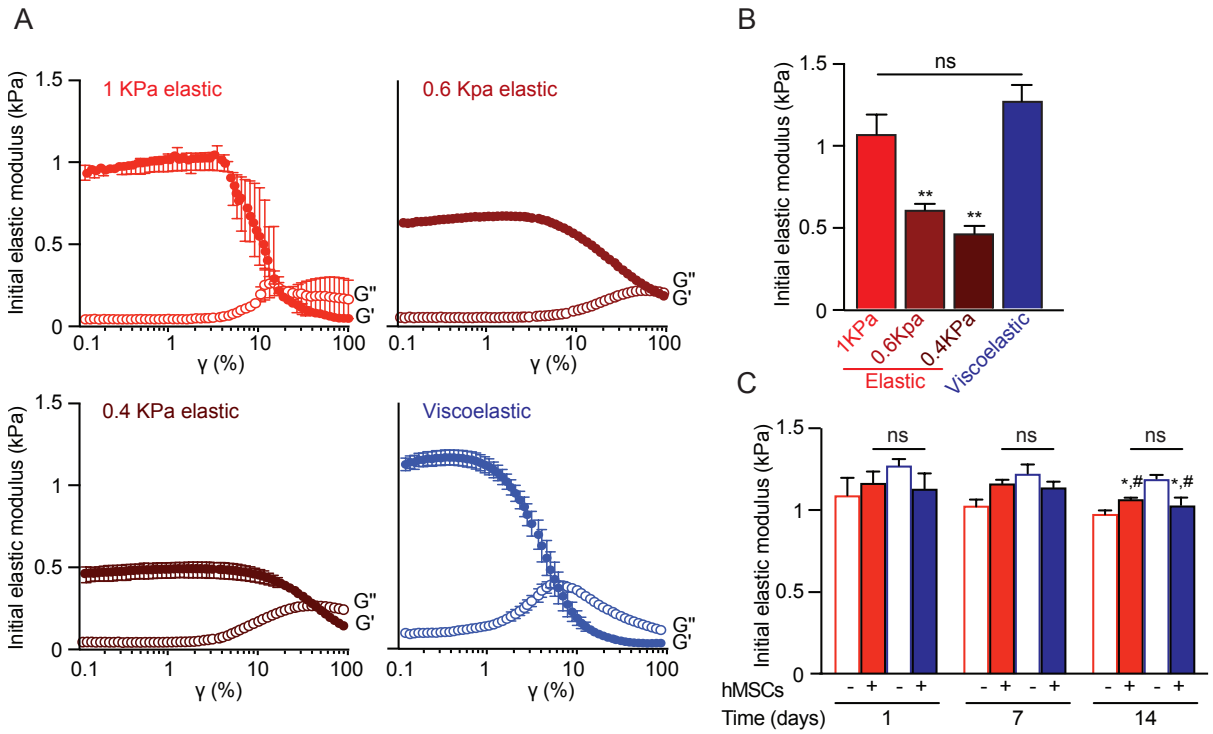

Figure 2.5 Rheological properties of elastic and viscoelastic silk hydrogels.

(A) Strain sweep, storage modulus (G') and loss modulus (G'') curves. Error bars are hidden in the plot symbols when not visible. (B) Initial elastic modulus of elastic and viscoelastic silk hydrogels. Elastic silk hydrogel samples with an elastic modulus of 1.0 kPa, 0.6 kPa and 0.4 kPa were generated using 2.25, 4.5 and 6.75 U/mg horseradish peroxidase, respectively (see the formulations in Table 2.2). Data are presented as mean ± SD, n=4 independent experiments. **($p \leq 0.01$) comparison among 3 different formulations of elastic silk hydrogels. (C) Initial elastic modulus (~1 kPa) of the hydrogels in the presence and absence of hMSCs for 14 days. Data are presented as mean ± SD, n=5 independent experiments. "ns" indicates no significance. For *($p \leq 0.05$) comparison of silk hydrogels at the same condition either day 7 or day 14 with day 1; # ($p \leq 0.05$) comparison of silk hydrogel with and without cell culture at the respective time point.

Table 2.2 Various HRP concentrations used for elastic silk hydrogels in total volume of 1 ml of 4% [w/v] silk solution

Conditions	HRP (µl)	H_2O_2 (µl)	Unit of HRP/mg of silk fibroin
0.4KPa elastic	450	450	6.75
0.6KPa elastic	300	300	4.5
1KPa elastic	150	150	2.25

2.4.2 Response of MSC Spreading and Proliferation by Substrate Mechanics.

The MSC response to substrate mechanics was monitored for up to 14 days. The DNA content was used to quantify cell proliferation. During the first 7 days, the MSCs showed a similar proliferation curve to the proliferation seen on plasma-treated tissue culture polystyrene, but the proliferation then stagnated, whereas the control cells continued to proliferate. The MSCs cultured on elastic and viscoelastic silk hydrogels showed different growth profiles, as the MSCs cultured on viscoelastic silk hydrogels had the slowest growth kinetics but eventually caught up with the cells on elastic hydrogels at day 14 (Figure 2.6A). Mitochondrial activity was also assessed in the MSCs, and the profiles closely mirrored the DNA content (Figure 2.6B). Semiquantitative assessment of cell proliferation showed similar confluency across all substrates during the first 3 days (Figure 2.6C). At day 14, the MSCs on both silk hydrogel substrates showed 80% confluency, whereas control cultures were 100% confluent (Figure 2.6C). The substrate stress relaxation had similar effects on cell spreading and cell proliferation, and a comparison of these data sets revealed no significant correlations among the tested. At day 3, cell spread vs cell proliferation on elastic hydrogels, R^2=0.6850, p=0.3749; cell spread vs cell proliferation on viscoelastic hydrogels, R^2=0.1625, p=0.7359).

On viscoelastic hydrogels, the MSCs at day 3 had assumed a more stretched and elongated morphology when compared to MSCs on elastic silk hydrogels. MSCs cultured on viscoelastic hydrogels showed signs of membrane protrusion, with intense local actin polymerization. These features were absent in MSCs cultured on elastic hydrogels or on the tissue culture plastic control substrate (Figure 2.6D). For both elastic and control substrates, the cells adopted a more cuboidal morphology. Quantification of the cell area, aspect ratio, roundness, and circularity revealed that the MSCs cultured on viscoelastic hydrogels had significantly greater cell areas and aspect ratios and concordantly lower roundness and circularity when compared to cells growing on elastic hydrogels (Figure 2.6E).

The influence of the ligand density on cell attachment and cell spreading of hMSCs was established by quantifying FN adsorption onto the surface of both hydrogel types. The surface density of the adsorbed FN increased with the solution concentration. The FN adsorption was significantly higher on the surface of the viscoelastic hydrogels than on the elastic hydrogels at 6 h for the low FN concentration (10 ng/ml) and at 1 h for the high FN concentration (100 ng/ml) (Figure 2.7). At 24 h, the FN adsorption on the surfaces of both hydrogel types was comparable, with no statistically significant differences.

The possibility that stress relaxation of the hydrogel substrates could alter downstream behaviors of hMSCs was assessed through evaluation of the Yes-associated protein/transcriptional co-activator (YAP/TAZ) mechanosensitive signalling pathways by determining the nuclear translocation of YAP.[131] The translocation of YAP from the cytoplasm into the nucleus became more apparent in hMSCs cultured on viscoelastic hydrogels than on elastic silk hydrogels (0.5-fold increase in the ratio of nuclear to cytoplasmic YAP/TAZ) (Figure 2.6F and 2.6G).

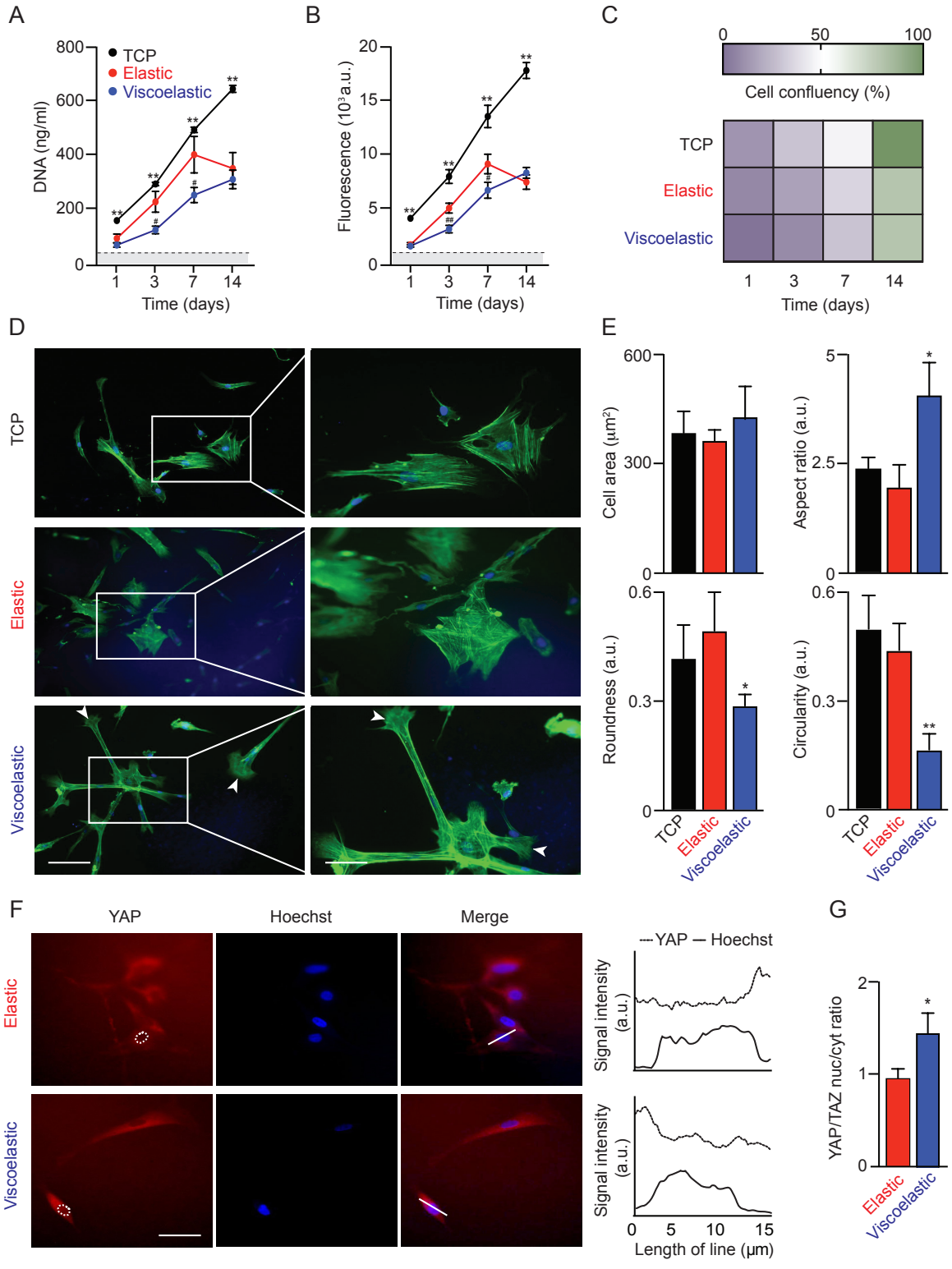
A
B
C
D
E
F
G
TCP
Elastic
Viscoelastic
DNA (ng/ml)
Time (days)
Fluorescence (10³ a.u.)
Cell confluency (%)
Cell area (μm²)
Aspect ratio (a.u.)
Roundness (a.u.)
Circularity (a.u.)
YAP
Hoechst
Merge
YAP — Hoechst
Signal intensity (a.u.)
Length of line (μm)
YAP/TAZ nuc/cyt ratio

Figure 2.6 Impact of substrate mechanics on MSC proliferation and morphology.

(A) MSC proliferation, (B) metabolic activity, and (C) confluency at day 14. Data were analyzed from four MSC donors and presented as mean ± SD, n = 4 independent experiments. Error bars are hidden in the plot symbols when not visible; *p ≤ 0.05 and **p ≤ 0.01 comparison of silk hydrogels with tissue culture plastic (TCP) control. For #p ≤ 0.05 and ##p ≤ 0.01 comparison of elastic and viscoelastic silk hydrogel cultures at the respective time point. (D) Representative images of cytoskeletal F- actin staining and (E) quantification of morphological characteristics of MSCs (92 cells in n = 21 images from three pooled experiments). For *p ≤ 0.05 and **p ≤ 0.01 comparison of silk hydrogels with control cultures. Scale bar 20 µm. (F) Representative images of YAP staining and (G) quantification of the nuclear-to-cytoplasmic ratio of YAP (50 MSCs in n = 18 images from three pooled experiments). For *p ≤ 0.05 comparison of elastic and viscoelastic silk hydrogel cultures. Scale bar, 20 µm. Dashed white lines represent nuclear outlines. The 15 µm line in the merged images were used for the profile plots to highlight nuclear localized YAP/TAZ.

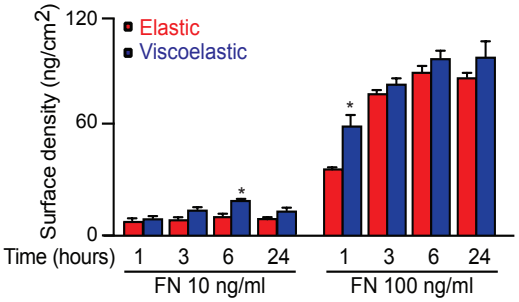

Figure 2.7 Protein adsorption on silk hydrogels.

Surface density of FN on the hydrogels exposed to 10 and 100 ng/ml of FN. For *(p≤0.05) comparison of elastic and viscoelastic silk hydrogels at the respective FN concentration and time point.

2.4.3 Gene and Protein Expression in Response to Mechanics.

The impact of culture substrates on MSC mRNA expression was assessed using pooled MSCs from four donors to minimize donor variability. The MSC response to elastic and viscoelastic hydrogels was characterized following 14 days of substrate priming (Figure 2.8A). The overall gene expression patterns for MSCs cultured on elastic hydrogels and viscoelastic hydrogels differed substantially, as the patterns for MSCs cultured on elastic hydrogels were clustered more closely to the patterns for the tissue culture controls than for the cells growing on viscoelastic hydrogels. Gene expression of *IL-1β, IL-6, LIF, BMP-*

6, BMP-7, and *protein tyrosine phosphatase receptor type C* were substantially higher in MSCs cultured on elastic hydrogels than on viscoelastic hydrogels, whereas this pattern was reversed for *insulin, HNF-1A, and SOX-2.* When compared to the tissue culture plastic controls, cells growing on both hydrogels showed an upregulation of *CSF3, IGF1,* and *Zinc finger protein 42 (ZFP42)* and downregulation of *bone gamma-carboxyglutamate protein (BGLAP), telomerase reverse transcriptase (TERT), and tumor necrosis factor (TNF)*. Across all three substrate types, the expression patterns of the cytoskeleton-related proteins *integrin β1, vimentin, RhoA, catenin beta1 (CTNNB1)* were similar or increased for silk culture substrates (Figure 2.8A and 2.9). By contrast, *integrin alphaX* was only expressed by hydrogel-cultured MSC and was absent in the tissue culture plastic control cultures.

The IPA software was used to generate interactive networks in response to the different substrates to better explain the biological relevance of the expressed genes. The overall trends were similar for both elastic and viscoelastic hydrogels. Nonetheless, some notable differences were observed in two pathways, and especially in the IL-1β canonical pathway (Figure 2.10). To obtain further insights, I clustered the differentially expressed genes and predicted the potential functional canonical pathway networks using IPA core analysis. The top five canonical pathways enriched in the differentially expressed genes included cellular development, cell-to-cell signaling and interaction, and cell death and cell survival, and also connective tissue and nervous system development and function (Table 2.2). Subsequently, the most consistent network-related gene expression in MSCs cultured on elastic hydrogels involved glucose metabolism disorders and inflammatory responses (consistency score +2.83 and +1.789, respectively), thereby predicting the regulation of these functions by an activation of *CRYAB, NR1H2,* and *PIM1* and by an inhibition of *IRF1* and *NR1/2*. By contrast, culture on viscoelastic hydrogels was associated with homing, fatty acid metabolism, and chemotaxis (consistency score +3.50, +3.32, and +3.21, respectively), mainly mediated through MAPKs and CHUK (Table 2.3 and 2.4).

The expression of selected target genes was also verified individually across the four hMSC donors (Figure 2.9). These results showed similarities across all the donors, as well as with the data sets generated from gene array analyses. For example, for all the donors the expression of *IL-1β, IL-6, integrin alphaV,* and *LIF* was significantly higher with elastic hydrogels than those with viscoelastic hydrogels, whereas *VCAM1* expression was significantly greater with viscoelastic hydrogels than with elastic hydrogels (Figure 2.9). The cytoskeleton-related genes, such as *integrin β1* and *RhoA*, showed no significant differences between the two hydrogel types. *Integrin alphaV* was upregulated with both hydrogels

compared to that with plasma-treated tissue culture plastic. Expression of *MMP2* was unchanged for either hydrogel substrate compared to that for plasma-treated tissue culture plastic.

The expression data sets were complemented with protein secretion profiles of the MSCs. Of the 108 analyzed proteins, 35 showed differential expression profiles in response to stress relaxation (Figure 2.8B and 2.11). The proteomic profiles of cells cultured on elastic and viscoelastic hydrogels shared some common proteins that were secreted at high levels from the MSCs (e.g., FGF basic, IL-6, IL-8, HGF, IGFBP-2, EGF, Endoglin, and VEGF). By contrast, elastic hydrogels induced the production of the cytokines angiopoietin-1, BDNF, LIF, FGF basic, IL-6, GDF-15, ENA-78, GRO alpha, complement factor D, IL-18 Bpa, and cystatin C. Growth on the viscoelastic hydrogels induced protein expression of apolipoprotein, MIF, thrombospondin, osteopontin, VEGF, IL-8, PDGF AB/BB, IGFBP-2, and VCAM-1. Moderately elevated signals for Dkk-1, DPP IV, lipocalin-2, PF4, adiponectin, and FGF-19 were found in cells growing on viscoelastic hydrogels compared to cells growing on elastic ones. Notably, a strong increase was observed in both gene expression and protein levels for the pro-inflammatory cytokines IL-1β, and LIF in the MSCs cultured on elastic hydrogels.

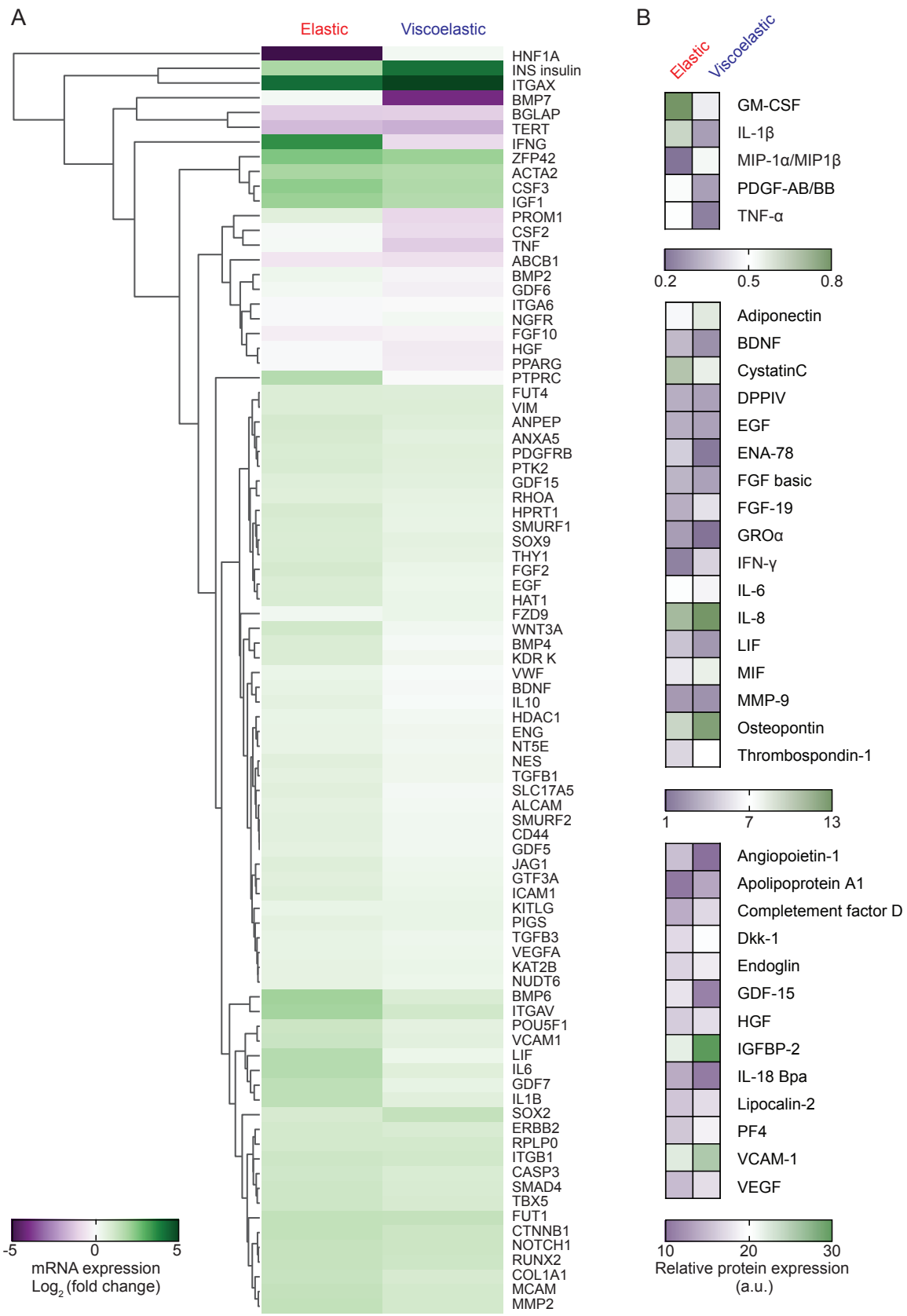
A
Elastic
Viscoelastic
HNF1A
INS insulin
ITGAX
BMP7
BGLAP
TERT
IFNG
ZFP42
ACTA2
CSF3
IGF1
PROM1
CSF2
TNF
ABCB1
BMP2
GDF6
ITGA6
NGFR
FGF10
HGF
PPARG
PTPRC
FUT4
VIM
ANPEP
ANXA5
PDGFRB
PTK2
GDF15
RHOA
HPRT1
SMURF1
SOX9
THY1
FGF2
EGF
HAT1
FZD9
WNT3A
BMP4
KDR K
VWF
BDNF
IL10
HDAC1
ENG
NT5E
NES
TGFB1
SLC17A5
ALCAM
SMURF2
CD44
GDF5
JAG1
GTF3A
ICAM1
KITLG
PIGS
TGFB3
VEGFA
KAT2B
NUDT6
BMP6
ITGAV
POU5F1
VCAM1
LIF
IL6
GDF7
IL1B
SOX2
ERBB2
RPLP0
ITGB1
CASP3
SMAD4
TBX5
FUT1
CTNNB1
NOTCH1
RUNX2
COL1A1
MCAM
MMP2
-5
0
5
mRNA expression
Log2 (fold change)
B
Elastic
Viscoelastic
GM-CSF
IL-1β
MIP-1α/MIP1β
PDGF-AB/BB
TNF-α
0.2
0.5
0.8
Adiponectin
BDNF
CystatinC
DPPIV
EGF
ENA-78
FGF basic
FGF-19
GROα
IFN-γ
IL-6
IL-8
LIF
MIF
MMP-9
Osteopontin
Thrombospondin-1
1
7
13
Angiopoietin-1
Apolipoprotein A1
Completement factor D
Dkk-1
Endoglin
GDF-15
HGF
IGFBP-2
IL-18 Bpa
Lipocalin-2
PF4
VCAM-1
VEGF
10
20
30
Relative protein expression
(a.u.)

Figure 2.8 Impact of substrate mechanics on MSCgene and secretome expression.

(A) Hierarchical cluster analysis of gene expression of MSCs cultured on silk hydrogels for 14 days using pooled RNA isolation from four MSC donors. Differential gene expression was calculated and shown as log2 fold change. (B) Expression pattern of secreted proteins over 14 days. A conditioned culture medium was pooled from four MSC donors prior to analysis.

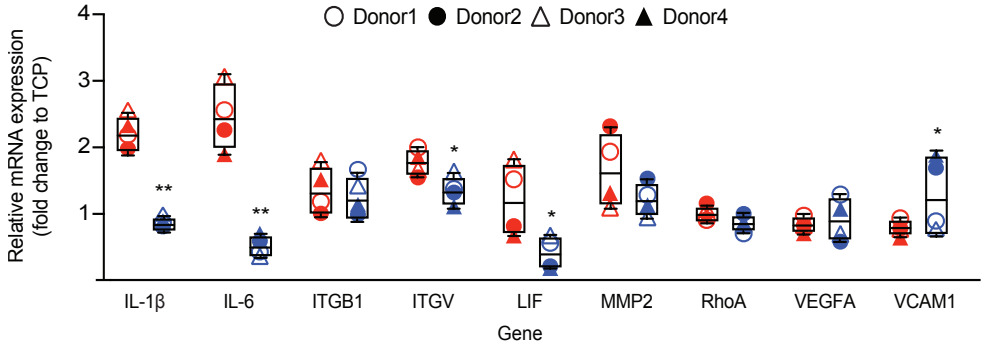

Figure 2.9 Differential gene expression of hMSCs cultured on mechanically tuned silk hydrogels.

Gene expression patterns were determined using RNA extracted from 4 individual healthy donor hMSCs and visualized by a Tukey boxplot. For *($p \leq 0.05$) and **($p \leq 0.01$) comparison of elastic (red) and viscoelastic (blue) silk hydrogels.

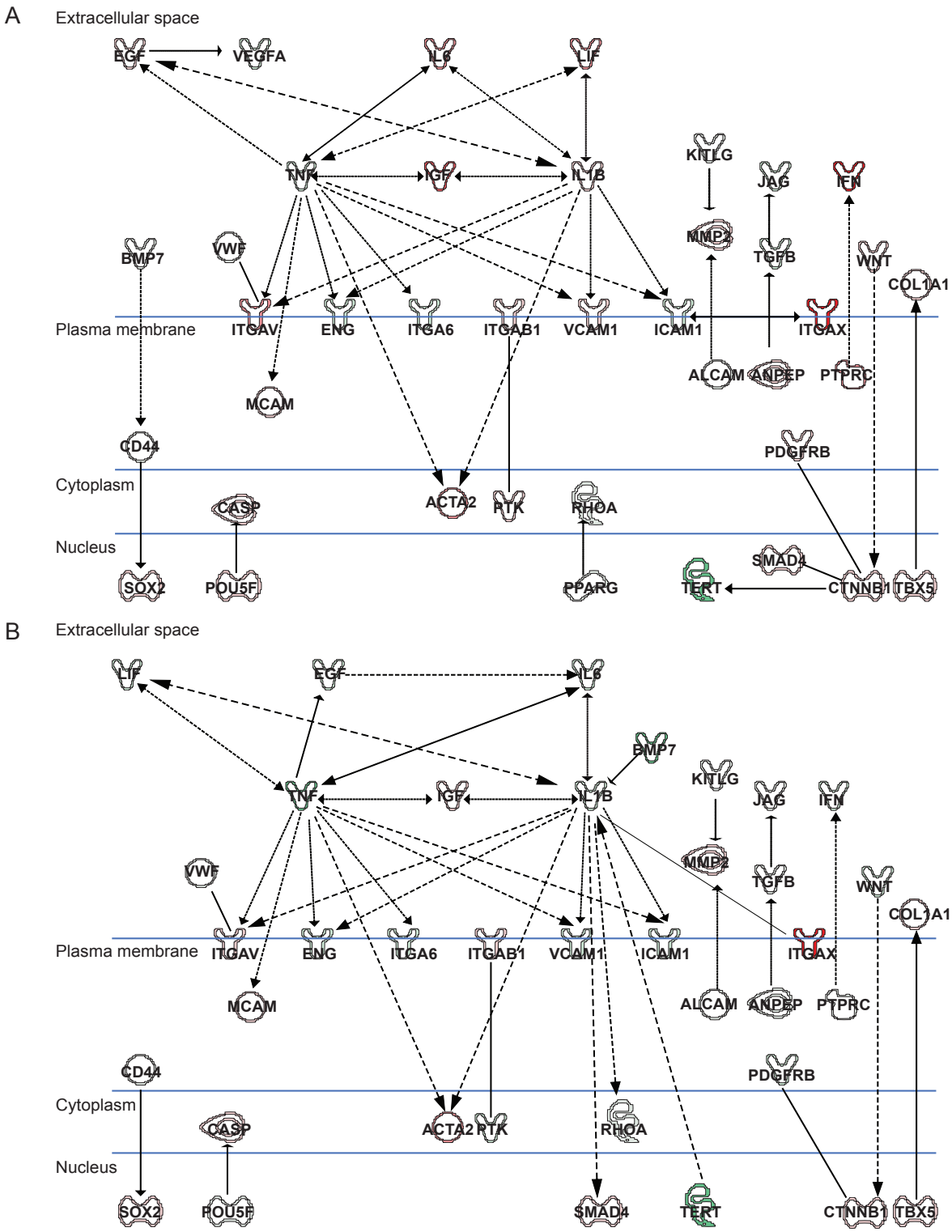
A
Extracellular space
EGF
VEGFA
IL6
LIF
TNF
IGF
IL1B
KITLG
JAG
IFN
MMP2
TGFB
WNT
COL1A1
BMP7
VWF
Plasma membrane
ITGAV
ENG
ITGA6
ITGAB1
VCAM1
ICAM1
ITGAX
ALCAM
ANPEP
PTPRC
MCAM
CD44
PDGFRB
Cytoplasm
CASP
ACTA2
PTK
RHOA
Nucleus
SMAD4
SOX2
POU5F
PPARG
TERT
CTNNB1
TBX5
B
Extracellular space
LIF
EGF
IL6
BMP7
TNF
IGF
IL1B
KITLG
JAG
IFN
MMP2
TGFB
WNT
COL1A1
VWF
Plasma membrane
ITGAV
ENG
ITGA6
ITGAB1
VCAM1
ICAM1
ITGAX
ALCAM
ANPEP
PTPRC
MCAM
CD44
PDGFRB
Cytoplasm
CASP
ACTA2
PTK
RHOA
Nucleus
SOX2
POU5F
SMAD4
TERT
CTNNB1
TBX5
Legend
Cytokine/Growth factor
Enzyme
Kinase
Ligand-dependent nuclear receptor
Peptidase
Phosphatase
Transcription regulator
Transmembrane receptor
Other
Relationship
Relationship

Figure 2.10 Pathway analysis of MSC exposed to elastic and viscoelastic silk hydrogels.

Tissue culture treated polystyrene culture controls were mapped against (A) elastic silk hydrogels and (B) viscoelastic silk hydrogels. The green color denotes a decrease in expression in cell culture on hydrogels relative to control and the red color denotes the respective increase.

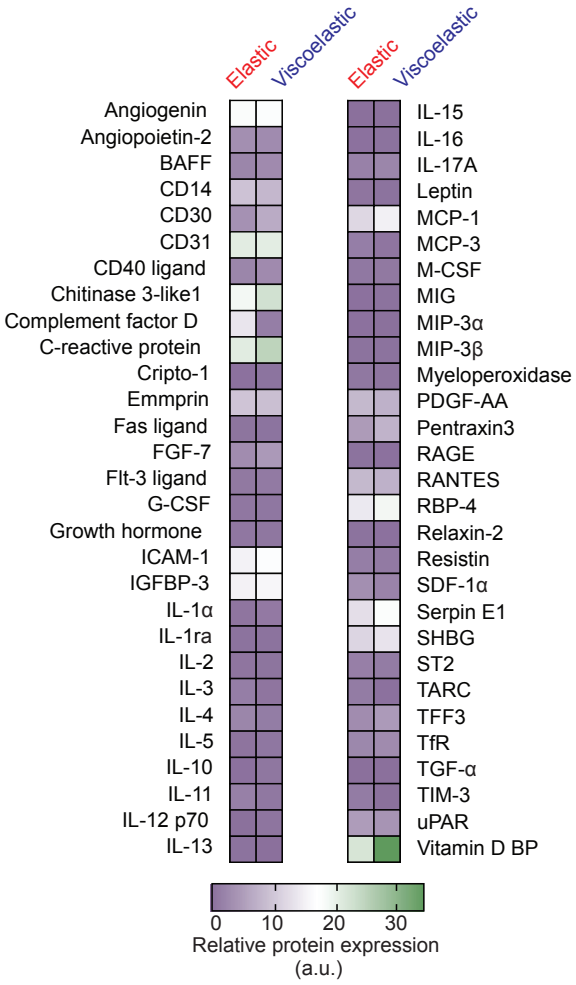

Figure 2.11 Impact of stress relaxation on MSC secretome.

Secreted proteins with similar expression patterns. MSCs were grown on elastic and viscoelastic silk hydrogels for 14 days. The complementary data sets are in Figure 2.3. Conditioned culture medium was pooled from 4 MSC donors.

2.4.4 MSCs Exometabolome Changes in Response to Mechanics.

The metabolic response to the culture substrate was monitored by analyzing conditioned cell culture medium (Figure 2.12). The data were shown as fold changes compared to the respective acellular media under the same incubation conditions, at day 7 and 14 for all four MSC donors. Control cells consistently consumed glucose, pyruvate, glutamine, and aspartate, while secreting lactate, formate, and glutamate at day 7, together with citrate and acetate at day 14. Cells growing on silk hydrogels showed most of these variations, although with different magnitudes. At both time points (but especially at day 7), the silk-cultured cells displayed lower metabolic activity than the control cells, as evidenced by the smaller fold changes in metabolite levels compared to those of acellular media. Only aspartate was consumed more appreciably by the silk-cultured cells. The levels of glycine were also higher in the medium of the silk-grown cells than those in the control medium. A comparison of the metabolites that MSC grown on the two hydrogels revealed a higher consumption of glucose and glutamine, together with a higher secretion of lactate, by cells growing on the elastic substrate than those on the viscoelastic substrate.

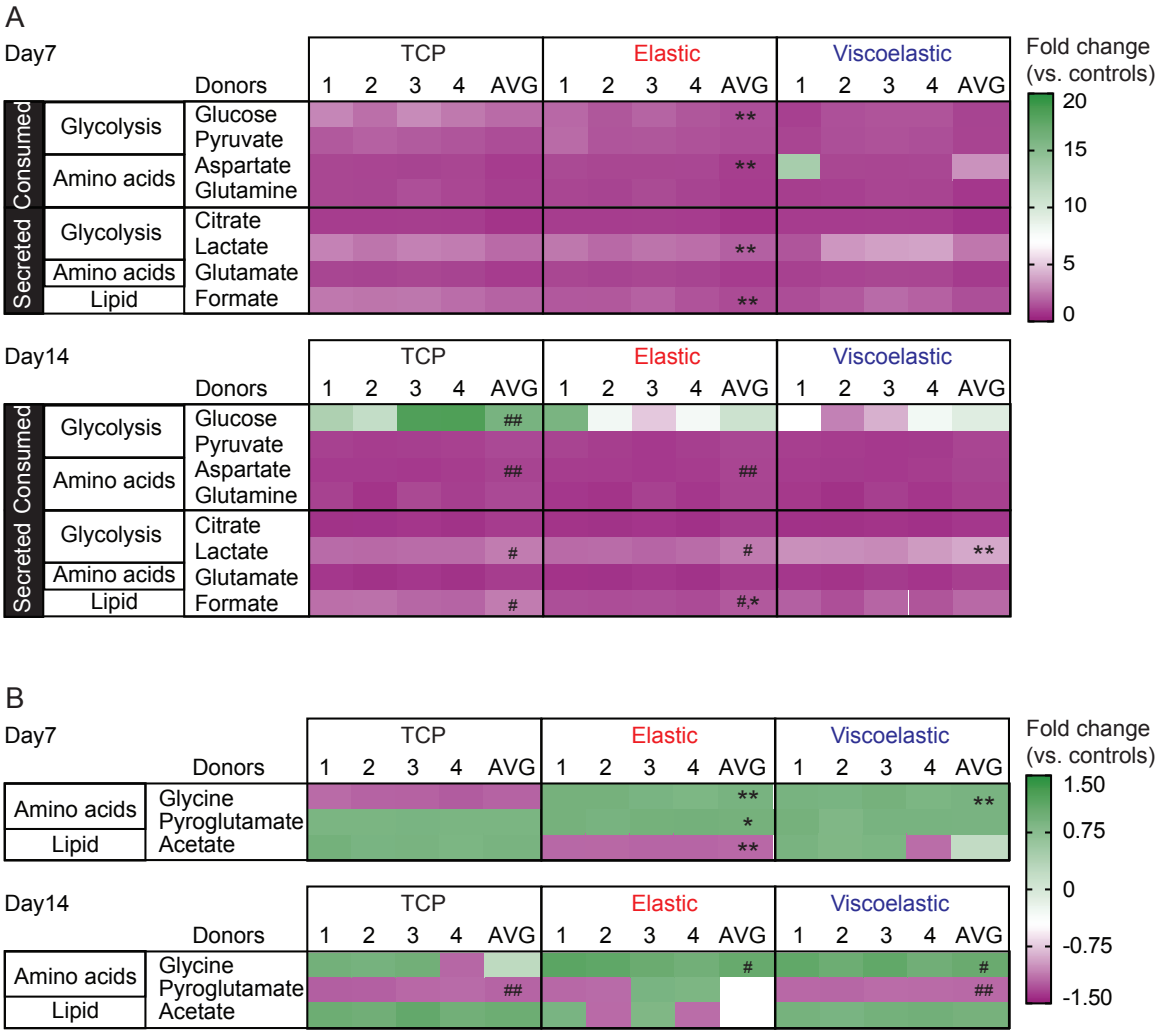

Figure 2.12 Impact of substrate mechanics on MSC metabolism.

Exometabolites of silk hydrogel MSC cultures at 7 and 14 days. The criterion for including a metabolite in the heatmap was (A) absolute fold change ≥1.05 grouped as distinct consumed or secreted metabolites, and (B) absolute fold change ≤ 1.05 represented as negative values for consumptions and positive values for secretions. Color codings are expressed as relative fold changes to matched acellular medium samples (negative values for consumptions; positive values for secretions). Control cultures used tissue culture plastic (TCP) as the culture substrates. For all treatment groups, a conditioned culture medium was collected from four MSC donors (denoted 1−4) and analyzed individually and combined (AVG: average). For statistical analyses #p ≤ 0.05 and ##p ≤ 0.01 impact of time for the respective culture substrate, whereas *p ≤ 0.05 and **p ≤ 0.01 denotes a comparison between the substrates and control at the respective time point.

Table 2.3 Top regulator effect networks responsible for cell cultured on elastic and viscoelastic silk hydrogels

Rank	Main molecules in network	Score	Focus molecule	Top functional networks
1	BGLAP, BMP2, BMP4, BMP6, BMP7, ENG, FUT4, GDF15, GDF7, Integrin alpha/beta1, RUNX2, SMAD4, Smooth muscle actin, SOX9, TGFBR	22	12	Cellular development, embryonic development, organismal development
2	CD44, CSF2, CSF3, FGF10, HGF, ICAM1, Interferon alpha, ITGB1, NOTCH1, PTK2, PTPRC, RPLP0, TNF, VCAM1	22	12	Cell-to-cell signaling and interaction, hematological system development and function, inflammatory response
3	CASP3, CTNNB1, ERBB2, FZD9, HDAC1, HNF1A, Insulin, POU5F1, RHOA, SMURF1, SOX2	22	12	Cancer, cellular development, organismal injury and abnormalities
4	ACTA2, ADCY, ADRB, COL1A1, EGF, FGF2, GDF5, GTF3A, IGF1, MMP2, NT5E, NUDT6, PTPase, SMURF2, VEGF	20	11	Connective tissue development and function, organismal injury and abnormalities, tissue morphology
5	ANXA5, BDNF, HPRT1, IL1B, LIF, NGFR, PDGFR, PDGFRB, VEGFA, WNT3A, ZFP42	18	10	Cardiovascular disease, cell death and survival, nervous system development and function

Table 2.4 Top regulator effect networks responsible for cell cultured on elastic silk hydrogels

Rank	Regulators	Disease & functions	Consistency score
1	CRYAB, NR1H2	Failure of heart, glucose metabolism disorder	2.828
2	Esrra, MMP9	Failure of heart	2.449
3	PIM1	Inflammatory response	1.789
4	IRF1	Glucose metabolism disorder	-3.536
5	NR 1/2	Inflammatory response	-4.158

Table 2.5 Top regulator effect networks responsible for cell cultured on viscoelastic silk hydrogels

Rank	Regulators	Disease & functions	Consistency score
1	p38 MAPK	Homing cells	3.5
2	ERK1/2	Fatty acid metabolism	3.317
3	ERK1/2	Chemotaxis	3.207
4	CHUK	Chemotaxis	3.175
5	poly rl:rC-RNA	Attachment of cells	3.015

2.5 Discussion

Model systems have contributed to our understanding of MSCs and culture materials and have provided a blueprint for the material design space. However, translating these findings requires materials that are suitable for use in humans. Silk fibroin is a clinically approved biopolymer, and a first-generation regenerated silk fibroin hydrogel product was approved in 2019 for use in humans. This milestone now catalyzes new bench-to-bedside translational opportunities. I have selected silk fibroin with different crosslinking modes to assess how hydrogel stress relaxation can prime MSC behavior in two dimensions. I have explored the MSC biological responses toward elastic and viscoelastic silk hydrogels in studies with human MSCs from four healthy donors to minimize potential donor variability.

The solid content is known to directly influence the mechanical properties of silk hydrogels.[25],[65],[97] Hydrogels with a greater mechanical strength are obtained with a higher silk content. To facilitate handling and a robust solution-gel transition, I used 4% [w/v] silk fibroin. The resulting secondary structure of silk hydrogels was similar to previously reported structures.[65],[97] For elastic hydrogels, the cross-linker concentration was fine-tuned to yield an initial elastic modulus of 1 kPa (Figure 2.5B) (Table 2.5), whereas matched viscoelastic hydrogels were assembled using physical cross-linking. The selected initial elastic modulus of 1 kPa is physiologically relevant[111] and is implicated in MSC self-renewal and reduced replicative senescence.[132] Recent work with nondegradable alginate hydrogels showed decoupling of irreversible creep from stress relaxation and modulus, thereby demonstrating that network plasticity drove cell spreading.[133] Cell spreading impacts cell behavior, whereas mechanical remodeling of the extracellular matrix, including matrix degradation, often occurs in health and disease, ultimately impacting cell biology. Although the silk biopolymers of the hydrogels are biodegradable, no signs of substrate degradation were evident during cell culture in our study. Importantly, the expression of the silk proteolytic enzyme MMP2 was unchanged for either hydrogel substrate compared to that of plasma-treated tissue culture plastic, suggesting that silk hydrogel mechanics, rather than hydrogel degradation, were responsible for the observed biological differences.

Both silk hydrogel types supported MSC proliferation, although elastic hydrogels supported greater cell proliferation (but still outpaced by polystyrene controls). Previous studies have shown that elastic silk hydrogels with a comparable stiffness and silk content could support human MSC attachment and proliferation and were able to compete with tissue culture plastic controls.[97] The underlying reasons for these subtle but distinct differences between our work and previous reports is not clear. However, cell heterogeneity and culture conditions can impact performance. For example, human corneal epithelial cells

cultured on chemical versus physically cross-linked silk hydrogels showed better growth on chemically cross-linked hydrogels, although the presence of serum in the culture medium abolished these effects.[134] By contrast, stress relaxation of alginate hydrogels increased mouse myoblast proliferation when compared to that of elastic controls.[49] MSC adhesion to silk is likely mediated both by factors present in the serum (e.g., fibronectin) and by factors secreted from the MSCs themselves (i.e., collagen type I) that adsorb to the silk substrate. I observed similar amounts of fibronectin adsorption to elastic and viscoelastic silk hydrogels, suggesting that the secondary structure and microstructure of silk hydrogels had no significant effect on the protein-surface adsorption.

Increasing the stiffness of purely elastic substrates contributes to cell spreading, cytoskeleton organization, and focal adhesion.[111] Stiffer substrates promote cell spreading by maintaining tensional homeostasis. For example, soft silk hydrogels (16 kPa) promoted less cell spreading than did stiffer ones (64 kPa).[25] However, I observed striking differences in morphology for cells grown on viscoelastic versus elastic silk hydrogels, independent of the elastic modulus. Previous work using alginate hydrogels proposed that hydrogels with fast stress relaxation reduced mechanical confinement and enhanced ligand clustering, leading to greater cell spreading.[46] Similar observations have been reported for other model substrates. For example, MSC spreading increased with greater loss modulus by increasing Rac1 and N-cadherin expression that, in turn, increased motility and lamellipodial protrusion.[50, 135] I observed no difference in vimentin expression, so I therefore speculate that stiffness, rather than viscoelasticity, is important for regulating vimentin expression. This speculation is supported by the observation that MSCs cultured on stiff gelatin hydrogels showed increased vimentin and decreased tropomyosin cytoskeleton protein expression when compared to soft hydrogels.[47]

Growth of MSCs on elastic hydrogels induced IL-1β signaling with the highest IPA network score. I observed increased IL-1β gene and protein expression in MSCs grown on elastic silk hydrogels. Previous work has linked IL-1β signaling to cell volume regulation via adhesion-independent mechano-transduction, which ultimately impacts differentiation.[41] Viscoelastic alginate hydrogels supported chondrocyte development, while elastic ones restricted chondrocyte volume expansion via IL-1β signaling, which negatively regulated chondrocyte gene expression and cell survival.[41] Consequently, designing therapeutic silk biomaterials to either encourage (or suppress) IL-1β signaling could represent a new tissue engineering approach. For example, increases in IL-1β signaling could promote normal wound repair during the inflammatory phase of healing.[136]

IL-1β signaling also impacts other downstream signaling pathways (Figure 2.10). For example, integrin β1 receptors are responsible for cell-ECM binding through RGD ligand clustering that, in turn, activates YAP/TAZ, which is implicated in mechanobiology.[26],[46],[42] Cells sense substrate mechanics through actomyosin contractility through a mechanism often mediated through Rho[137] and Rac signaling[135] that can impacting linage commitment. For example, low levels of activated RhoA commit hMSCs to become adipocytes, while constitutive expression of activated RhoA protein promotes osteogenesis.[138] The study demonstrated an increased expression of integrin β1 and RhoA in MSCs cultured on both viscoelastic and elastic substrates compared to the controls. IPA downstream effector analysis revealed a direct involvement of PPAR gamma transcription factor with RhoA activation in MSCs grown on an elastic substrate but not on a viscoelastic one. Additionally, monitoring the nuclear localization of mechanically sensitive transcription regulators (e.g., YAP/TAZ) provided compelling evidence that fast-relaxing substrates enhanced downstream mechanosensitive signaling via the RhoA and/or YAP/TAZ signaling pathways, ultimately priming the MSCs.[131]

Substrate mechanics impacts both MSC gene and secretome expression[139] that are implicated in tissue repair. For example, MSCs cultured on stiff polyethylene glycol/HA/gelatin hydrogels showed upregulated VEGF, urokinase plasminogen activator, and IL-8 when compared to cells grown on soft hydrogels.[127] Physically cross-linked silk hydrogels with an elastic modulus of 10 kPa promoted brain injury repair via TGF β1 secretions[63],[64] and TGF β1 production has also been reported as important in bone tissue engineering.[57] I also observed a substantial TGF β1 increase in MSCs growing on both elastic and viscoelastic silk hydrogels, whereas BMP- 7 was differentially expressed in response to elastic versus viscoelastic silks. Therefore, mechanically tuned silk hydrogels are expected to further enhance bone regeneration beyond the current state of the art.[120]

I also observed other differentially expressed transcriptome and secretome profiles in response to substrate mechanics. For example, apolipoprotein A1, VEGF, and VCAM 1 were strongly expressed in MSCs growing on viscoelastic silk hydrogels, whereas growth/differentiation factor 15 (GDF15) was higher in MSCs growing on elastic silk hydrogels. The GDF15–stress response cytokine, which belongs to the TGF β1 superfamily, is strongly upregulated during tissue injury.[140] In agreement with the IPA core analyses, gene expression in MSCs cultured on elastic silk hydrogels was primarily involved in regulatory effects on inflammation, whereas growth on viscoelastic silk hydrogels affected the chemotaxis and fatty acid metabolism networks (Table 2.3 and 2.4).

Assessment of metabolic pathways is crucial for obtaining a better understanding of the cellular responses to substrate mechanics, especially in cells proposed for regenerative therapies.[141] Growth on silk hydrogels significantly changed the magnitude of consumption of glucose, pyruvate, and some amino acids (mainly glutamine and aspartate), along with the amounts of secreted metabolites (lactate, glutamate, formate, citrate, and acetate). MSCs exposed to silk hydrogels consumed less glucose and secreted less lactate compared to controls, suggesting a lower glycolytic flux. Similar reductions were observed for glutamine consumption and glutamate excretion, suggesting decreased glutaminolytic activity. However, consumption of pyruvate, the main fuel for the TCA cycle, was only substantially decreased in cells growing on viscoelastic hydrogels. Interestingly, aspartate consumption from the medium was higher in MSCs growing on silk hydrogels than in control cells. I speculate that this increased aspartate uptake replenished the TCA cycle via the aspartate arginosuccinate shunt used by cells like inflammatory macrophages.[142] Cells exposed to silk hydrogels for 14 days also showed a decreased secretion of citrate (a TCA cycle intermediate) and of acetate, a metabolite that may be produced from glycolytic pyruvate, especially under conditions of metabolic overflow.[143] These lower releases of citrate and acetate also hint at possible effects on lipid metabolism, a hypothesis to be verified in future studies. Finally, glycine levels increased only in the medium of cells exposed to silk hydrogels (14 days) and not in silk-containing acellular media, indicating that this variation was not attributable to passive glycine leakage. Instead, glycine excretion must have been triggered via cellular events (e.g., metabolism). This result is similar to observations made previously in macrophages exposed to silk nanoparticles.[144]

2.6 Conclusions

I have examined the impact of silk hydrogel stress relaxation on human MSC biology. Both elastic and viscoelastic silk hydrogels supported cell proliferation but impacted several aspects of cell biology, including morphology, metabolism, and gene and protein expression. Data sets subjected to pathway analysis highlighted that silk hydrogel mechanics primed MSC biology. For example, elastic cultures activated IL-1β signaling in response to hydrogel mechanics. An elastic substrate also induced higher consumption of glucose and glutamine, coupled with a higher secretion of lactate, than that observed in MSCs grown on viscoelastic substrate. However, both silk hydrogels significantly changed the magnitude of consumption of glucose, pyruvate, glutamine, and aspartate, and also metabolite secretion, resulting in an overall lower metabolic activity than that found in control cells. Overall, this study demonstrated that

silk hydrogel mechanics impacts MSC biology in two dimensions. Therefore, the fine-tuning of silk hydrogels has the potential to maximize MSC performance.

CHAPTER 3

IMPACT OF THE CHRONIC ISCHEMIC STROKE MICROENVIRONMENT ON SILK FIBROIN HYDROGEL BIODEGRADATION AND DE NOVO TISSUE FORMATION

Chapter summary:

For this Chapter I designed, analysed and carried out all experimental work and also wrote an accompanying manuscript draft. I received help from Dr Natalia Gorenkova to perform the experimental stoke and streotactic injections. Panicha Aruvornlop supported me in monitoring animals over the 12 month study period.

This chapter highlighted the use of engineered native-like ECM silk hydrogels as supportive matrix in an experimental stroke model. Sol-gel transition of silk was delivered into stroke lesion and long tern study on tissue regeneration was evidenced by histology. Engineered injectable silk hydrogels are thought to be a potentially implant material for neural tissue engineering.

3.1 Abstract

The brain has limited tissue regeneration capacity; therefore, tissue lost due to stroke is not spontaneously regenerated. In addition, the absence of extracellular matrix further impedes endogenous repair mechanisms. One emerging strategy to support endogenous brain tissue repair is to fill the stroke cavity with a self-assembling silk fibroin hydrogel that can serve as a tissue-mimetic extracellular matrix. However, development of these silk fibroin hydrogels for subacute and chronic stroke therapies requires a comprehensive understanding of the long-term performance and biodegradation of silk fibroin hydrogels. Here, silk fibroin hydrogels that can undergo a solution-gel transition were injected directly into an established stroke cavity, and biodegradation of the hydrogels was followed over 12 months. The histology of silk fibroin hydrogel-treated brains showed reduced inflammation post stroke due to infiltration of astrocytes (GFAP+) and microglia/macrophages (CD11b+) into the hydrogels rather than into astrocytic scars. At 6 months, the majority of invading cells were found at the tissue/hydrogel boundary and displayed a typical M2-like phenotype (CD206+), whereas the cells that substantially infiltrated the center of the hydrogels at 12 months showed both M1 (CD86+)-like and M2 (CD206+)-like phenotypes. The hydrogel areas surrounded by macrophages showed evidence of degradation, potentially providing a niche for endogenous neuronal progenitor cell proliferation and migration (DCX+/Ki67+) into the hydrogel. Overall, this study provides insight into the chronic 12-month tissue response, indicating

both silk fibroin hydrogel degradation and cell support. These are important features for the development of next-generation stroke therapies.

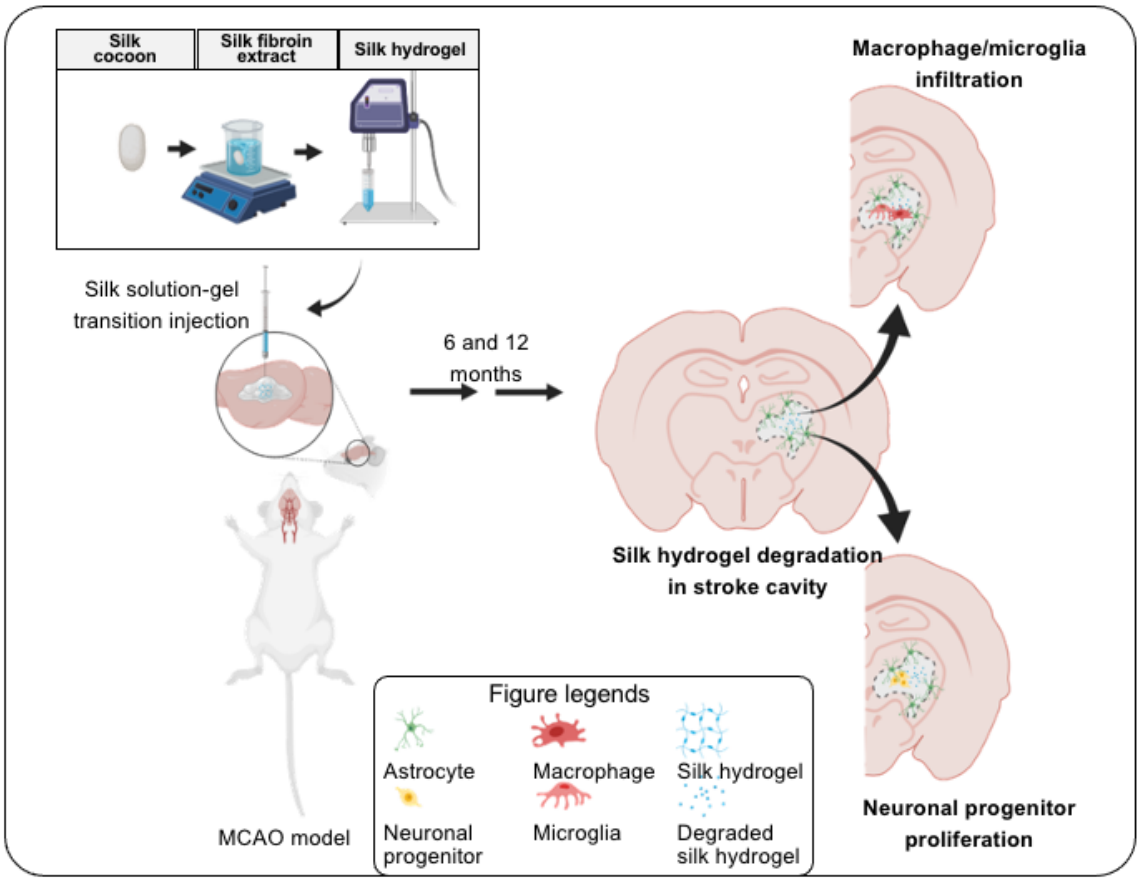

Figure 3.1 Graphical abstract

3.2 Introduction

Stroke remains the most common cause of severe and long-term disability in adults worldwide[67]. Ischemic stroke, the most frequent form of stroke, is caused by the occlusion of cerebral blood flow due to an embolus or local thrombosis. Unsuccessful reperfusion causes brain tissue damage and loss of function[145]. At present, intravenous injection of tPA is the only effective stroke therapy approved for routine clinical use[69]. However, tPA has only a 4.5 h administration window after the onset of symptoms; thus, few stroke patients can benefit from these treatments[70]. To date, no effective treatment options can target the subacute and chronic phases of ischemic stroke. While physical therapy is important for post-stroke recovery, no U.S. Food and Drug Administration [FDA]-approved drugs promote a satisfactory degree of functional

recovery. Thus, most patients who do not receive acute reperfusion therapies show long-lasting neurological impairment[146].

Cell-based therapies, including the use of MSCs, are now attracting widespread interest as safe and effective candidates for the repair of damaged tissues, including the stroked brain. However, a major problem with MSC administration encountered in both pre-clinical and clinical studies is a low cell retention at the application site due to rapid cell death (because of an absence of supporting signals)[147]. One solution to overcome this limitation is to use a biomaterial as a carrier [148]. Here, cells are co-administered during transplantation with a carrier that can enhance stem cell viability, proliferation, and retention at the target site[149]. Hydrogels are key contenders for this mission because they have the potential to (i) support cell behavior by presenting cues (e.g., RGD peptide motifs), (ii) provide a fibrillary structure to support cells, and (iii) furnish tunable mechanical and biochemical properties[91].

Unlike other central nervous system diseases, ischemic stroke is characterized by infiltration of large numbers of macrophage/microglia into the infarct area to promote clearance of necrotic cell debris, and this ultimately forms a stroke cavity in severe cases[150]. For this reason, injectable biomaterials offer a potential opportunity for treatment of chronic ischemia strokes. One key aim in this therapy is to elicit endogenous brain tissue repair mechanisms, including post-stroke angiogenesis and neurogenesis[151]. However, the typical candidate materials have thus far failed in their translation to the clinic, mainly due to fast/slow degradation and/or toxicity of the degradation by products[152]. However, engineered biomaterials are believed to have the potential to tip the balance toward regeneration[153]. For example, the Injectable Collagen Scaffold™ is presently being used in human clinical trials to deliver MSCs to intracranial hematoma cavities for functional recovery in patients with traumatic brain injury and stroke (ClinicalTrials.gov Identifier: NCT02767817)[148].

Silk fibroin-based hydrogels have also been studied for a broad range of tissue engineering applications, both *in vitro* and *in vivo*. The historic track record of silk biocompatibility, its excellent mechanical properties, and its controllable biodegradation rates[154] support the use of silk in these applications. For example, silk has been tuned for both soft (e.g., adipose and brain) and hard (e.g., bone and cartilage) tissue engineering applications. The *in vivo* degradation rates of silk material formats can be altered from minutes to years by controlling the structure and morphology[155]. Experience with silk based biomaterials in humans includes the clinically approved SERI® Surgical Scaffold and the Silk Voice® injectable implant [156]. However, the use of silk in the stroke setting requires verification because material performance is context specific[157].

Over the past 5 years, my host laboratory and others have investigated the use of injectable silk fibroin hydrogels for post-stroke brain repair[63,158] because the externally triggered solution-to-gel transition enables minimally invasive stereotactic injection. This administration route results in an excellent conformal fit of silk fibroin within the stroke cavity[65], while the resulting soft viscoelastic silk fibroin hydrogel (1 kPa) positively impacts cell biology[106] while also showing good *in vivo* biocompatibility after transplantation for up to 2 months. Treated animals showed a substantially reduced inflammatory response and increased peri-infarct vascularization compared to stroke-only controls[158]. However, the long-term fate of the silk fibroin hydrogel, as well as the tissue response to the hydrogel and its degradation byproducts, are currently unknown.

The feasibility of injectable silk hydrogels to promote brain repair in the post-stroke setting was demonstred with the middle cerebral artery occlusion model (insert intraluminal suture from the internal carotid artery to occlude the origin of the MCA) . This model does not require craniotomy, mimics the gradual reperfusion seen in human ischemic stroke, and fully generates cavity formation by less than 2 weeks post-injury[159]. The model is also commonly used in my group[65, 158].

In vivo silk fibroin degradation in part relies on host immune cells, specifically macrophages and foreign-body giant cells, and occurs via immune cell-mediated pathways (i.e., phagocytosis and extracellular proteolytic degradation)[160]. However, several knowledge gaps currently exist[148], including the long-term host response toward silk fibroin hydrogels in stroked brains (e.g., material degradation, tissue recovery, etc.). Here, I show that acellular silk hydrogels can potentially support tissue reconstruction in the stroke-damaged brain over a 12-month duration by generating a pro-repair environment within the hospital stroke cavity and activating endogenous repair processes, including neurogenesis.

3.3 Materials and Methods

3.3.1 Silk fibroin hydrogel manufacture.

The silk solution was prepared from *Bombyx mori* cocoons, as previously reported in Chapter 2. In brief, the cocoons were degummed by boiling for 60 min in 25 mM Na_2CO_3. The degummed silk was dissolved in 9.3 M LiBr at 60°C for 3 h and then dialyzed against water for 48 h (molecular weight cut-off 3,500 Da), yielding a 5–6% [w/v] silk fibroin solution. Next, 10× phosphate buffered saline (PBS) was added to the silk fibroin solution to obtain a physiological osmolarity for the final preparation. The resulting 4% [w/v] silk fibroin solution was filter-sterilized. Physically crosslinked silk hydrogels were manufactured by ultrasonication with a digitally controlled probe sonicator (Sonoplus HD 2070, Bandelin, Berlin,

Germany) fitted with a 23 cm long sonication tip (0.3 cm diameter tip and tapered over 8 cm). A total volume of 4 mL of 4% [w/v] silk fibroin solution in water was placed on ice in 15 mL Falcon tubes (1.4 cm diameter and 11 cm long) (Greiner Bio-One GmbH, Kremsmünster, Austria) and exposed to 3 sonication cycles at 30% amplitude (one cycle consisted of 30s on and 30s off) to induce the solution-gel transition. The sonicated silk fibroin samples were then drawn up into Hamilton syringes and injected into the animals. These parameters were adjusted based on the study by Osama *et al.* where 4% [w/v] silk hydrogels mimicked of brain mechanics best (~1 kPa reported in literature) compared to either 2 or 3% [w/v] silk hydrogels. Osama et al a reported that a sonication time of 30 seconds and power amplitude at 30% were best for generating injectable silk hydrogels for intracerebral injection. Injetability was demonstrated with tissue substitutes[65]. These 4% [w/v] hydrogels completed their solution-gel transition within <1 h *in vitro*.

3.3.2 Middle cerebral artery occlusion (MCAo).

Animal procedures were performed in accordance with the UK Animals (Scientific) Procedures Act (1986) and the Ethical Review Process of the Institute of Pharmacy and Biomedical Sciences of the University of Strathclyde, in adherence with ARRIVE guidelines. The rat model of stroke was established as previously described[161]. All animal procedures were approved by the Home Office of the United Kingdom (Project License number 60/4469). Male Sprague−Dawley rats (weight 240−290 g, 8−9 weeks old, Harlan, UK, n = 10) were maintained on a 12 h light/dark schedule, with food and water available *ad libitum*. For the right MCAo rat model of stroke, the animal was placed under isoflurane anesthesia (4% for induction, 2% for maintenance in 30% oxygen), and the body temperature was maintained at 37 ± 1 °C. A propylene filament (Doccol Corporation, USA, tip diameter with coating 0.33 ± 0.02 mm) was then advanced to the ostium of the MCA in the circle of Willis. The MCA was occluded for 1 h prior to reperfusion by retracting the filament to the common carotid bifurcation; this produced an occlusion similar to the scenario in 2/3 of all cases of human ischemic stroke [82]. After recovery from anesthesia, the animals were assessed for forelimb flexion and contralateral circling. Daily post-operative care and neurological assessment were performed until the animals recovered pre-operative weight. Animals not exhibiting signs of MCA damage (i.e., unilateral forelimb flexion) or any animal found to be moribund due to excessive weight loss (>20% of start weight) were excluded from the study[162]. The severity of the stroke-induced deficits was established by monitoring animals for the following two-week period and before euthanasia. This included a neurological deficit scoring using a grading scale of 0 to 4, where 0 =

no observable deficit; 1 = forelimb flexion; 2 = decreased resistance to lateral push (and forelimb flexion) without circling; and 3 = decreased resistance to lateral push (and forelimb flexion) with circling. An additional score = 4 was added if the animal appeared unstable or exhibited reduced spontaneous motility.

3.3.3 Stereotactic surgery.

Two weeks after MCAo, the rats were anesthetized with isoflurane (4% induction, 2% maintenance) and randomly assigned to receive 4% [w/v] self-assembling silk fibroin hydrogel (n = 10). Animals were placed in a stereotactic frame, and injections (10 μL, at a rate of 2 μL/min) were performed at coordinates (L) −1.5 mm, (A-P) −3.5 mm, and (V) −6.5 mm, using a 10 μL Hamilton syringe with a 22G blunt-tip needle.

3.3.4 Histologic analysis.

3.3.4.1 Perfusion-fixation of tissue

The *in situ* distribution of the silk hydrogel and cell infiltration within the hydrogel were determined in the rats (n=5/ group) at 6 and 12 months post-implantation by transcardial perfusion with 0.9% saline followed by 4% ice-cold paraformaldehyde in 0.2 M phosphate buffered saline (PBS) to fix brain tissue prior to craniotomy. Brains were postfixed in 4% paraformaldehyde for 24 h prior to cryopreservation in 30% sucrose in PBS with 0.01% sodium azide for 72 h at 4 °C. Histologic sections (30 μm thickness) were prepared on a cryostat (Leica CM1850, UK) and placed directly onto microscopic slides to preserve tissue morphology.

3.3.4.2 Hematoxylin and eosin (H&E) and Masson trichrome staining

The tissues were stained with hematoxylin and eosin to identify lesion/graft localization in whole brain tissue. Masson trichrome staining was performed to visualize the gross morphology of the silk hydrogel implants within the cavity according to the manufacturer's protocol (ab 150686, Abcam, UK). The stained sections were viewed and photographed with a bright field microscope.

3.3.4.3 Immunohistochemistry

Brain sections were washed three times for 5 min in PBS, followed by a 40 min permeabilization in 10% v/v blocking sera and in PBS with 0.3% v/v Triton X-100 (Sigma) at room temperature. Primary antibodies were diluted in PBS with 10% v/v normal serum and 0.3% v/v Triton X-100 and applied to the sections, followed by incubation at 4 °C overnight. The primary antibodies used (Table 3.1) were: rabbit anti- GFAP (1:1000, Z0334, DAKO, CA, USA) to visualize the glial scar and to quantify the volume of the cavity; rat

anti-CD11b (1:200, ab1211, Abcam, UK) to detect microglia/macrophages, rabbit anti-CD86 (1:100, ab269587, Abcam, UK) to visualize M1-like macrophages, mouse anti-CD206 (1:50, sc376108, Santa Cruz Biotechnology, Texas, USA) to detect M2-like macrophages, rabbit anti-Ki67 (1:500, ab15580, Abcam, UK) to visualize proliferating cells, and chicken anti- DCX (1:150, ab153668, Abcam, UK) to visualize neural progenitor cells. The unreacted primary antibodies were removed from the sections by three 5 min rinses in PBS, and appropriate secondary Alexa Fluor 488 or Alexa Fluor 555 antibodies (1:500, Invitrogen, UK) were applied for 2 h at room temperature, followed by three 5 min PBS washes. All secondary antibodies were highly cross-absorbed variants to minimize background fluorescence. The sections were coverslipped with DAPI containing Vectashield (Vector Laboratories, UK) and stored at 4 °C prior to imaging. Images were captured and analyzed using WinFluor V3.9.1 (Nikon Eclipse E600).

Table 3.1 Primary antibodies

Antibody	Host	Manufacturer	Dilution	Marker
GFAP	rabbit	DAKO-Z0334	1:1000	Active astrocytes
CD11b	rat	Abcam-ab1211	1:200	Microglia/macrophages
CD86	rabbit	Abcam-ab269587	1:100	M1-like macrophages
CD206	mouse	Santa Cruz-sc376108	1:50	M2-like macrophages
Ki67	rabbit	Abcam-ab15580	1:500	Proliferating cells
DCX	chicken	Abcam-ab153668	1:150	Neural progenitor cells

3.4 Results

3.4.1 The silk hydrogel–host tissue interface.

Brain ischemic stroke in the caudate putamen (striatum) was successfully created by MCAo. This model creates a complex array of microenvironments, with cavitation representing the most severe form of damage[163]. Sonicated silk hydrogels in the solution−gel transition (10 μL) were injected into the cavity at 14 days post stroke, and histology was determined at 6 and 12 months post-injection (Figure 3.2A). During the post-MCAo recovery period, prior to grafting, 1 rat showed full restoration of its neurological functions, with no observable deficit (score = 0), whereas the other 9 animals showed partial recovery (those with striatal stroke) (score = 1-2). The highest neurologic deficit was observed at 1 week post-implant. After 6 months post-implantation, the neurological score was significantly decreased and approached the original baseline levels. All stroke signs were recovered within 1 year post-implantation in all animals (Figure 3.2B). The hydrogel implants did not cause any loss of body weight during the study period (Figure 3.2C). Injection of silk fibroin into the lesion cavity resulted in a robust in situ gelation,

with a good interface formed between the hydrogels and the host tissue, as indicated by a light pink color following eosin staining (Figure 3.3) and light blue (Figure 3.4) following trichrome staining. Small gaps were observed and could potentially be artifacts that arose during sample preparation. Silk hydrogel remnants were still present, although with visibly reduced material integrity, at 1 year post-implantation (Figure 3.3 and Figure 3.4).

A

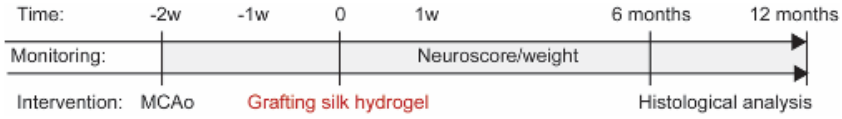

B

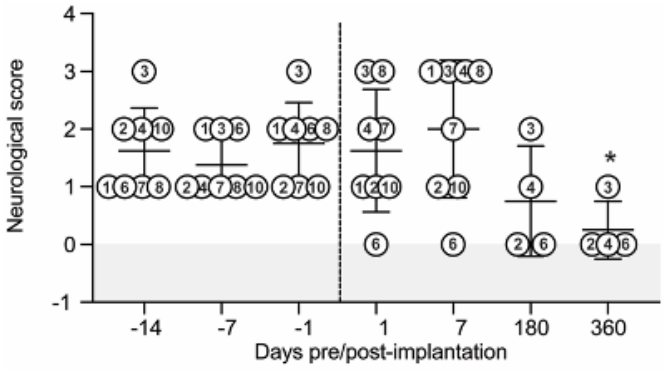

C

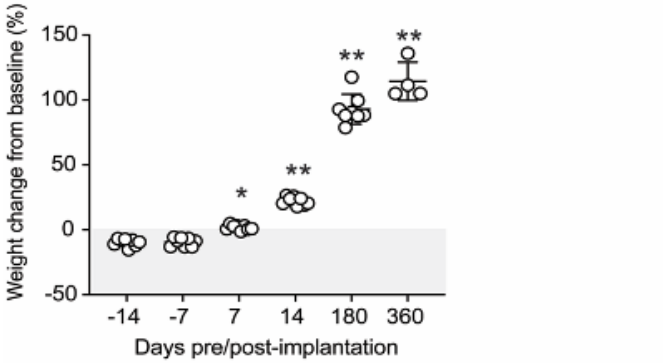

D

	Animals	Sign of stroke	SH graft position
6 months (n=4)	JHS01	minor stroke	-2.2/-3.6
	JHS07	minor stroke	-2.2
	JHS08	stroke	-0.4/-2.2
	JHS10	stroke	-0.4
12 months (n=4)	JHS02*	minor stroke	silk in cavity
	JHS03	stroke	-0.4/-2.2
	JHS04	minor stroke	silk in cavity
	JHS06	minor stroke	silk not found

Figure 3.2 Neurological function and body weight were unaffected by silk fibroin hydrogel implants. (A) Experimental timeline, stroke intervention, and assessment. Right transient MCAo was performed on 10 rats at 2 weeks prior to the grafting surgery. At time 0, animals (n = 8) were given stereotactic intracerebral injections of 4% [w/v] self-assembling silk hydrogels. A hydrogel was prepared by sonication, and stereotactic injection into the stroke cavity was performed during the sol-gel transition. (B) Neurological score was assessed, and (C) body weight was determined at 2 weeks during post-MCAo recovery (after 24 h; day −14 and after 7 days; day −7) and again at 1 week, 6 months, and 12 months after grafting. Animals were euthanized at 6 months and 12 months after grafting and subjected to (immuno)-histochemical analysis. (D) Striatal lesions were found in all animals after MCAo, indicating minor or striatal stroke.

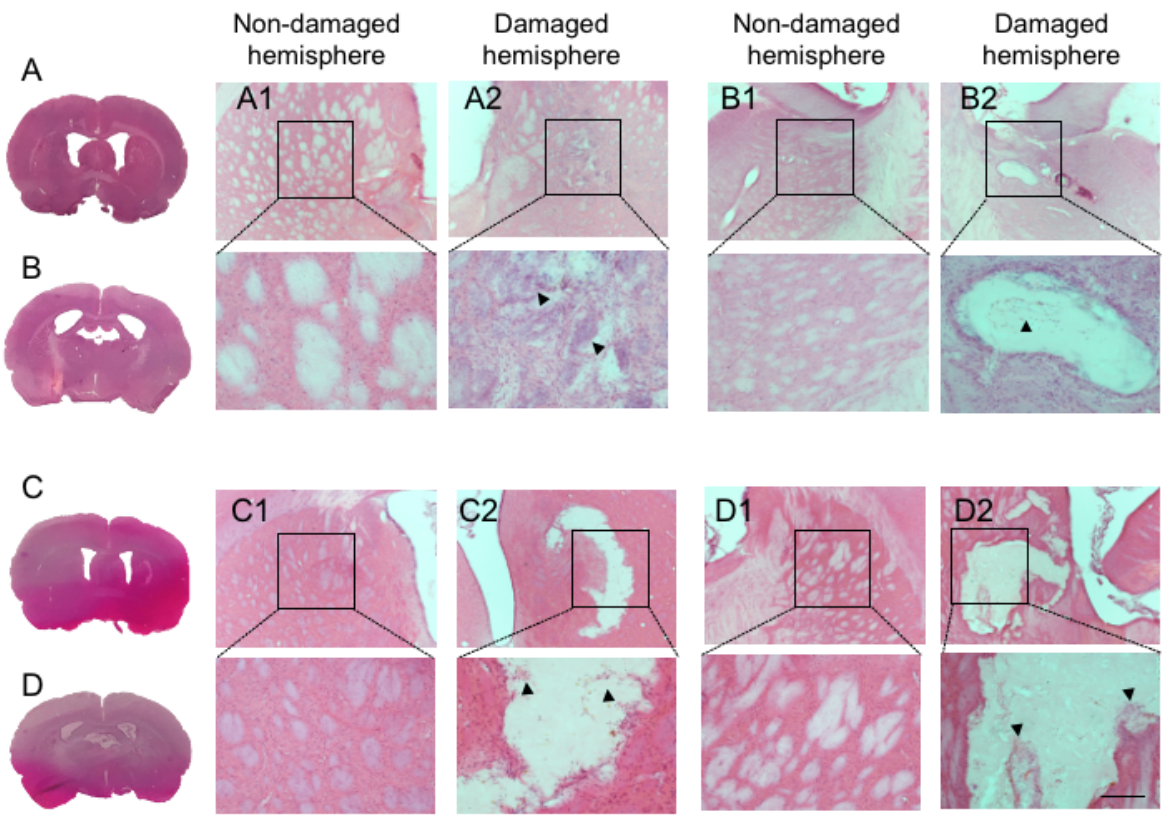

Figure 3.3 Endogenous cells present in the silk hydrogel graft.

Representative hematoxylin and eosin stained coronal brain sections at (A, C) the level of the globus pallidus (IA 7.68 mm) and (B, D) the level of the anterior hypothalamus (IA 6.84 mm) at (A, B) 6 or (C, D) 12 months after transplantation with self-assembling silk fibroin hydrogels (dotted line represents higher magnification, below panels). The whole brain sections and magnified figures illustrate (A1, B1, C1, D1) the non-damaged hemisphere and (A2, B2, C2, D2) the damaged hemisphere with the presence of the silk fibroin hydrogel graft in the striatal lesions (visualized by light pink eosin staining), surrounded by endogenous invading cells (nuclei showing purple hematoxylin staining; arrow). Scale bars: 200 μm.

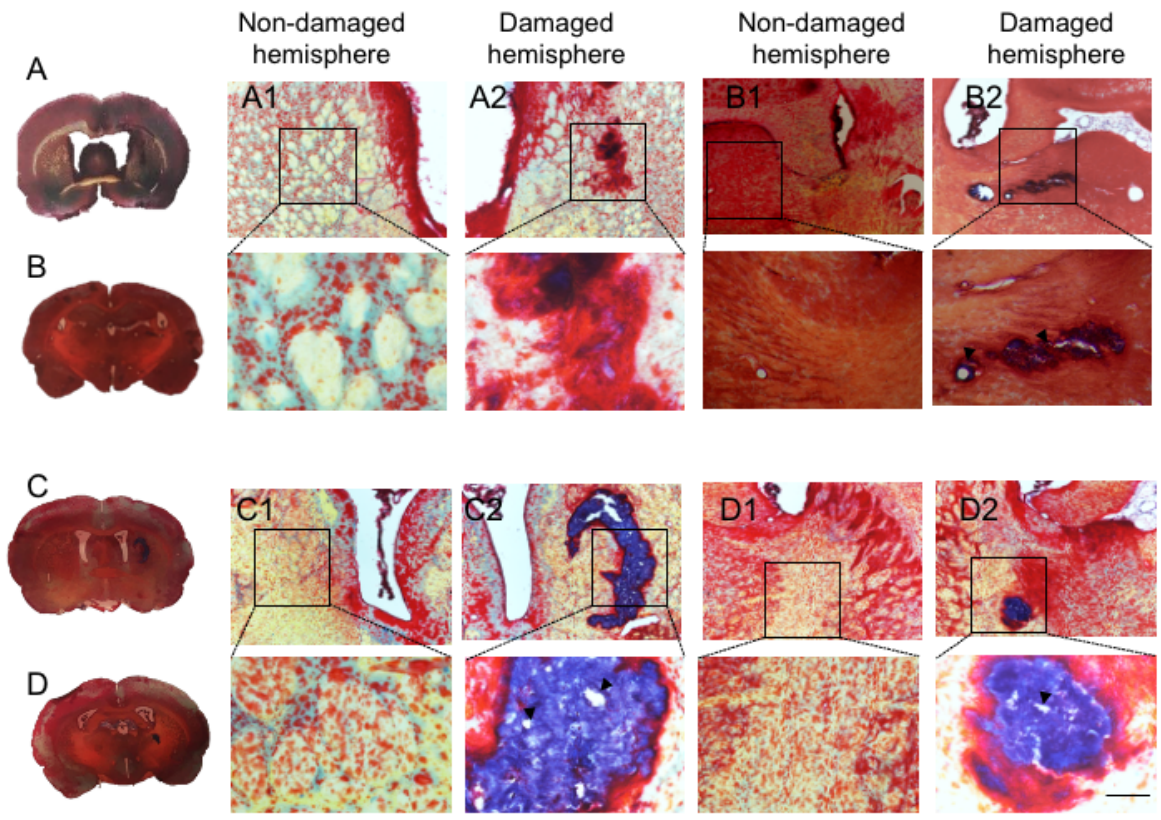

Figure 3.4 The silk hydrogel graft degraded over time.

Representative trichrome stained images of coronal brain sections at (A, C) the level of the globus pallidus (IA 7.68 mm) and (B, D) the level of the anterior hypothalamus (IA 6.84 mm) at (A, B) 6 or (C, D) 12 months after transplantation with self-assembling silk fibroin hydrogels (dotted line represents higher magnification, below panels). The whole brain sections and magnified figures illustrate (A1, B1, C1, D1) the non-damaged hemisphere and (A2, B2, C2, D2) the damaged hemisphere, with the presence of a good space confirming silk hydrogel deposits in the stroke lesion (visualized by dark purple collagen/silk fibroin staining). Signs of hydrogel degradation were observed (i.e., looser structure; arrow). Scale bars: 200 µm. (Blue = collagen/ silk fibroin; red = muscle fiber; black/blue = nucleus)

3.4.2 Silk hydrogels-macrophage infiltration.

At 6 months, astrocytes surrounded the implanted hydrogels, defining the boundary between silk hydrogels and host tissue, but a typical astrocytic scar was absent. At 12 months, a drastic decrease was evident in this astrocytic accumulation at the silk hydrogel tissue interface when compared to stroked animals without intervention (Figure 3.5 and Figure 3.6). Both structural support and inductive cues are necessary for cells to migrate into the hydrogel. The majority of cells that infiltrated the hydrogels were macrophages/microglia (CD11b+). At 6 months post-implant, both macrophage/microglia and astrocytes were found in abundance around the small silk fibroin hydrogel remnants that were spread across the stroked area. However, only a very few cells invaded the hydrogel itself (Figure 3.5), while a substantial infiltration was evident at the small gaps present between the hydrogel and the host tissue. This was especially the case in areas where the cavitation was small and resulted in an increased macrophage density within the hydrogels at 1 year post-implant (Figure 3.6). Infiltrating macrophage/microglia were located close to astrocytes.

Degradation of the silk hydrogels could be another key factor that enabled host cell infiltration and brain tissue reconstruction. Some cases showed invasion by microglia/macrophages, which are necessary for both tissue clearing and silk fibroin hydrogel degradation. I distinguished the phenotypes of these cells and examined inflammatory M1 (CD86+) and/or anti-inflammatory M2 (CD206+) phenotypes implicated in tissue remodeling. At 6 months post-implantation, M2-like phenotype macrophages dominated in the hydrogels (Figure 3.7). By contrast, macrophages co-expressing the M1-like and M2-like phenotypes were the most common cell phenotypes infiltrating silk fibroin hydrogels at 1 year (Figure 3.8).

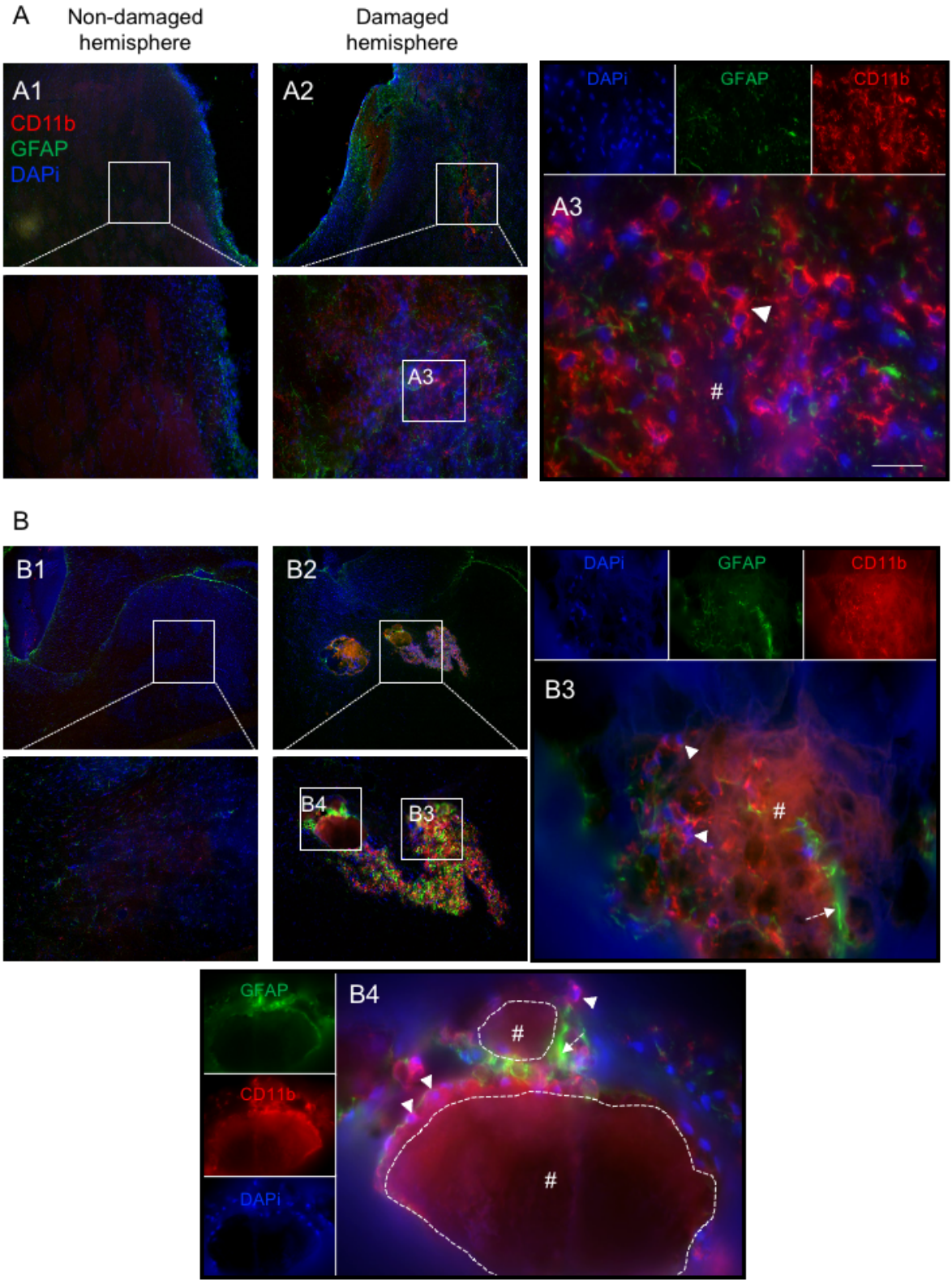
A
Non-damaged hemisphere
Damaged hemisphere
A1
CD11b
GFAP
DAPi
A2
A3
DAPi
GFAP
CD11b
A3
#
B
B1
B2
B4
B3
DAPi
GFAP
CD11b
B3
#
GFAP
CD11b
DAPi
B4
#
#

Figure 3.5 Silk hydrogels promoted microglia/macrophage infiltration at 6 months post-grafting. Representative CD11b+ (red)/ GFAP+ (green)/ DAPI (nuclei in blue) staining images of coronal brain sections at (A) the level of the globus pallidus (IA 7.68 mm) and (B) the level of the anterior hypothalamus (IA 6.84 mm) at 6 months after transplantation with self-assembling silk fibroin hydrogels (dotted line represents higher magnification, below panels). The whole brain sections and magnified figures illustrate (A1, B1) the non-damaged hemisphere and (A2-A3 and B2-B4) the damaged hemisphere with substantial CD11b/DAPI -positive cells (arrows nearby hash symbol with white outline) surrounding a grafted hydrogel (hash symbols). GFAP+ astrocytes also invaded the silk hydrogels (B3, B4 dotted arrows), but they were not adjacent to migrating microglia/macrophages (B3, B4 arrow). Scale bars: 50 μm.

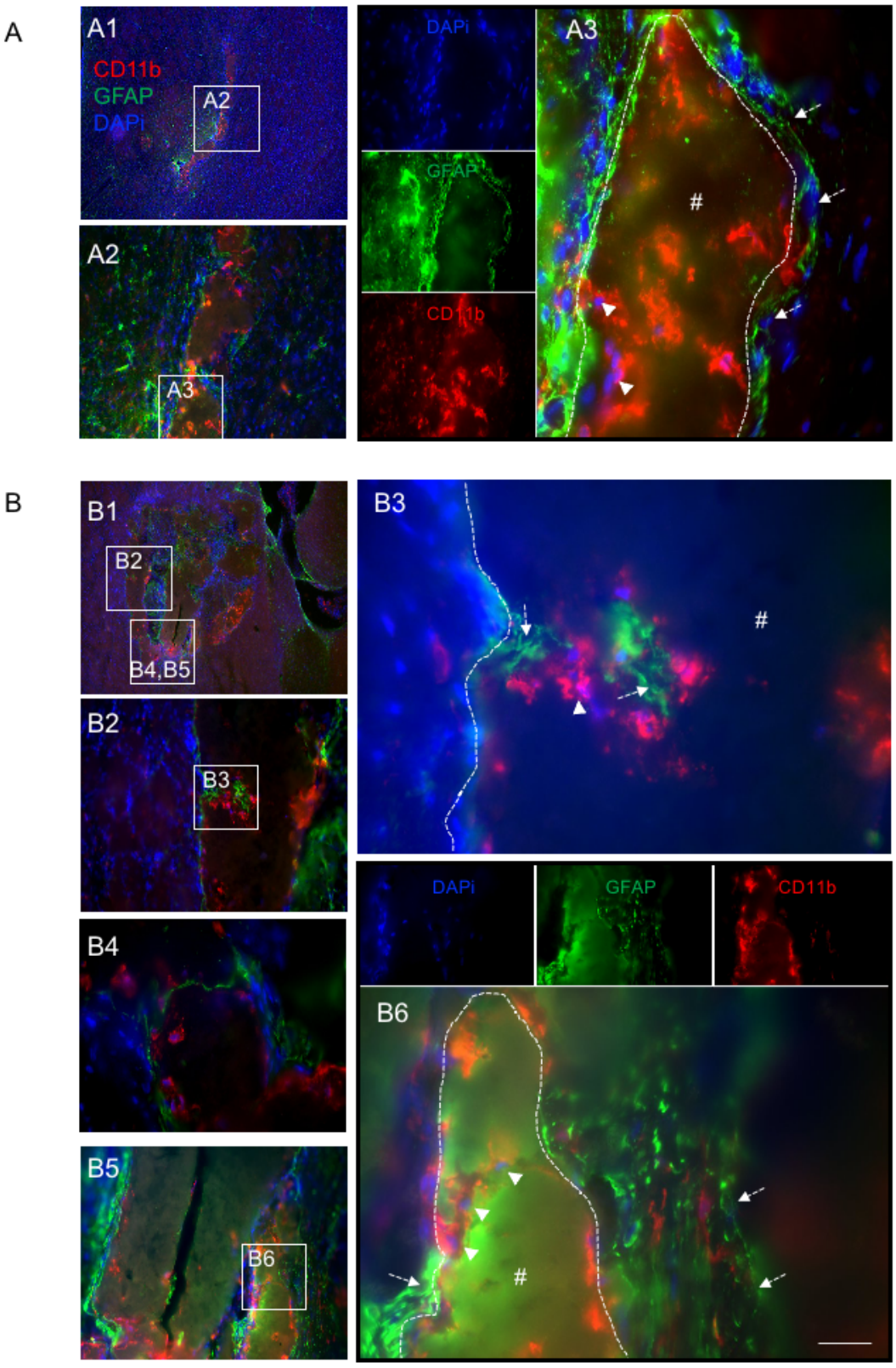
A
A1
CD11b
GFAP
DAPi
A2
A2
A3
DAPi
GFAP
CD11b
A3
#
B
B1
B2
B4,B5
B2
B3
B4
B5
B6
B3
#
DAPi
GFAP
CD11b
B6
#

Figure 3.6 Silk hydrogel promoted microglia/macrophage infiltration at 12 months post-grafting. Representative CD11b+ (red)/ GFAP+ (green)/ DAPI (nuclei in blue) stained images of coronal brain sections at (A) the level of the globus pallidus (IA 7.68 mm) and (B) the level of the anterior hypothalamus (IA 6.84 mm) at 12 months after transplantation of self-assembling silk fibroin hydrogels. The whole brain sections and magnified figures illustrate (A, B) damaged hemisphere with substantial CD11b/DAPI - positive cells (arrows in hash symbol with white outline) located inside a grafted hydrogel (hash symbols) in both (A3) posterior (globus pallidus) and (B3,B6) anterior (hypothalamus) of the striatal area, indicating a possible association with the degradation of the silk hydrogels. GFAP+ astrocytes were observed some distance away from the grafted silk hydrogels, whereas a silk fibroin hydrogel−astrocytic scar (GFAP+) interface was less visible (A3, B6 dotted arrows). Scale bars: 100 μm.

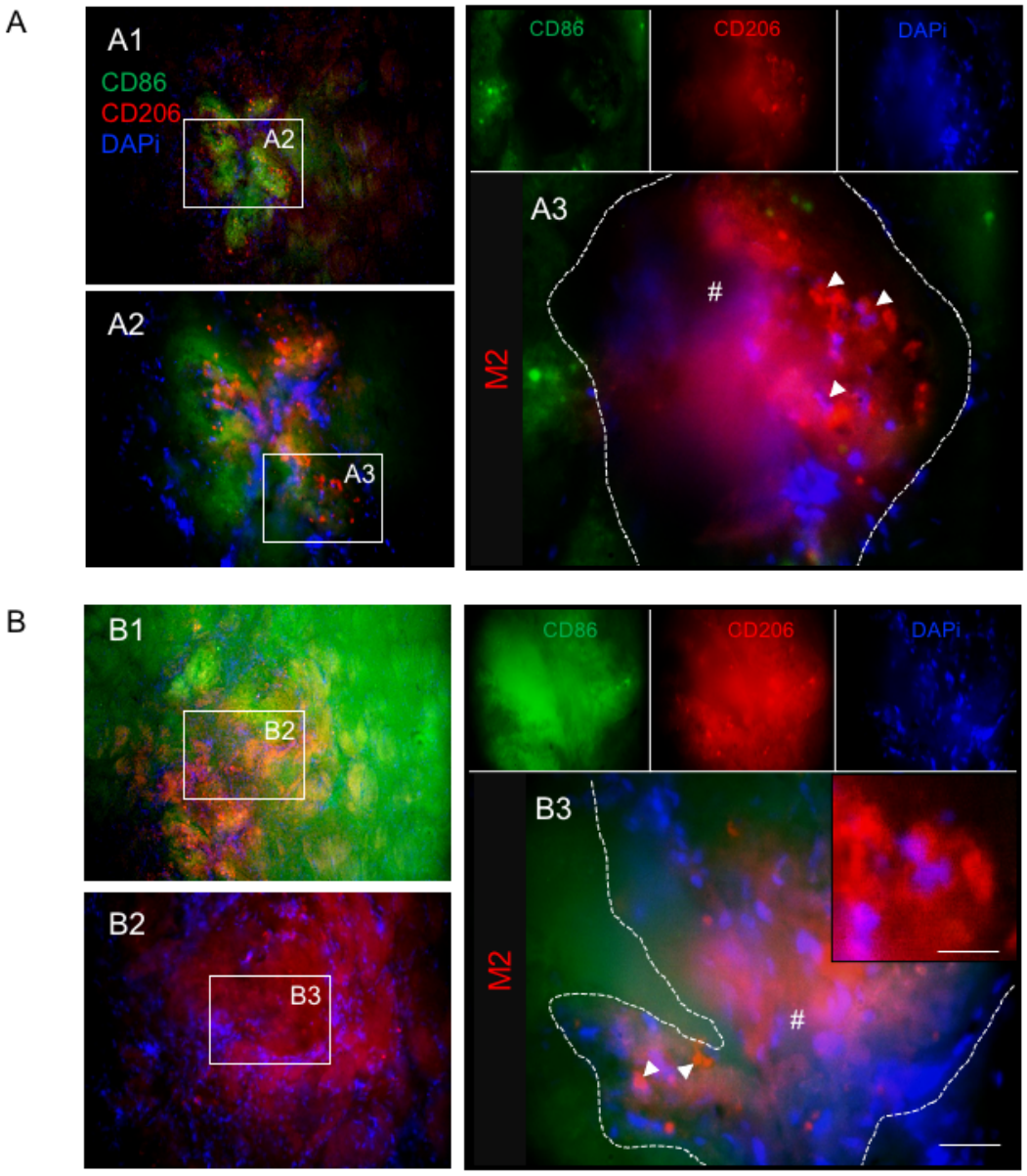

Figure 3.7 Silk hydrogels promoted M2-like macrophage infiltration at 6 months post-grafting. Representative CD86 (green)/ CD206 (red)/ DAPI (nuclei in blue) stained images of coronal brain sections at (A) the level of the globus pallidus (IA 7.68 mm) and (B) the level of the anterior hypothalamus (IA 6.84 mm) at 6 months after transplantation with self-assembling silk fibroin hydrogels. The whole brain sections and magnified figures illustrate (A, B) damaged hemisphere with substantial M2-like (CD206+) (arrows in hash symbol with white outline) located inside a grafted hydrogel (hash symbols), indicating this could promote brain tissue remodeling during stroke recovery. Scale bars: 100 μm; zoom10 μm.

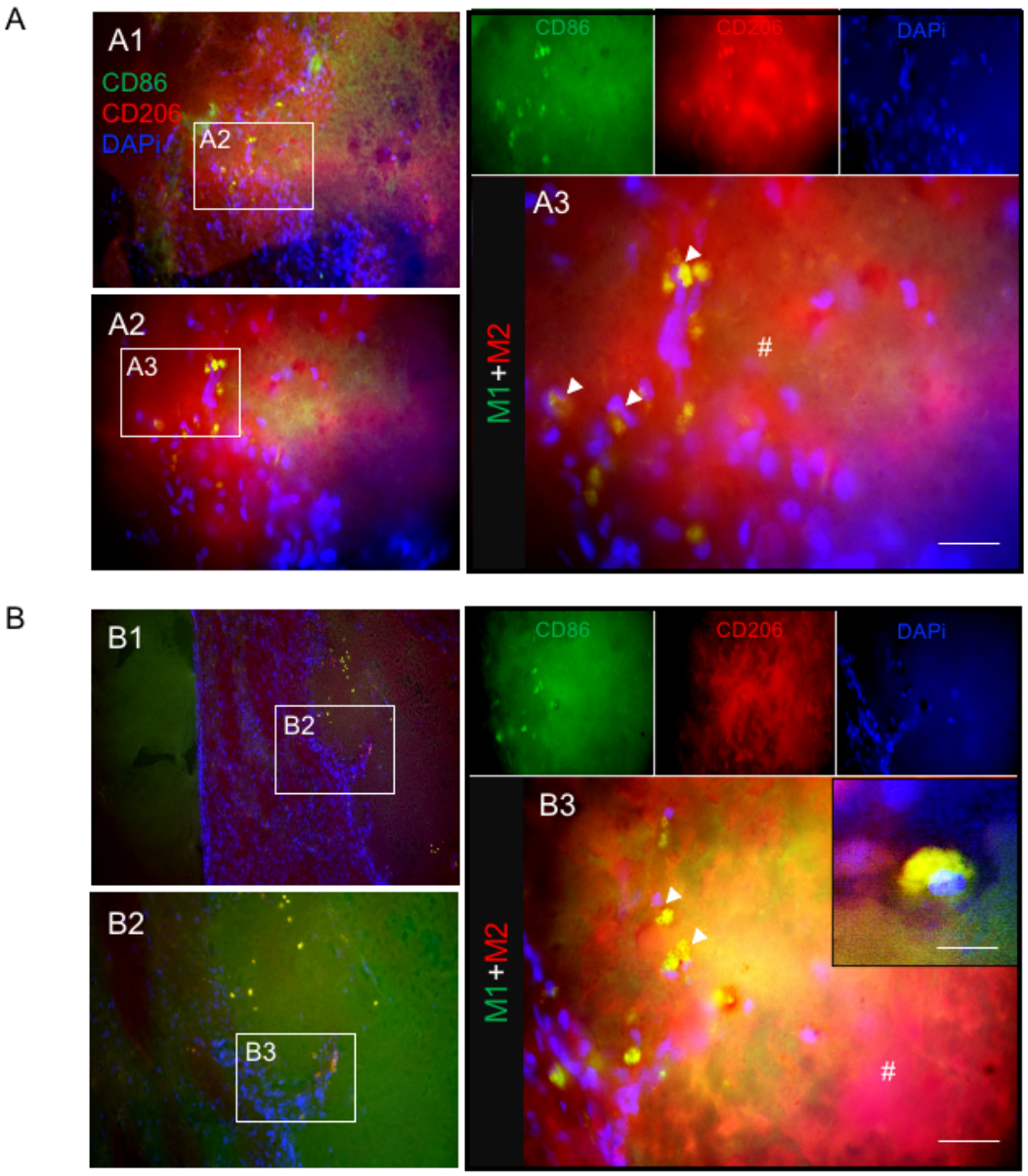

Figure 3.8 Silk hydrogel promoted hybrid M1-like and M2-like macrophage infiltration at 12 months after grafting.

Representative CD86 (green)/ CD206 (red)/ DAPI (nuclei in blue) stained images of coronal brain sections at (A) the level of the globus pallidus (IA 7.68 mm) and (B) the level of the anterior hypothalamus (IA 6.84 mm) at 12 months after transplantation with self-assembling silk fibroin hydrogels. The whole brain sections and magnified images illustrate (A, B) damaged hemisphere with substantial CD86/CD206-positive cells (arrows in hash symbol with white outline) located inside a grafted hydrogel (hashmark symbols), indicating that hybrid M1- and M2-like macrophages increased in the long-term period. Scale bars: 50 μm in Figure A and 100 μm; zoom10 μm in Figure B.

3.4.3 Silk hydrogels-neuronal progenitor cell infiltration.

I observed cells within the hydrogels that did not show staining for astrocytes or macrophage/microglia. In the brain, neural progenitor cell [NPC] migration toward the damaged tissue is a spontaneous endogenous post-stroke response that elicits tissue remodelling and new brain tissue formation. I determined whether our material enhanced neuronal NPC proliferation and migration from the subventricular zone to lesion sites by examining DCX and Ki67 as NPC and proliferating cell markers, respectively. Double positive DCX and Ki67 cells, which were considered proliferating NPCs, were found both in the peri-infarct area and in the infarct area of the hydrogels (Figure 3.9). This observation was consistently observed in all animals treated with silk fibroin hydrogels.

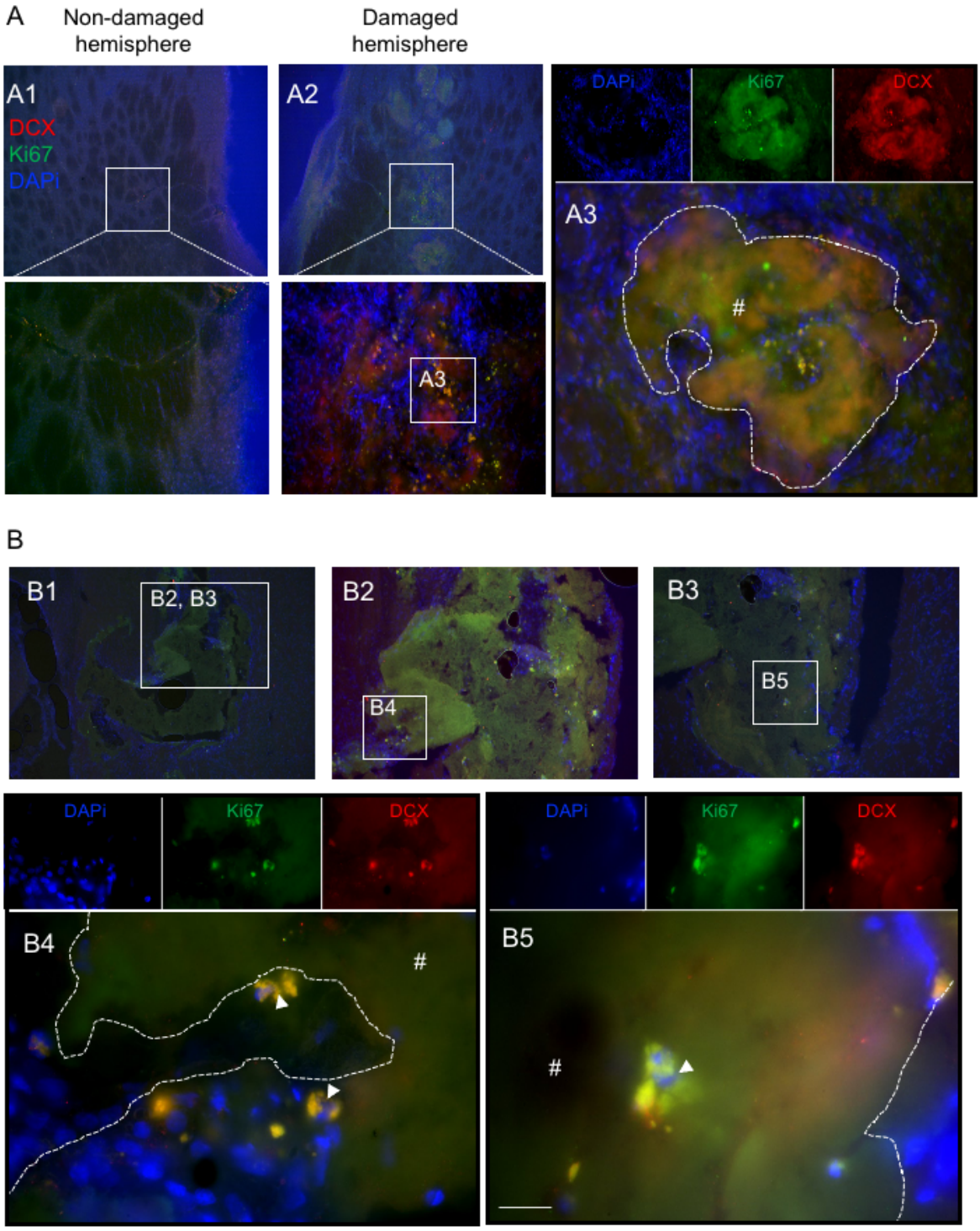
A
Non-damaged hemisphere
Damaged hemisphere
A1
DCX
Ki67
DAPi
A2
A3
DAPi
Ki67
DCX
#
B
B1
B2, B3
B2
B4
B3
B5
DAPi
Ki67
DCX
B4
#
DAPi
Ki67
DCX
B5
#

Figure 3.9 Neuronal progenitor cells invaded into silk hydrogels.

Representative DCX+ (red)/ Ki67+ (green)/ DAPI (nuclei in blue) stained images of coronal brain sections at (A) 6 or (B) 12 months after transplantation with self-assembling silk fibroin hydrogels (dotted line represents higher magnification, below panels). The whole brain sections and magnified figures illustrate (A1) non-damaged hemisphere and (A2-A3 and B1-B5) damaged hemisphere with a number of DCX+ colocalized with Ki67+ cells (arrows in hash symbol with white outline) at the host-biomaterial interface and inside the grafted hydrogels (hash symbols), indicating the proliferation of these migrating neural progenitors inside and this could promote brain tissue repair after stroke. A few more DCX/Ki67/DAPI-positive cells were present in the hydrogels at 12 months after grafting (B4, B5 arrows in dotted white outline; yellow = red+green). Scale bars: 100 μm.

3.5 Discussion

In the search for better stroke therapies, injectable hydrogels are promising contenders in minimally invasive therapeutic interventions, especially in the context of cell therapies [80]. The advantage of self-assembling silk hydrogels with a minutes to hour gelation timeline is that their solution-gel transition enables their administration through a thin needle to the lesion site and subsequent *in situ* gelation. This ultimately provides structural support but without swelling and tissue-like mechanics[116]. In addition, central nervous system damage in stroke is typically irregular in shape; therefore, the use of shape-adaptable hydrogels allows the filling of irregular defects, thereby facilitating good host tissue integration[150].

In the current study, I examined the long-term biocompatibility and degradation of silk hydrogels in the stroke microenvironment by monitoring *in vivo* hydrogel biodegradation over 12 months. The histology of silk fibroin hydrogel-treated brains indicated reduced post-stroke inflammation due to the promotion of astrocyte (GFAP+) and microglia/macrophage (CD11b+) infiltration into the hydrogels, rather than the promotion of astrocytic scar formation. At 6 months, the majority of the invading cells were found at the tissue/hydrogel boundary and typically were macrophages with an M2-like phenotype (CD206+). By contrast, at 12 months, a substantial infiltration was observed in the center of the hydrogels by macrophages that co-expressed the M1 (CD86+)-like and M2 (CD206+)-like phenotypes. The areas surrounded by macrophages showed evidence of hydrogel degradation, with the degraded sites potentially providing a niche for endogenous neuronal progenitor cell proliferation and migration (DCX+/Ki67+).

Injecting silk hydrogels into the stroke cavity provided tissue integration and modulation, as evidenced by a reduction in tissue scarring (GFAP+) around the implant site and the infiltration and proliferation of host cells (DCX+/Ki67+) within the hydrogels (Figure 3.9). The glial scar creates a physical barrier that seals off the stroked area as a way to limit damage and tissue cavitation in adjacent areas[164]. However, this scarring also impedes tissue regeneration by limiting access to appropriate immune cells while obstructing neuronal ingrowth[165]. Silk fibroin hydrogels reduced the formation of this impermeable glial scar for 6 months after the stroke, so that residual scarring was not a limitation for attracting host cells into the implants. Similar observations have been made with other degradable materials, including IKVAV peptides[166] and poly(lactic-co-glycolic acid) (PLGA)-modified HA[167]. Hydrogels provide a structure that supports both cell infiltration and ingrowth[168,169]; however, achieving suitable mechanical properties for the hydrogels and their sufficient tissue residence time is difficult without resorting to hydrogel crosslinking. The available crosslinker materials are often cytotoxic, so they can adversely affect biocompatibility[78]. Here, the use of physical, rather than chemical, crosslinking of the silk hydrogels eliminated the need for these harsh chemicals. I used 4% [w/v] silk hydrogels that have a 1 kPa stiffness and a reliable solution-gel transition[65], and our processed silk material achieved a mechanical stiffness matching that of brain tissue[106]. This work also complements our earlier studies that examined the performance of these hydrogels in stroked brains during the first 7 weeks post stroke[158]. Self-assembled 4% [w/v] silk hydrogels are viscoelastic, making them particularly suitable for neural tissues[170].

In the present study, injectable silk hydrogels evoked the colocalization of microglia/macrophages with infiltrating astrocytes. This mobilization of microglia/macrophages might be followed by a “chain-like” migration of pioneering astrocytes. In line with the expected acute tissue response, I have previously shown that macrophage infiltration is also a typical foreign-body response toward silk fibroin hydrogels[157]. How these innate immune cells guide astrocyte migration into the damaged area or the exact sequence of events remains to be elucidated. I speculate that “invasion trails” likely arise due to a combination of cell-cell signaling by invading immune cells[77] and changes in the conductive mechanical properties. For example, the internal architecture of a hydrogel, such as its porosity and topographical cues, offers potential mechanisms for modulation of nutrient/trophic factor diffusion and cell motility—factors that ultimately affect the development of neural progenitors [81]. I know that self-assembling silk hydrogels are viscoelastic, with various impacts on cell biology factors[106], including phenotype, trophic factor release, and possible migration behavior. The injectable silk fibroin hydrogels used here were conducive to the formation of new tissue through recruitment and proliferation. I speculate that innate

immune cells ultimately recruit other brain cells that gradually repopulated the hydrogel material. However, more work is required to understand the molecular mechanisms and functional consequences.

Macrophage density within the hydrogel, and particularly the density of the M2-like phenotype macrophages, is key to promoting rapid hydrogel biodegradation, suggesting that cells were able to better access the implanted hydrogels following degradation (Figure 3.7 and Figure 3.8). Materials promoting *de novo* tissue formation must be biodegradable, as the invading host cells must be able to remodel and degrade the biomaterial to facilitate the formation of a new neuronal network[72]. Infiltrating macrophages are critical for the initiation of hydrogel material degradation. The M1-like macrophages are associated with a foreign-body response, while the anti-inflammatory M2-like phenotype is thought to be crucial for attracting cells from the host tissues to repopulate the tissue damage site and to replace the implanted material with new tissue[163,82]. Upregulation of matrix metalloproteinases-2 and -9 in macrophages after stroke is responsible for degradation of native ECM, breakdown of blood brain barrier, and increase of immune cell invasion at the injury site[171]. This tissue response potentially triggers further macrophage/microglia recruitment into the implanted materials, leading to material remodeling and degradation[9]. I observed phenotypic changes in macrophages over time: the M2-like macrophage response dominated at 6 months post-implantation, but the M1-like response, with a shift toward an M2-like phenotype, occurred after 12 months. I speculate that this shift is mediated by signaling factors arising from the silk hydrogel and/or its degradation products. A similar shift has been observed in response to the long-term degradation of porcine-derived urinary bladder ECM hydrogels. The matrix in that study showed an approximately 80% degradation of the low-strength area within 14 days, and 32% of the high-intensity area was degraded by 3 months. The material resorption profile was matched by glial cell activity and a phenotypic macrophage shift from an M1- to an M2-like state [82].

The current paradigm is to match hydrogel degradation with tissue remodeling, ultimately resulting in material replacement (i.e., degradation) with newly formed tissue [55]. A mismatch typically results in failure to guide proliferation and differentiation of local progenitor cells. For example, soft collagen hydrogels often degrade faster than desired[172], and they pose an additional theoretical risk of introducing prion diseases into the brain. HA hydrogels cause toxicity to parenchyma host tissues, leading to accelerated aging and demyelinating diseases[173,174]. Studies on the performance of silk in healthy and pathological brains are scarce. This is the first study to report the long-term performance of silk in the stroked brain. However, silk hydrogel performance and degradation have been studied in other soft and hard tissues[175]. Both silk secondary structure and format are known to modulate silk degradation and,

ultimately, tissue performance, and several studies have reported improved *in vivo* tissue repair in response to silk[155,176]. For example, intramyocardially injected silk hydrogels 2% [w/v] were completely degraded within 1 month and prevented negative left ventricle remodeling [177], whereas physically crosslinked silk hydrogels 2% [w/v] in a rat femoral segmental defect model were degraded within 3 months and promoted bone regeneration[178].

Ultrasound imaging has also been used to track material degradation [179,180], while non-invasive imaging was used to monitor the innate immune response[157]. However, little is known about silk hydrogel performance in the immune-privileged central nervous system. Implantation of self-assembling silk hydrogels 2% [w/v] containing MSCs showed a 50% material reduction after 1 month in the absence of an inflammatory response[63]. Our present study showed that self-assembling silk hydrogels were slowly degraded in the chronic stroked brain, with a substantial silk material loss occurring over 12 months. Silk degradation did not evoke any overt adverse tissue response (Figure 3.5 and Figure 3.6), and our data suggest a mild acute response that further declined over time.

I also examined the impact of silk hydrogels on endogenous neuronal cells. Neural progenitor cells are promising for stroke tissue repair because these cells have the potential to generate all neural cell types present in the brain. Stroke triggers neural progenitor cell proliferation in the subventricular zone[181]. However, these neural progenitor cells cannot reach the stroke site; one barrier is the glial scar[182]. Therefore, materials that can suppress glial scar formation while also supporting neural progenitor cell migration into the stroke area are promising because this harnesses the endogenous repair mechanisms that ultimately contribute to tissue regeneration. *In vitro* studies indicate that silk is able to protect human induced pluripotent stem cells -derived neurons and glial cells in long-term (2-year) cultures[183], suggesting that this supportive microenvironment might also be present *in vivo*. In the present study, neural progenitor cells were able to migrate along the anterior and posterior lateral ventricle toward the damaged tissues. I also observed neural-like cell proliferation and infiltration within the silk hydrogel. This observation is exciting because it suggests that silk hydrogel placement turned the stroke microenvironment into a hospitable microenvironment.

The cellular mechanism(s) underlying these microenvironment changes remain to be elucidated, but newly formed blood vessels or direct infiltration through the surrounding parenchyma host tissue are potentially involved. This scenario is plausible because endothelial cell survival, growth, and microvascular network formation were already evident at 2 months post stroke[158]. Similar findings have been reported for porcine-derived urinary bladder ECM hydrogels[83]. Clearly, cells are required for improving functional outcomes

in stroke. Endogenous cell recruitment is desirable to reduce treatment complexity, but its effects are likely to be finite. Therefore, exogenous cell applications are important. For example, application of MSCs to acute stroke lesions using self-assembling silk hydrogels 2% [w/v] improved functional recovery and restitution of stroke-damaged neuronal circuitry[63].

3.6 Conclusion

I demonstrate that injection of silk hydrogels into a chronic stroke lesion resulted in retention of the silk hydrogel within the lesion cavity and excellent host tissue integration. Evidence of silk hydrogel degradation, mediated by invading macrophages, was evident at 6 months and was more widespread at 12 months. The applied silk hydrogel triggered tissue remodeling by decreasing post-stroke astrogliosis and inflammation, thereby leading to an enhanced polarization toward an M2-like macrophage phenotype. Endogenous proliferation of neural progenitor cells was also observed in the silk hydrogel. Our findings show that silk hydrogels are degraded over time in the stroke epicenter and reduce glial scarring, while supporting neural progenitor cell proliferation.

CHAPTER 4
THESIS CONCLUSION AND FUTURE DIRECTION

Chapter summary:

This chapter provides a summary of the outcomes of this thesis and suggestions for future work. The research outputs of the thesis included: (i) the impact of viscoelasticity on cell proliferation, cellular gene expression, and paracrine release by hMSCs cultured on 2D silk hydrogels (Phuagkhaopong *et al.* 2021. ACS Appl. Mater. Interfaces. 13(26): 30420–30433)[106], and (ii) assessment of biodegradation and de novo tissue formation mediated by an engineered self-assembling silk fibroin hydrogel implant in a rat model of chronic ischemic stroke (manuscript in preparation). I have also contributed to additional manuscripts as a co-author (see Appendix). For future work, based on the main findings of this thesis, there are many areas that would benefit from further investigation for example an examination of the impact of stress relaxation on MSCs embedded within 3D silk hydrogels and the establishment of the effects of an MSC−silk hydrogel system in an experimental stroke model.

4.1 Thesis conclusions

Renewed interest in silk for biomedical applications over the past two decades has resulted in the translation of several silk products from bench to bedside. For example, in 2013, Prof. David Kaplan and co-workers at Tufts University launched the Seri Surgical Scaffold™, which was the first new Class II silk-based medical device introduced to the market in more than 100 years. This scaffold is used in plastic surgeries, such as breast reconstructions. The approval of Seri Surgical Scaffold™ has been followed by an increasing number of research reports on silk biomaterials. In 2018, the FDA approved Silk Voice® for vocal cord augmentation. Silk Voice® contains reverse-engineered silk and is the first product approved for human use that has used this technology. Reverse-engineered silk has also been used to generate silk hydrogels for use as delivery matrices for controlled drug release [56] and cell-based therapy. Since the start of this PhD, a few studies have used cell-loaded silk hydrogels for stroke treatment.[65,66] However, many aspects relating to self-assembled silk hydrogels are still unknown, including their viscoelastic behavior. Therefore, the mission of this thesis was to fill in some of these knowledge gaps, especially those related to the development of self-assembling silk hydrogels that can serve as ECM mimetics for cell therapy.

The first part of this thesis examined the impact of stress relaxation of silk hydrogels on primary hMSCs cultured in 2D culture. Bone marrow-derived hMSCs, which are widely used for cell-based therapies,

were cultured on viscoelastic and elastic hydrogels. The faster stress relaxation of viscoelastic hydrogels enhanced the expression of genes for insulin, HNF-1A, and SOX-2 in the cultured hMSCs, whereas elastic silk hydrogel substrates promoted the expression of IL-1β, IL-6, LIF, BMP-6, BMP-7, and protein tyrosine phosphatase receptor type C. The two hydrogel types also induced different extracellular protein and metabolomic profiles in the hMSCs. For example, cells cultured on elastic hydrogels showed greater activation of IL-1β signaling and a higher consumption of glucose and glutamine, coupled with a higher secretion of lactate, compared with MSCs grown on viscoelastic substrates. These cellular responses to substrate stress relaxation were mediated by mechanosensitive RhoA and/or YAP/TAZ signaling.

The second part of this thesis explored the long-term tissue response toward silk hydrogels implanted into an experimental stroke model. One of the most interesting observation was that transplanted silk material promoted brain tissue repair, as this confirmed that silk, on its own, and even in the absence of a therapeutic payload, could positively modulate the disease microenvironment. Viscoelastic hydrogels were chosen for this study because this type of crosslinking best matches brain tissue mechanics. Stereotactic injection of a hydrogel into the ischemic stroke epicenter in rats induced a host cell response that cumulated in an invasion of astrocytes (GFAP+) and neuronal progenitor cells (DCX+/Ki67+) into the lesion. These cells then promoted tissue remodeling to form "new brain tissue" that provided new neuronal capacity. One can only speculate how this capacity might be utilized (or already contributes to improvement in disease symptoms). Degradation of the implanted silk hydrogel was evidenced by an increase in the numbers of positive CD11b macrophages/ microglia identified as M2 macrophages and co-occurrence of M1 and M2 macrophages. Overall, this study demonstrated that silk hydrogels are able to mimic the ECM and provide a supportive matrix that cells can populate.

4.2 Future directions

The results from this thesis now indicate interesting new avenues to pursue and new questions to address by other researchers (i.e., this thesis advances our knowledge, answers the questions it was intended to address, and its findings now can guide new research directions). I have summarized some of these potential research directions below.

4.2.1 Impact of stress relaxation on cellular response in 3D culture.

The findings of this thesis confirm the emergence of silk fibroin-based materials as promising platforms for mimicking the ECM to impact cell biology. MSCs clearly respond to their surrounding culture

microenvironment, including the presence of ECM-like substrates. Here, substrate stress relaxation was investigated (Chapter 2); however, the use of a flat 2D cell culture model cannot fully mimic the physiologically relevant microenvironment of cells in tissues. Under physiologically normal conditions, cells typically experience a 3D substrate interface; this architecture is also relevant in the context of the delivery of cells to lesioned areas. Therefore, these studies on the impact of stress relaxation in silk hydrogels should next be studied using 3D cultures to confirm the validity of data obtained using oversimplified 2D models and unrepresentative physiological conditions. This knowledge is important for refining and translating the design of hydrogel-based biomaterials for tissue engineering applications. For this future work, hMSCs will be cultured on 3D silk hydrogels that show slow and fast rates of stress relaxation. The cellular responses will be monitored using the currently established toolbox to assess the potential of silk hydrogels to support MSC biology.

4.2.2 Impact of viscoplasticity of silk hydrogels on cell responses.

This thesis has demonstrated that viscoelastic culture substrates regulate MSC behavior by triggering cell–matrix mechanotransduction. However, unlike cells in culture, cells in tissues exhibit complex mechanical behaviors because tissues can contain purely viscous fluids, where all the input deformation energy can be dissipated, as well as combinations of viscoelastic (time-dependent stress relaxation, e.g., brain[26], fat[28], breast[29], muscle, and liver tissue[30]) and viscoplastic (irreversible or plastic deformations, e.g., skin, tendon, traumatic brain injury, and traumatic aortic rupture) components[184]. Some materials may also have both viscoelastic and viscoplastic mechanics or exhibit irreversible deformations in response to an applied stress. For example, Mooney et al. created viscoelastic and viscoplastic PEG-alginate hydrogels that showed similar plasticity to native ECM collagen networks and subsequently showed that matrix plasticity controlled MSC spreading, proliferation, and gene expression[133]. Therefore, the design of biomaterials for regenerative medicine should also interrogate the importance of viscoplasticity, independent of storage modulus, stress relaxation, and matrix degradation. Plasticity measurements of a hydrogel (i.e., tests of its ability to irreversibly deform in response to applied stress) should include creep tests (strain [ϵ] response by time at constant stress [σ]) and creep–recovery tests (stress release after a creep test). The degree of plasticity will be determined by the ratio of irreversible strain to total strain [185]. Silk hydrogels with desired plasticity characteristics could be designed by a combination of covalent and weak crosslinks with low connectivity[186]. Understanding the biological responses of MSCs to these characteristics of silk hydrogels is likely to further enhance the potential of silk hydrogel materials for use in cell-based therapy.

4.2.3 Advancing cell characterization.

Obtaining spatially localized metabolic profiles of M1-like and M2-like macrophages in rat brain tissues using time-of-flight secondary ion mass spectrometry (ToF-SIMS) analysis would help to further understand the immune response to trigger tissue regeneration. Chapter 3 presented immunofluorescence data used to subdivide the macrophages found in the silk hydrogel implants into M1-like and M2-like phenotypes. Off-shoot studies should now use ToF-SIMS analysis to distinguish M1 and M2 macrophages according to the atomic mass spectra (m/z) of their unique spatial metabolic profiles (i.e., amino acid and lipid fragment ions) [187]. Metal-conjugated antibody labeling could be used in ToF-SIMS to probe M1 and M2 macrophage distributions in brain sections. The resulting metabolite profiles could then be used to provide high spatial resolution images of metabolites specific to M1 and M2 macrophages. To conduct this work, brain sections would be placed on glass slides and stained with specific antibodies directly conjugated to metals (such as gadolinium or neodymium) [188]. The working hypothesis is that the amounts of secondary metal ions detected by ToF-SIMS should reflect both the distribution and the amount of protein to which the corresponding antibodies were raised. In addition, ToF-SIMS can be particularly beneficial because multiplexed protein profiles can be simultaneously detected in one sample by conjugating primary antibodies with different metal isotopes. The ToF-SIMS technique could help to visualize normal brain and the ischemic border by detecting the atomic mass of ischemia-related molecules that are generally produced around the damaged areas (e.g., lipid peroxide 4-hydroxy-2-nonenal ($C_9H_{16}O_2$, MW 156.11) and a deoxyribose nucleic acid (DNA) fragment 8-OHdG ($C_{10}H_{13}N_5O_5$, MW 283.09) [189]. These types of studies could be conducted, with the metrology expertise provided by National Physical Laboratory Scotland, in the ToF-SIMS facility available at CMAC, located at the Technology Innovation Centre at the University of Strathclyde.

4.2.4 Optimizing MSC−silk hydrogel systems in an experimental stroke model.

This thesis research has confirmed the potential use of self-assembling silk hydrogels in the context of stroke therapy (Chapter 3). However, the stereotactic injections were performed without imaging guidance, which is one limitation of the present study. Locating the stroke lesion area was difficult using non-invasive imaging, as was identifying silk hydrogel degradation over time. Therefore, the future use of non-invasive image-guided techniques, such as magnetic resonance imaging, would be invaluable for understanding and further advancing this hydrogel technology.

Another limitation identified by this thesis research is that *B. mori* silk fibroin lacks the RGD sequence required for integrin-mediated cell attachment. This lack of RGD reduces the ability of MSCs to readily grow on/in silk hydrogels. Cell attachment could conceivably be improved by modification of silk fibroin with the cell attachment cues (e.g., RGD) found in native ECM.

Chapter 3 presented the results for the implantation of silk hydrogels without any exogenous cells. The next step would be to establish the ability of self-assembling silk hydrogels to both encapsulate and deliver MSCs to the stroke epicenter to promote brain repair. One important consideration for the tissue remodeling process is to balance the rate of material degradation to that of tissue formation. This type of evaluation would establish when the embedded cells cease proliferation and the longevity of the implanted silk hydrogels in the brain. This knowledge is important for understanding the cellular/molecular mechanisms of tissue remodeling and, ultimately, *in vivo* repair. This thesis research explored the use of only one silk hydrogel concentration 4% [w/v]. Therefore, future work should determine whether degradation of silk hydrogel depends on the silk hydrogel concentration.

In recent years, an unprecedented amount of scientific work has advanced the development of cell-based strategies, particularly those using hMSCs. However, clinical outcomes have not achieved the results that were anticipated based on promising preclinical work[186]. Several additional factors (e.g., patient-to-patient variability, long-term survival of the grafted cells) might have contributed to these disappointing clinical failures and will also need to be investigated in future[108].

REFERENCES

(1) Andersson, M.; Johansson, J.; Rising, A. Silk Spinning in Silkworms and Spiders. *Int J Mol Sci* **2016**, *17* (8). DOI: 10.3390/ijms17081290.

(2) Cho, S. Y.; Yun, Y. S.; Lee, S.; Jang, D.; Park, K. Y.; Kim, J. K.; Kim, B. H.; Kang, K.; Kaplan, D. L.; Jin, H. J. Carbonization of a stable beta-sheet-rich silk protein into a pseudographitic pyroprotein. *Nat Commun* **2015**, *6*, 7145. DOI: 10.1038/ncomms8145.

(3) Holland, C.; Numata, K.; Rnjak-Kovacina, J.; Seib, F. P. The Biomedical Use of Silk: Past, Present, Future. *Adv Healthc Mater* **2019**, *8* (1), e1800465. DOI: 10.1002/adhm.201800465.

(4) Vollrath, F.; Knight, D. P. Liquid crystalline spinning of spider silk. *Nature* **2001**, *410* (6828), 541-548. DOI: 10.1038/35069000.

(5) Chalmers, I. Provision of consent. *Lancet* **2003**, *362* (9384), 663-664. DOI: 10.1016/S0140-6736(03)14164-5.

(6) Kwak, H. W.; Ju, J. E.; Shin, M.; Holland, C.; Lee, K. H. Sericin Promotes Fibroin Silk I Stabilization Across a Phase-Separation. *Biomacromolecules* **2017**, *18* (8), 2343-2349. DOI: 10.1021/acs.biomac.7b00549.

(7) Qi, Y.; Wang, H.; Wei, K.; Yang, Y.; Zheng, R. Y.; Kim, I. S.; Zhang, K. Q. A Review of Structure Construction of Silk Fibroin Biomaterials from Single Structures to Multi-Level Structures. *Int J Mol Sci* **2017**, *18* (3). DOI: 10.3390/ijms18030237.

(8) Muffly, T. M.; Tizzano, A. P.; Walters, M. D. The history and evolution of sutures in pelvic surgery. *J R Soc Med* **2011**, *104* (3), 107-112. DOI: 10.1258/jrsm.2010.100243.

(9) Thurber, A. E.; Omenetto, F. G.; Kaplan, D. L. In vivo bioresponses to silk proteins. *Biomaterials* **2015**, *71*, 145-157. DOI: 10.1016/j.biomaterials.2015.08.039.

(10) Aramwit, P.; Kanokpanont, S.; De-Eknamkul, W.; Srichana, T. Monitoring of inflammatory mediators induced by silk sericin. *J Biosci Bioeng* **2009**, *107* (5), 556-561. DOI: 10.1016/j.jbiosc.2008.12.012.

(11) Wang, Z.; Zhang, Y.; Zhang, J.; Huang, L.; Liu, J.; Li, Y.; Zhang, G.; Kundu, S. C.; Wang, L. Exploring natural silk protein sericin for regenerative medicine: an injectable, photoluminescent, cell-adhesive 3D hydrogel. *Sci Rep* **2014**, *4*, 7064. DOI: 10.1038/srep07064.

(12) Bachmann, C.; Schmidt, S.; Staebler, A.; Fehm, T.; Fend, F.; Schittenhelm, J.; Wallwiener, D.; Grischke, E. CNS metastases in breast cancer patients: prognostic implications of tumor subtype. *Med Oncol* **2015**, *32* (1), 400. DOI: 10.1007/s12032-014-0400-2.

(13) Reeves, A. R.; Spiller, K. L.; Freytes, D. O.; Vunjak-Novakovic, G.; Kaplan, D. L. Controlled release of cytokines using silk-biomaterials for macrophage polarization. *Biomaterials* **2015**, *73*, 272-283. DOI: 10.1016/j.biomaterials.2015.09.027.

(14) Numata, K.; Cebe, P.; Kaplan, D. L. Mechanism of enzymatic degradation of beta-sheet crystals. *Biomaterials* **2010**, *31* (10), 2926-2933. DOI: 10.1016/j.biomaterials.2009.12.026.

(15) Wang, Y.; Rudym, D. D.; Walsh, A.; Abrahamsen, L.; Kim, H. J.; Kim, H. S.; Kirker-Head, C.; Kaplan, D. L. In vivo degradation of three-dimensional silk fibroin scaffolds. *Biomaterials* **2008**, *29* (24-25), 3415-3428. DOI: 10.1016/j.biomaterials.2008.05.002.

(16) Brown, J.; Lu, C. L.; Coburn, J.; Kaplan, D. L. Impact of silk biomaterial structure on proteolysis. *Acta Biomater* **2015**, *11*, 212-221. DOI: 10.1016/j.actbio.2014.09.013.

(17) Elisseeff, J. Hydrogels: structure starts to gel. *Nat Mater* **2008**, *7* (4), 271-273. DOI: 10.1038/nmat2147.

(18) Geckil, H.; Xu, F.; Zhang, X.; Moon, S.; Demirci, U. Engineering hydrogels as extracellular matrix mimics. *Nanomedicine (Lond)* **2010**, *5* (3), 469-484. DOI: 10.2217/nnm.10.12.

(19) Lee, K. Y.; Mooney, D. J. Hydrogels for tissue engineering. *Chem Rev* **2001**, *101* (7), 1869-1879.

(20) Hennink, W. E.; van Nostrum, C. F. Novel crosslinking methods to design hydrogels. *Advanced Drug Delivery Reviews* **2012**, *64*, 223-236. DOI: 10.1016/j.addr.2012.09.009.

(21) Ribeiro, V. P.; Pina, S.; Oliveira, J. M.; Reis, R. L. Silk Fibroin-Based Hydrogels and Scaffolds for Osteochondral Repair and Regeneration. *Adv Exp Med Biol* **2018**, *1058*, 305-325. DOI: 10.1007/978-3-319-76711-6_14.

(22) Han, H.; Ning, H.; Liu, S.; Lu, Q. P.; Fan, Z.; Lu, H.; Lu, G.; Kaplan, D. L. Silk Biomaterials with Vascularization Capacity. *Adv Funct Mater* **2016**, *26* (3), 421-436. DOI: 10.1002/adfm.201504160.

(23) Levental, I.; Georges, P. C.; Janmey, P. A. Soft biological materials and their impact on cell function. *Soft Matter* **2007**, *3* (3), 299-306. DOI: 10.1039/b610522j.

(24) Whitehead, A. K.; Barnett, H. H.; Caldorera-Moore, M. E.; Newman, J. J. Poly (ethylene glycol) hydrogel elasticity influences human mesenchymal stem cell behavior. *Regen Biomater* **2018**, *5* (3), 167-175. DOI: 10.1093/rb/rby008.

(25) Floren, M.; Bonani, W.; Dharmarajan, A.; Motta, A.; Migliaresi, C.; Tan, W. Human mesenchymal stem cells cultured on silk hydrogels with variable stiffness and growth factor differentiate into mature smooth muscle cell phenotype. *Acta Biomater* **2016**, *31*, 156-166. DOI: 10.1016/j.actbio.2015.11.051.

(26) Chaudhuri, O.; Gu, L.; Klumpers, D.; Darnell, M.; Bencherif, S. A.; Weaver, J. C.; Huebsch, N.; Lee, H. P.; Lippens, E.; Duda, G. N.; et al. Hydrogels with tunable stress relaxation regulate stem cell fate and activity. *Nat Mater* **2016**, *15* (3), 326-334. DOI: 10.1038/nmat4489.

(27) Green, E. M.; Mansfield, J. C.; Bell, J. S.; Winlove, C. P. The structure and micromechanics of elastic tissue. *Interface Focus* **2014**, *4* (2), 20130058. DOI: 10.1098/rsfs.2013.0058.

(28) Geerligs, M.; Peters, G. W.; Ackermans, P. A.; Oomens, C. W.; Baaijens, F. P. Linear viscoelastic behavior of subcutaneous adipose tissue. *Biorheology* **2008**, *45* (6), 677-688.

(29) Sinkus, R.; Siegmann, K.; Xydeas, T.; Tanter, M.; Claussen, C.; Fink, M. MR elastography of breast lesions: understanding the solid/liquid duality can improve the specificity of contrast-enhanced MR mammography. *Magn Reson Med* **2007**, *58* (6), 1135-1144. DOI: 10.1002/mrm.21404.

(30) Liu, Z.; Bilston, L. On the viscoelastic character of liver tissue: experiments and modelling of the linear behaviour. *Biorheology* **2000**, *37* (3), 191-201.

(31) Sommerfeld, S. D.; Elisseeff, J. H. Time to Relax: Mechanical Stress Release Guides Stem Cell Responses. *Cell Stem Cell* **2016**, *18* (2), 166-167. DOI: 10.1016/j.stem.2016.01.020.

(32) Lee, J. H.; Kim, H. W. Emerging properties of hydrogels in tissue engineering. *J Tissue Eng* **2018**, *9*, 2041731418768285. DOI: 10.1177/2041731418768285.

(33) Oliviero, O.; Ventre, M.; Netti, P. A. Functional porous hydrogels to study angiogenesis under the effect of controlled release of vascular endothelial growth factor. *Acta Biomater* **2012**, *8* (9), 3294-3301. DOI: 10.1016/j.actbio.2012.05.019.

(34) Dziubla, T. D.; Lowman, A. M. Vascularization of PEG-grafted macroporous hydrogel sponges: a three-dimensional in vitro angiogenesis model using human microvascular endothelial cells. *J Biomed Mater Res A* **2004**, *68* (4), 603-614. DOI: 10.1002/jbm.a.20023.

(35) Zeng, L.; Yao, Y.; Wang, D. A.; Chen, X. Effect of microcavitary alginate hydrogel with different pore sizes on chondrocyte culture for cartilage tissue engineering. *Mater Sci Eng C Mater Biol Appl* **2014**, *34*, 168-175. DOI: 10.1016/j.msec.2013.09.003.

(36) Matsiko, A.; Gleeson, J. P.; O'Brien, F. J. Scaffold mean pore size influences mesenchymal stem cell chondrogenic differentiation and matrix deposition. *Tissue Eng Part A* **2015**, *21* (3-4), 486-497. DOI: 10.1089/ten.TEA.2013.0545.

(37) Phadke, A.; Hwang, Y.; Kim, S. H.; Kim, S. H.; Yamaguchi, T.; Masuda, K.; Varghese, S. Effect of scaffold microarchitecture on osteogenic differentiation of human mesenchymal stem cells. *Eur Cell Mater* **2013**, *25*, 114-129.

(38) Abdeen, A. A.; Weiss, J. B.; Lee, J.; Kilian, K. A. Matrix composition and mechanics direct proangiogenic signaling from mesenchymal stem cells. *Tissue Eng Part A* **2014**, *20* (19-20), 2737-2745. DOI: 10.1089/ten.TEA.2013.0661.

(39) Kasper, G.; Dankert, N.; Tuischer, J.; Hoeft, M.; Gaber, T.; Glaeser, J. D.; Zander, D.; Tschirschmann, M.; Thompson, M.; Matziolis, G.; et al. Mesenchymal stem cells regulate angiogenesis according to their mechanical environment. *Stem Cells* **2007**, *25* (4), 903-910. DOI: 10.1634/stemcells.2006-0432.

(40) Seib, F. P.; Prewitz, M.; Werner, C.; Bornhauser, M. Matrix elasticity regulates the secretory profile of human bone marrow-derived multipotent mesenchymal stromal cells (MSCs). *Biochem Biophys Res Commun* **2009**, *389* (4), 663-667. DOI: 10.1016/j.bbrc.2009.09.051.

(41) Lee, H. P.; Gu, L.; Mooney, D. J.; Levenston, M. E.; Chaudhuri, O. Mechanical confinement regulates cartilage matrix formation by chondrocytes. *Nat Mater* **2017**, *16* (12), 1243-1251. DOI: 10.1038/nmat4993.

(42) Tang, S.; Ma, H.; Tu, H. C.; Wang, H. R.; Lin, P. C.; Anseth, K. S. Adaptable Fast Relaxing Boronate-Based Hydrogels for Probing Cell-Matrix Interactions. *Adv Sci (Weinh)* **2018**, *5* (9), 1800638. DOI: 10.1002/advs.201800638.

(43) McKinnon, D. D.; Domaille, D. W.; Cha, J. N.; Anseth, K. S. Biophysically defined and cytocompatible covalently adaptable networks as viscoelastic 3D cell culture systems. *Adv Mater* **2014**, *26* (6), 865-872. DOI: 10.1002/adma.201303680.

(44) McKinnon, D. D.; Domaille, D. W.; Brown, T. E.; Kyburz, K. A.; Kiyotake, E.; Cha, J. N.; Anseth, K. S. Measuring cellular forces using bis-aliphatic hydrazone crosslinked stress-relaxing hydrogels. *Soft Matter* **2014**, *10* (46), 9230-9236. DOI: 10.1039/c4sm01365d.

(45) Lou, J.; Stowers, R.; Nam, S.; Xia, Y.; Chaudhuri, O. Stress relaxing hyaluronic acid-collagen hydrogels promote cell spreading, fiber remodeling, and focal adhesion formation in 3D cell culture. *Biomaterials* **2018**, *154*, 213-222. DOI: 10.1016/j.biomaterials.2017.11.004.

(46) Chaudhuri, O.; Gu, L.; Darnell, M.; Klumpers, D.; Bencherif, S. A.; Weaver, J. C.; Huebsch, N.; Mooney, D. J. Substrate stress relaxation regulates cell spreading. *Nat Commun* **2015**, *6*, 6364. DOI: 10.1038/ncomms7365.

(47) Kuboki, T.; Kantawong, F.; Burchmore, R.; Dalby, M. J.; Kidoaki, S. 2D-DIGE proteomic analysis of mesenchymal stem cell cultured on the elasticity-tunable hydrogels. *Cell Struct Funct* **2012**, *37* (2), 127-139.

(48) Yeung, T.; Georges, P. C.; Flanagan, L. A.; Marg, B.; Ortiz, M.; Funaki, M.; Zahir, N.; Ming, W.; Weaver, V.; Janmey, P. A. Effects of substrate stiffness on cell morphology, cytoskeletal structure, and adhesion. *Cell Motil Cytoskeleton* **2005**, *60* (1), 24-34. DOI: 10.1002/cm.20041.

(49) Bauer, A.; Gu, L.; Kwee, B.; Li, W. A.; Dellacherie, M.; Celiz, A. D.; Mooney, D. J. Hydrogel substrate stress-relaxation regulates the spreading and proliferation of mouse myoblasts. *Acta Biomater* **2017**, *62*, 82-90. DOI: 10.1016/j.actbio.2017.08.041.

(50) Cameron, A. R.; Frith, J. E.; Gomez, G. A.; Yap, A. S.; Cooper-White, J. J. The effect of time-dependent deformation of viscoelastic hydrogels on myogenic induction and Rac1 activity in mesenchymal stem cells. *Biomaterials* **2014**, *35* (6), 1857-1868. DOI: 10.1016/j.biomaterials.2013.11.023.

(51) Engler, A. J.; Sen, S.; Sweeney, H. L.; Discher, D. E. Matrix elasticity directs stem cell lineage specification. *Cell* **2006**, *126* (4), 677-689. DOI: 10.1016/j.cell.2006.06.044.

(52) Darnell, M.; Young, S.; Gu, L.; Shah, N.; Lippens, E.; Weaver, J.; Duda, G.; Mooney, D. Substrate Stress-Relaxation Regulates Scaffold Remodeling and Bone Formation In Vivo. *Adv Healthc Mater* **2017**, *6* (1). DOI: 10.1002/adhm.201601185.

(53) Wang, X.; Wenk, E.; Matsumoto, A.; Meinel, L.; Li, C.; Kaplan, D. L. Silk microspheres for encapsulation and controlled release. *J Control Release* **2007**, *117* (3), 360-370. DOI: 10.1016/j.jconrel.2006.11.021.

(54) Yan, L. P.; Oliveira, J. M.; Oliveira, A. L.; Reis, R. L. Core-shell silk hydrogels with spatially tuned conformations as drug-delivery system. *J Tissue Eng Regen Med* **2017**, *11* (11), 3168-3177. DOI: 10.1002/term.2226.

(55) Nazarov, R.; Jin, H. J.; Kaplan, D. L. Porous 3-D scaffolds from regenerated silk fibroin. *Biomacromolecules* **2004**, *5* (3), 718-726. DOI: 10.1021/bm034327e.

(56) Seib, F. P.; Pritchard, E. M.; Kaplan, D. L. Self-assembling doxorubicin silk hydrogels for the focal treatment of primary breast cancer. *Adv Funct Mater* **2013**, *23* (1), 58-65. DOI: 10.1002/adfm.201201238.

(57) Fini, M.; Motta, A.; Torricelli, P.; Giavaresi, G.; Nicoli Aldini, N.; Tschon, M.; Giardino, R.; Migliaresi, C. The healing of confined critical size cancellous defects in the presence of silk fibroin hydrogel. *Biomaterials* **2005**, *26* (17), 3527-3536. DOI: 10.1016/j.biomaterials.2004.09.040.

(58) Morita, Y.; Tomita, N.; Aoki, H.; Sonobe, M.; Wakitani, S.; Tamada, Y.; Suguro, T.; Ikeuchi, K. Frictional properties of regenerated cartilage in vitro. *J Biomech* **2006**, *39* (1), 103-109. DOI: 10.1016/j.jbiomech.2004.10.031.

(59) Lin, Y.; Xia, X.; Shang, K.; Elia, R.; Huang, W.; Cebe, P.; Leisk, G.; Omenetto, F.; Kaplan, D. L. Tuning chemical and physical cross-links in silk electrogels for morphological analysis and mechanical reinforcement. *Biomacromolecules* **2013**, *14* (8), 2629-2635. DOI: 10.1021/bm4004892.

(60) Yucel, T.; Cebe, P.; Kaplan, D. L. Vortex-induced injectable silk fibroin hydrogels. *Biophys J* **2009**, *97* (7), 2044-2050. DOI: 10.1016/j.bpj.2009.07.028.

(61) Koch, F.; Muller, M.; Konig, F.; Meyer, N.; Gattlen, J.; Pieles, U.; Peters, K.; Kreikemeyer, B.; Mathes, S.; Saxer, S. Mechanical characteristics of beta sheet-forming peptide hydrogels are dependent on peptide sequence, concentration and buffer composition. *R Soc Open Sci* **2018**, *5* (3), 171562. DOI: 10.1098/rsos.171562.

(62) Fernandez-Garcia, L.; Mari-Buye, N.; Barios, J. A.; Madurga, R.; Elices, M.; Perez-Rigueiro, J.; Ramos, M.; Guinea, G. V.; Gonzalez-Nieto, D. Safety and tolerability of silk fibroin hydrogels implanted into the mouse brain. *Acta Biomater* **2016**, *45*, 262-275. DOI: 10.1016/j.actbio.2016.09.003.

(63) Fernandez-Garcia, L.; Perez-Rigueiro, J.; Martinez-Murillo, R.; Panetsos, F.; Ramos, M.; Guinea, G. V.; Gonzalez-Nieto, D. Cortical Reshaping and Functional Recovery Induced by Silk Fibroin Hydrogels-Encapsulated Stem Cells Implanted in Stroke Animals. *Front Cell Neurosci* **2018**, *12*, 296. DOI: 10.3389/fncel.2018.00296.

(64) Martín-Martín, Y.; Fernández-García, L.; Sanchez-Rebato, M. H.; Marí-Buyé, N.; Rojo, F. J.; Pérez-Rigueiro, J.; Ramos, M.; Guinea, G. V.; Panetsos, F.; González-Nieto, D. Evaluation of Neurosecretome from Mesenchymal Stem Cells Encapsulated in Silk Fibroin Hydrogels. *Sci Rep* **2019**, *9* (1), 8801. DOI: 10.1038/s41598-019-45238-4.

(65) Osama, I.; Gorenkova, N.; McKittrick, C. M.; Wongpinyochit, T.; Goudie, A.; Seib, F. P.; Carswell, H. V. O. In vitro studies on space-conforming self-assembling silk hydrogels as a mesenchymal stem cell-support matrix suitable for minimally invasive brain application. *Sci Rep* **2018**, *8* (1), 13655. DOI: 10.1038/s41598-018-31905-5.

(66) Gorenkova, N.; Osama, I.; Seib, F. P.; Carswell, H. V. O. In Vivo Evaluation of Engineered Self-Assembling Silk Fibroin Hydrogels after Intracerebral Injection in a Rat Stroke Model. *ACS Biomaterials Science & Engineering* **2018**, *5* (2), 859-869. DOI: 10.1021/acsbiomaterials.8b01024.

(67) Donkor, E. S. Stroke in the 21. *Stroke Res Treat* **2018**, *2018*, 3238165. DOI: 10.1155/2018/3238165.

(68) Sofroniew, M. V.; Vinters, H. V. Astrocytes: biology and pathology. *Acta Neuropathol* **2010**, *119* (1), 7-35. DOI: 10.1007/s00401-009-0619-8.

(69) Gravanis, I.; Tsirka, S. E. Tissue-type plasminogen activator as a therapeutic target in stroke. *Expert Opin Ther Targets* **2008**, *12* (2), 159-170. DOI: 10.1517/14728222.12.2.159.

(70) Saver, J. L.; Fonarow, G. C.; Smith, E. E.; Reeves, M. J.; Grau-Sepulveda, M. V.; Pan, W.; Olson, D. M.; Hernandez, A. F.; Peterson, E. D.; Schwamm, L. H. Time to treatment with intravenous tissue plasminogen activator and outcome from acute ischemic stroke. *JAMA* **2013**, *309* (23), 2480-2488. DOI: 10.1001/jama.2013.6959.

(71) Moreau, F.; Patel, S.; Lauzon, M. L.; McCreary, C. R.; Goyal, M.; Frayne, R.; Demchuk, A. M.; Coutts, S. B.; Smith, E. E. Cavitation after acute symptomatic lacunar stroke depends on time, location, and MRI sequence. *Stroke* **2012**, *43* (7), 1837-1842. DOI: 10.1161/STROKEAHA.111.647859.

(72) Modo, M.; Badylak, S. F. A roadmap for promoting endogenous in situ tissue restoration using inductive bioscaffolds after acute brain injury. *Brain Res Bull* **2019**, *150*, 136-149. DOI: 10.1016/j.brainresbull.2019.05.013.

(73) Love, C. J.; Selim, M.; Spector, M.; Lo, E. H. Biomaterials for Stroke Therapy. *Stroke* **2019**, *50* (8), 2278-2284. DOI: 10.1161/STROKEAHA.118.023721.

(74) Wieloch, T.; Nikolich, K. Mechanisms of neural plasticity following brain injury. *Curr Opin Neurobiol* **2006**, *16* (3), 258-264. DOI: 10.1016/j.conb.2006.05.011.

(75) Cook, J.; Lewandowsky, S.; Ecker, U. K. H. Neutralizing misinformation through inoculation: Exposing misleading argumentation techniques reduces their influence. *PLoS One* **2017**, *12* (5), e0175799. DOI: 10.1371/journal.pone.0175799.

(76) Massensini, A. R.; Ghuman, H.; Saldin, L. T.; Medberry, C. J.; Keane, T. J.; Nicholls, F. J.; Velankar, S. S.; Badylak, S. F.; Modo, M. Concentration-dependent rheological properties of ECM hydrogel for intracerebral delivery to a stroke cavity. *Acta Biomater* **2015**, *27*, 116-130. DOI: 10.1016/j.actbio.2015.08.040.

(77) Modo, M. Bioscaffold-Induced Brain Tissue Regeneration. *Front Neurosci* **2019**, *13*, 1156. DOI: 10.3389/fnins.2019.01156.

(78) Nih, L. R.; Carmichael, S. T.; Segura, T. Hydrogels for brain repair after stroke: an emerging treatment option. *Curr Opin Biotechnol* **2016**, *40*, 155-163. DOI: 10.1016/j.copbio.2016.04.021.

(79) González-Nieto, D.; Fernández-García, L.; Pérez-Rigueiro, J.; Guinea, G. V.; Panetsos, F. Hydrogels-Assisted Cell Engraftment for Repairing the Stroke-Damaged Brain: Chimera or Reality. *Polymers (Basel)* **2018**, *10* (2). DOI: 10.3390/polym10020184.

(80) Lin, P. H.; Dong, Q.; Chew, S. Y. Injectable hydrogels in stroke and spinal cord injury treatment: a review on hydrogel materials, cell–matrix interactions and glial involvement. *Materials Advances* **2021**, *2* (8), 2561-2583.

(81) Nih, L. R.; Sideris, E.; Carmichael, S. T.; Segura, T. Injection of Microporous Annealing Particle (MAP) Hydrogels in the Stroke Cavity Reduces Gliosis and Inflammation and Promotes NPC Migration to the Lesion. *Adv Mater* **2017**, *29* (32). DOI: 10.1002/adma.201606471.

(82) Ghuman, H.; Mauney, C.; Donnelly, J.; Massensini, A. R.; Badylak, S. F.; Modo, M. Biodegradation of ECM hydrogel promotes endogenous brain tissue restoration in a rat model of stroke. *Acta Biomater* **2018**, *80*, 66-84. DOI: 10.1016/j.actbio.2018.09.020.

(83) Ghuman, H.; Gerwig, M.; Nicholls, F. J.; Liu, J. R.; Donnelly, J.; Badylak, S. F.; Modo, M. Long-term retention of ECM hydrogel after implantation into a sub-acute stroke cavity reduces lesion volume. *Acta Biomater* **2017**, *63*, 50-63. DOI: 10.1016/j.actbio.2017.09.011.

(84) Jian, W. H.; Wang, H. C.; Kuan, C. H.; Chen, M. H.; Wu, H. C.; Sun, J. S.; Wang, T. W. Glycosaminoglycan-based hybrid hydrogel encapsulated with polyelectrolyte complex nanoparticles for endogenous stem cell regulation in central nervous system regeneration. *Biomaterials* **2018**, *174*, 17-30. DOI: 10.1016/j.biomaterials.2018.05.009.

(85) Sundin, M.; Ringden, O.; Sundberg, B.; Nava, S.; Gotherstrom, C.; Le Blanc, K. No alloantibodies against mesenchymal stromal cells, but presence of anti-fetal calf serum antibodies, after transplantation in allogeneic hematopoietic stem cell recipients. *Haematologica* **2007**, *92* (9), 1208-1215. DOI: 10.3324/haematol.11446.

(86) In 't Anker, P. S.; Scherjon, S. A.; Kleijburg-van der Keur, C.; de Groot-Swings, G. M.; Claas, F. H.; Fibbe, W. E.; Kanhai, H. H. Isolation of mesenchymal stem cells of fetal or maternal origin from human placenta. *Stem Cells* **2004**, *22* (7), 1338-1345. DOI: 10.1634/stemcells.2004-0058.

(87) Bieback, K.; Kern, S.; Kluter, H.; Eichler, H. Critical parameters for the isolation of mesenchymal stem cells from umbilical cord blood. *Stem Cells* **2004**, *22* (4), 625-634. DOI: 10.1634/stemcells.22-4-625.

(88) Bortolotti, F.; Ukovich, L.; Razban, V.; Martinelli, V.; Ruozi, G.; Pelos, B.; Dore, F.; Giacca, M.; Zacchigna, S. In vivo therapeutic potential of mesenchymal stromal cells depends on the source and the isolation procedure. *Stem Cell Reports* **2015**, *4* (3), 332-339. DOI: 10.1016/j.stemcr.2015.01.001.

(89) Kean, T. J.; Lin, P.; Caplan, A. I.; Dennis, J. E. MSCs: Delivery Routes and Engraftment, Cell-Targeting Strategies, and Immune Modulation. *Stem Cells Int* **2013**, *2013*, 732742. DOI: 10.1155/2013/732742.

(90) Wechsler, L. R. Clinical trials of stroke therapy: which cells, which patients? *Stroke* **2009**, *40* (3 Suppl), S149-151. DOI: 10.1161/STROKEAHA.108.533208.

(91) Drury, J. L.; Mooney, D. J. Hydrogels for tissue engineering: scaffold design variables and applications. *Biomaterials* **2003**, *24* (24), 4337-4351.

(92) Detante, O.; Jaillard, A.; Moisan, A.; Barbieux, M.; Favre, I. M.; Garambois, K.; Hommel, M.; Remy, C. Biotherapies in stroke. *Rev Neurol (Paris)* **2014**, *170* (12), 779-798. DOI: 10.1016/j.neurol.2014.10.005.

(93) Bhasin, A.; Srivastava, M. V.; Mohanty, S.; Bhatia, R.; Kumaran, S. S.; Bose, S. Stem cell therapy: a clinical trial of stroke. *Clin Neurol Neurosurg* **2013**, *115* (7), 1003-1008. DOI: 10.1016/j.clineuro.2012.10.015.

(94) Taguchi, A. [Cell-Based Therapy for Stroke Patients]. *No Shinkei Geka* **2015**, *43* (12), 1071-1079. DOI: 10.11477/mf.1436203183.

(95) Kim, D. H.; Seo, Y. K.; Thambi, T.; Moon, G. J.; Son, J. P.; Li, G.; Park, J. H.; Lee, J. H.; Kim, H. H.; Lee, D. S.; et al. Enhancing neurogenesis and angiogenesis with target delivery of stromal cell derived factor-1alpha using a dual ionic pH-sensitive copolymer. *Biomaterials* **2015**, *61*, 115-125. DOI: 10.1016/j.biomaterials.2015.05.025.

(96) Aeschbach, R.; Amado, R.; Neukom, H. Formation of dityrosine cross-links in proteins by oxidation of tyrosine residues. *Biochim Biophys Acta* **1976**, *439* (2), 292-301. DOI: 10.1016/0005-2795(76)90064-7.

(97) Partlow, B. P.; Hanna, C. W.; Rnjak-Kovacina, J.; Moreau, J. E.; Applegate, M. B.; Burke, K. A.; Marelli, B.; Mitropoulos, A. N.; Omenetto, F. G.; Kaplan, D. L. Highly tunable elastomeric silk biomaterials. *Adv Funct Mater* **2014**, *24* (29), 4615-4624. DOI: 10.1002/adfm.201400526.

(98) Chirila, T. V.; Suzuki, S.; Papolla, C. A comparative investigation of Bombyx mori silk fibroin hydrogels generated by chemical and enzymatic cross-linking. *Biotechnol Appl Biochem* **2017**, *64* (6), 771-781. DOI: 10.1002/bab.1552.

(99) Su, D.; Yao, M.; Liu, J.; Zhong, Y.; Chen, X.; Shao, Z. Enhancing Mechanical Properties of Silk Fibroin Hydrogel through Restricting the Growth of beta-Sheet Domains. *ACS Appl Mater Interfaces* **2017**, *9* (20), 17489-17498. DOI: 10.1021/acsami.7b04623.

(100) Ribeiro, V. P.; Silva-Correia, J.; Goncalves, C.; Pina, S.; Radhouani, H.; Montonen, T.; Hyttinen, J.; Roy, A.; Oliveira, A. L.; Reis, R. L.; et al. Rapidly responsive silk fibroin hydrogels as an artificial matrix for the programmed tumor cells death. *PLoS One* **2018**, *13* (4), e0194441. DOI: 10.1371/journal.pone.0194441.

(101) Yan, L. P.; Silva-Correia, J.; Ribeiro, V. P.; Miranda-Goncalves, V.; Correia, C.; da Silva Morais, A.; Sousa, R. A.; Reis, R. M.; Oliveira, A. L.; Oliveira, J. M.; et al. Tumor Growth Suppression Induced by Biomimetic Silk Fibroin Hydrogels. *Sci Rep* **2016**, *6*, 31037. DOI: 10.1038/srep31037.

(102) Matsumoto, A.; Chen, J.; Collette, A. L.; Kim, U. J.; Altman, G. H.; Cebe, P.; Kaplan, D. L. Mechanisms of silk fibroin sol-gel transitions. *J Phys Chem B* **2006**, *110* (43), 21630-21638. DOI: 10.1021/jp056350v.

(103) Kim, U. J.; Park, J.; Li, C.; Jin, H. J.; Valluzzi, R.; Kaplan, D. L. Structure and properties of silk hydrogels. *Biomacromolecules* **2004**, *5* (3), 786-792. DOI: 10.1021/bm0345460.

(104) Sun, W.; Incitti, T.; Migliaresi, C.; Quattrone, A.; Casarosa, S.; Motta, A. Viability and neuronal differentiation of neural stem cells encapsulated in silk fibroin hydrogel functionalized with an IKVAV peptide. *J Tissue Eng Regen Med* **2017**, *11* (5), 1532-1541. DOI: 10.1002/term.2053.

(105) Wang, X.; Kluge, J. A.; Leisk, G. G.; Kaplan, D. L. Sonication-induced gelation of silk fibroin for cell encapsulation. *Biomaterials* **2008**, *29* (8), 1054-1064. DOI: 10.1016/j.biomaterials.2007.11.003.

(106) Phuagkhaopong, S.; Mendes, L.; Müller, K.; Wobus, M.; Bornhäuser, M.; Carswell, H. V. O.; Duarte, I. F.; Seib, F. P. Silk Hydrogel Substrate Stress Relaxation Primes Mesenchymal Stem Cell Behavior in 2D. *ACS Appl Mater Interfaces* **2021**, *13* (26), 30420-30433. DOI: 10.1021/acsami.1c09071.

(107) Prasad, S. Transconjunctival sutureless haptic fixation of posterior chamber IOL: a minimally traumatic approach for IOL rescue or secondary implantation. *Retina* **2013**, *33* (3), 657-660. DOI: 10.1097/IAE.0b013e31827b6499.

(108) Galipeau, J.; Sensébé, L. Mesenchymal Stromal Cells: Clinical Challenges and Therapeutic Opportunities. *Cell Stem Cell* **2018**, *22* (6), 824-833. DOI: 10.1016/j.stem.2018.05.004.

(109) Galleu, A.; Riffo-Vasquez, Y.; Trento, C.; Lomas, C.; Dolcetti, L.; Cheung, T. S.; von Bonin, M.; Barbieri, L.; Halai, K.; Ward, S.; et al. Apoptosis in mesenchymal stromal cells induces in vivo recipient-mediated immunomodulation. *Sci Transl Med* **2017**, *9* (416). DOI: 10.1126/scitranslmed.aam7828.

(110) Mao, A. S.; Özkale, B.; Shah, N. J.; Vining, K. H.; Descombes, T.; Zhang, L.; Tringides, C. M.; Wong, S. W.; Shin, J. W.; Scadden, D. T.; et al. Programmable microencapsulation for enhanced mesenchymal stem cell persistence and immunomodulation. *Proc Natl Acad Sci U S A* **2019**, *116* (31), 15392-15397. DOI: 10.1073/pnas.1819415116.

(111) Vining, K. H.; Mooney, D. J. Mechanical forces direct stem cell behaviour in development and regeneration. *Nat Rev Mol Cell Biol* **2017**, *18* (12), 728-742. DOI: 10.1038/nrm.2017.108.

(112) Bennett, M.; Cantini, M.; Reboud, J.; Cooper, J. M.; Roca-Cusachs, P.; Salmeron-Sanchez, M. Molecular clutch drives cell response to surface viscosity. *Proc Natl Acad Sci U S A* **2018**, *115* (6), 1192-1197. DOI: 10.1073/pnas.1710653115.

(113) Janani, G.; Kumar, M.; Chouhan, D.; Moses, J. C.; Gangrade, A.; Bhattacharjee, S.; Mandal, B. B. Insight into silk-based biomaterials: From physicochemical attributes to recent biomedical applications. *ACS Applied Bio Materials* **2019**, *2* (12), 5460-5491.

(114) Jewell, M.; Daunch, W.; Bengtson, B.; Mortarino, E. The development of SERI® Surgical Scaffold, an engineered biological scaffold. *Ann N Y Acad Sci* **2015**, *1358*, 44-55. DOI: 10.1111/nyas.12886.

(115) Reagan, M. R.; Seib, F. P.; McMillin, D. W.; Sage, E. K.; Mitsiades, C. S.; Janes, S. M.; Ghobrial, I. M.; Kaplan, D. L. Stem Cell Implants for Cancer Therapy: TRAIL-Expressing Mesenchymal Stem Cells Target Cancer Cells In Situ. *J Breast Cancer* **2012**, *15* (3), 273-282. DOI: 10.4048/jbc.2012.15.3.273.

(116) Seib, F. P. Reverse-engineered silk hydrogels for cell and drug delivery. *Ther Deliv* **2018**, *9* (6), 469-487. DOI: 10.4155/tde-2018-0016.

(117) Guan, Y.; You, H.; Cai, J.; Zhang, Q.; Yan, S.; You, R. Physically crosslinked silk fibroin/hyaluronic acid scaffolds. *Carbohydr Polym* **2020**, *239*, 116232. DOI: 10.1016/j.carbpol.2020.116232.

(118) Cui, X.; Soliman, B. G.; Alcala-Orozco, C. R.; Li, J.; Vis, M. A. M.; Santos, M.; Wise, S. G.; Levato, R.; Malda, J.; Woodfield, T. B. F.; et al. Rapid Photocrosslinking of Silk Hydrogels with High Cell Density and Enhanced Shape Fidelity. *Adv Healthc Mater* **2020**, *9* (4), e1901667. DOI: 10.1002/adhm.201901667.

(119) Zheng, X.; Ding, Z.; Cheng, W.; Lu, Q.; Kong, X.; Zhou, X.; Lu, G.; Kaplan, D. L. Microskin-Inspired Injectable MSC-Laden Hydrogels for Scarless Wound Healing with Hair Follicles. *Adv Healthc Mater* **2020**, *9* (10), e2000041. DOI: 10.1002/adhm.202000041.

(120) Melke, J.; Midha, S.; Ghosh, S.; Ito, K.; Hofmann, S. Silk fibroin as biomaterial for bone tissue engineering. *Acta Biomater* **2016**, *31*, 1-16. DOI: 10.1016/j.actbio.2015.09.005.

(121) Yodmuang, S.; McNamara, S. L.; Nover, A. B.; Mandal, B. B.; Agarwal, M.; Kelly, T. A.; Chao, P. H.; Hung, C.; Kaplan, D. L.; Vunjak-Novakovic, G. Silk microfiber-reinforced silk hydrogel composites for functional cartilage tissue repair. *Acta Biomater* **2015**, *11*, 27-36. DOI: 10.1016/j.actbio.2014.09.032.

(122) Hamilton, D. C.; Shih, H. H.; Schubert, R. A.; Michie, S. A.; Staats, P. N.; Kaplan, D. L.; Fontaine, M. J. A silk-based encapsulation platform for pancreatic islet transplantation improves islet function in vivo. *J Tissue Eng Regen Med* **2017**, *11* (3), 887-895. DOI: 10.1002/term.1990.

(123) Gorenkova, N.; Osama, I.; Seib, F. P.; Carswell, H. V. In vivo evaluation of engineered self-assembling silk fibroin hydrogels after intracerebral injection in a rat stroke model. *ACS Biomaterials Science & Engineering* **2018**, *5* (2), 859-869.

(124) Kapoor, S.; Kundu, S. C. Silk protein-based hydrogels: Promising advanced materials for biomedical applications. *Acta Biomater* **2016**, *31*, 17-32. DOI: 10.1016/j.actbio.2015.11.034.

(125) Rockwood, D. N.; Preda, R. C.; Yücel, T.; Wang, X.; Lovett, M. L.; Kaplan, D. L. Materials fabrication from Bombyx mori silk fibroin. *Nat Protoc* **2011**, *6* (10), 1612-1631. DOI: 10.1038/nprot.2011.379.

(126) Hu, X.; Kaplan, D.; Cebe, P. Determining beta-sheet crystallinity in fibrous proteins by thermal analysis and infrared spectroscopy. *Macromolecules* **2006**, *39* (18), 6161-6170.

(127) Seib, F. P.; Prewitz, M.; Werner, C.; Bornhäuser, M. Matrix elasticity regulates the secretory profile of human bone marrow-derived multipotent mesenchymal stromal cells (MSCs). *Biochem Biophys Res Commun* **2009**, *389* (4), 663-667. DOI: 10.1016/j.bbrc.2009.09.051.

(128) Schneider, C. A.; Rasband, W. S.; Eliceiri, K. W. NIH Image to ImageJ: 25 years of image analysis. *Nat Methods* **2012**, *9* (7), 671-675. DOI: 10.1038/nmeth.2089.

(129) Walters, B.; Uynuk-Ool, T.; Rothdiener, M.; Palm, J.; Hart, M. L.; Stegemann, J. P.; Rolauffs, B. Engineering the geometrical shape of mesenchymal stromal cells through defined cyclic stretch regimens. *Sci Rep* **2017**, *7* (1), 6640. DOI: 10.1038/s41598-017-06794-9.

(130) Totten, J. D.; Wongpinyochit, T.; Seib, F. P. Silk nanoparticles: proof of lysosomotropic anticancer drug delivery at single-cell resolution. *J Drug Target* **2017**, *25* (9-10), 865-872. DOI: 10.1080/1061186X.2017.1363212.

(131) Panciera, T.; Azzolin, L.; Cordenonsi, M.; Piccolo, S. Mechanobiology of YAP and TAZ in physiology and disease. *Nat Rev Mol Cell Biol* **2017**, *18* (12), 758-770. DOI: 10.1038/nrm.2017.87.

(132) Kureel, S. K.; Mogha, P.; Khadpekar, A.; Kumar, V.; Joshi, R.; Das, S.; Bellare, J.; Majumder, A. Soft substrate maintains proliferative and adipogenic differentiation potential of human mesenchymal stem cells on long-term expansion by delaying senescence. *Biol Open* **2019**, *8* (4). DOI: 10.1242/bio.039453.

(133) Grolman, J. M.; Weinand, P.; Mooney, D. J. Extracellular matrix plasticity as a driver of cell spreading. *Proc Natl Acad Sci U S A* **2020**, *117* (42), 25999-26007. DOI: 10.1073/pnas.2008801117.

(134) Chirila, T. V.; Suzuki, S.; Bray, L. J.; Barnett, N. L.; Harkin, D. G. Evaluation of silk sericin as a biomaterial: in vitro growth of human corneal limbal epithelial cells on Bombyx mori sericin membranes. *Prog Biomater* **2013**, *2* (1), 14. DOI: 10.1186/2194-0517-2-14.

(135) Cameron, A. R.; Frith, J. E.; Cooper-White, J. J. The influence of substrate creep on mesenchymal stem cell behaviour and phenotype. *Biomaterials* **2011**, *32* (26), 5979-5993. DOI: 10.1016/j.biomaterials.2011.04.003.

(136) Hübner, G.; Brauchle, M.; Smola, H.; Madlener, M.; Fässler, R.; Werner, S. Differential regulation of pro-inflammatory cytokines during wound healing in normal and glucocorticoid-treated mice. *Cytokine* **1996**, *8* (7), 548-556. DOI: 10.1006/cyto.1996.0074.

(137) Khetan, S.; Guvendiren, M.; Legant, W. R.; Cohen, D. M.; Chen, C. S.; Burdick, J. A. Degradation-mediated cellular traction directs stem cell fate in covalently crosslinked three-dimensional hydrogels. *Nat Mater* **2013**, *12* (5), 458-465. DOI: 10.1038/nmat3586.

(138) McBeath, R.; Pirone, D. M.; Nelson, C. M.; Bhadriraju, K.; Chen, C. S. Cell shape, cytoskeletal tension, and RhoA regulate stem cell lineage commitment. *Dev Cell* **2004**, *6* (4), 483-495. DOI: 10.1016/s1534-5807(04)00075-9.

(139) Kusuma, G. D.; Carthew, J.; Lim, R.; Frith, J. E. Effect of the Microenvironment on Mesenchymal Stem Cell Paracrine Signaling: Opportunities to Engineer the Therapeutic Effect. *Stem Cells Dev* **2017**, *26* (9), 617-631. DOI: 10.1089/scd.2016.0349. Liu, F. D.; Tam, K.; Pishesha, N.; Poon, Z.; Van Vliet, K. J. Improving hematopoietic recovery through modeling and modulation of the mesenchymal stromal cell secretome. *Stem Cell Res Ther* **2018**, *9* (1), 268. DOI: 10.1186/s13287-018-0982-2.

(140) Wischhusen, J.; Melero, I.; Fridman, W. H. Growth/Differentiation Factor-15 (GDF-15): From Biomarker to Novel Targetable Immune Checkpoint. *Front Immunol* **2020**, *11*, 951. DOI: 10.3389/fimmu.2020.00951.

(141) Yang, F.; Mei, Y.; Langer, R.; Anderson, D. G. High throughput optimization of stem cell microenvironments. *Comb Chem High Throughput Screen* **2009**, *12* (6), 554-561. DOI: 10.2174/138620709788681916.

(142) Jha, A. K.; Huang, S. C.; Sergushichev, A.; Lampropoulou, V.; Ivanova, Y.; Loginicheva, E.; Chmielewski, K.; Stewart, K. M.; Ashall, J.; Everts, B.; et al. Network integration of parallel metabolic and transcriptional data reveals metabolic modules that regulate macrophage polarization. *Immunity* **2015**, *42* (3), 419-430. DOI: 10.1016/j.immuni.2015.02.005.

(143) Liu, X.; Cooper, D. E.; Cluntun, A. A.; Warmoes, M. O.; Zhao, S.; Reid, M. A.; Liu, J.; Lund, P. J.; Lopes, M.; Garcia, B. A.; et al. Acetate Production from Glucose and Coupling to Mitochondrial Metabolism in Mammals. *Cell* **2018**, *175* (2), 502-513.e513. DOI: 10.1016/j.cell.2018.08.040.

(144) Totten, J. D.; Wongpinyochit, T.; Carrola, J.; Duarte, I. F.; Seib, F. P. PEGylation-Dependent Metabolic Rewiring of Macrophages with Silk Fibroin Nanoparticles. *ACS Appl Mater Interfaces* **2019**, *11* (16), 14515-14525. DOI: 10.1021/acsami.8b18716.

(145) Moskowitz, M. A.; Lo, E. H.; Iadecola, C. The science of stroke: mechanisms in search of treatments. *Neuron* **2010**, *67* (2), 181-198. DOI: 10.1016/j.neuron.2010.07.002.

(146) George, P. M.; Steinberg, G. K. Novel Stroke Therapeutics: Unraveling Stroke Pathophysiology and Its Impact on Clinical Treatments. *Neuron* **2015**, *87* (2), 297-309. DOI: 10.1016/j.neuron.2015.05.041.

(147) Martin, R. L.; Lloyd, H. G.; Cowan, A. I. The early events of oxygen and glucose deprivation: setting the scene for neuronal death? *Trends Neurosci* **1994**, *17* (6), 251-257. DOI: 10.1016/0166-2236(94)90008-6.

(148) John, T. D.; Hani, A. A.; Essam, J. H.; Calum, M.; Philipp, S. F.; Hilary, C. V. O. Towards clinical translation of 'second-generation' regenerative stroke therapies: hydrogels as game changers? In *Trends in Biotechnology*, In press ed.; 2021.

(149) Ho, M. T.; Teal, C. J.; Shoichet, M. S. A hyaluronan/methylcellulose-based hydrogel for local cell and biomolecule delivery to the central nervous system. *Brain Res Bull* **2019**, *148*, 46-54. DOI: 10.1016/j.brainresbull.2019.03.005.

(150) Garcia, J. H.; Lassen, N. A.; Weiller, C.; Sperling, B.; Nakagawara, J. Ischemic stroke and incomplete infarction. *Stroke* **1996**, *27* (4), 761-765. DOI: 10.1161/01.str.27.4.761.

(151) Ghuman, H.; Modo, M. Biomaterial applications in neural therapy and repair. *Chinese Neurosurgical Journal* **2016**, *2* (1), 1-8.

(152) Peppas, N. A.; Khademhosseini, A. Make better, safer biomaterials. *Nature* **2016**, *540* (7633), 335-337. DOI: 10.1038/540335a.

(153) Williams, D. F. Specifications for Innovative, Enabling Biomaterials Based on the Principles of Biocompatibility Mechanisms. *Front Bioeng Biotechnol* **2019**, *7*, 255. DOI: 10.3389/fbioe.2019.00255.

(154) Hopkins, A. M.; De Laporte, L.; Tortelli, F.; Spedden, E.; Staii, C.; Atherton, T. J.; Hubbell, J. A.; Kaplan, D. L. Silk hydrogels as soft substrates for neural tissue engineering. *Advanced functional materials* **2013**, *23* (41), 5140-5149.

(155) Guo, C.; Li, C.; Kaplan, D. L. Enzymatic Degradation of. *Biomacromolecules* **2020**, *21* (5), 1678-1686. DOI: 10.1021/acs.biomac.0c00090.

(156) Fine, N. A.; Lehfeldt, M.; Gross, J. E.; Downey, S.; Kind, G. M.; Duda, G.; Kulber, D.; Horan, R.; Ippolito, J.; Jewell, M. SERI surgical scaffold, prospective clinical trial of a silk-derived biological scaffold in two-stage breast reconstruction: 1-year data. *Plast Reconstr Surg* **2015**, *135* (2), 339-351. DOI: 10.1097/PRS.0000000000000987.

(157) Gorenkova, N.; Maitz, M. F.; Böhme, G.; Alhadrami, H. A.; Jiffri, E. H.; Totten, J. D.; Werner, C.; Carswell, H. V. O.; Seib, F. P. The innate immune response of self-assembling silk fibroin hydrogels. *Biomater Sci* **2021**, *9* (21), 7194-7204. DOI: 10.1039/d1bm00936b.

(158) Gorenkova, N.; Osama, I.; Seib, F. P.; Carswell, H. V. O. In Vivo Evaluation of Engineered Self-Assembling Silk Fibroin Hydrogels after Intracerebral Injection in a Rat Stroke Model. *ACS Biomater Sci Eng* **2019**, *5* (2), 859-869. DOI: 10.1021/acsbiomaterials.8b01024.

(159) Rewell, S. S.; Churilov, L.; Sidon, T. K.; Aleksoska, E.; Cox, S. F.; Macleod, M. R.; Howells, D. W. Evolution of ischemic damage and behavioural deficit over 6 months after MCAo in the rat: Selecting the optimal outcomes and statistical power for multi-centre preclinical trials. *PLoS One* **2017**, *12* (2), e0171688. DOI: 10.1371/journal.pone.0171688.

(160) Li, C.; Guo, C.; Fitzpatrick, V.; Ibrahim, A.; Zwierstra, M. J.; Hanna, P.; Lechtig, A.; Nazarian, A.; Lin, S. J.; Kaplan, D. L. Design of biodegradable, implantable devices towards clinical translation. *Nature Reviews Materials* **2020**, *5* (1), 61-81.

(161) Kilkenny, C.; Browne, W. J.; Cuthill, I. C.; Emerson, M.; Altman, D. G. Improving bioscience research reporting: The ARRIVE guidelines for reporting animal research. *J Pharmacol Pharmacother* **2010**, *1* (2), 94-99. DOI: 10.4103/0976-500X.72351.

(162) Modo, M. Long-term survival and serial assessment of stroke damage and recovery - practical and methodological considerations. *J Exp Stroke Transl Med* **2009**, *2* (2), 52-68. DOI: 10.6030/1939-067X-2.2.52.

(163) Ghuman, H.; Massensini, A. R.; Donnelly, J.; Kim, S. M.; Medberry, C. J.; Badylak, S. F.; Modo, M. ECM hydrogel for the treatment of stroke: Characterization of the host cell infiltrate. *Biomaterials* **2016**, *91*, 166-181. DOI: 10.1016/j.biomaterials.2016.03.014.

(164) Cregg, J. M.; DePaul, M. A.; Filous, A. R.; Lang, B. T.; Tran, A.; Silver, J. Functional regeneration beyond the glial scar. *Exp Neurol* **2014**, *253*, 197-207. DOI: 10.1016/j.expneurol.2013.12.024.

(165) Yiu, G.; He, Z. Glial inhibition of CNS axon regeneration. *Nat Rev Neurosci* **2006**, *7* (8), 617-627. DOI: 10.1038/nrn1956.

(166) Cheng, T. Y.; Chen, M. H.; Chang, W. H.; Huang, M. Y.; Wang, T. W. Neural stem cells encapsulated in a functionalized self-assembling peptide hydrogel for brain tissue engineering. *Biomaterials* **2013**, *34* (8), 2005-2016. DOI: 10.1016/j.biomaterials.2012.11.043.

(167) Ju, R.; Wen, Y.; Gou, R.; Wang, Y.; Xu, Q. The experimental therapy on brain ischemia by improvement of local angiogenesis with tissue engineering in the mouse. *Cell Transplant* **2014**, *23 Suppl 1*, S83-95. DOI: 10.3727/096368914X684998.

(168) Lam, J.; Lowry, W. E.; Carmichael, S. T.; Segura, T. Delivery of iPS-NPCs to the Stroke Cavity within a Hyaluronic Acid Matrix Promotes the Differentiation of Transplanted Cells. *Adv Funct Mater* **2014**, *24* (44), 7053-7062. DOI: 10.1002/adfm.201401483.

(169) Hoban, D. B.; Newland, B.; Moloney, T. C.; Howard, L.; Pandit, A.; Dowd, E. The reduction in immunogenicity of neurotrophin overexpressing stem cells after intra-striatal transplantation by encapsulation in an in situ gelling collagen hydrogel. *Biomaterials* **2013**, *34* (37), 9420-9429. DOI: 10.1016/j.biomaterials.2013.08.073.

(170) Hiscox, L. V.; Johnson, C. L.; Barnhill, E.; McGarry, M. D.; Huston, J.; van Beek, E. J.; Starr, J. M.; Roberts, N. Magnetic resonance elastography (MRE) of the human brain: technique, findings and clinical applications. *Phys Med Biol* **2016**, *61* (24), R401-R437. DOI: 10.1088/0031-9155/61/24/R401.

(171) del Zoppo, G. J.; Milner, R.; Mabuchi, T.; Hung, S.; Wang, X.; Berg, G. I.; Koziol, J. A. Microglial activation and matrix protease generation during focal cerebral ischemia. *Stroke* **2007**, *38* (2 Suppl), 646-651. DOI: 10.1161/01.STR.0000254477.34231.cb.

(172) Nicholas, A. P.; McInnis, C.; Gupta, K. B.; Snow, W. W.; Love, D. F.; Mason, D. W.; Ferrell, T. M.; Staas, J. K.; Tice, T. R. The fate of biodegradable microspheres injected into rat brain. *Neuroscience letters* **2002**, *323* (2), 85-88.

(173) Back, S. A.; Tuohy, T. M.; Chen, H.; Wallingford, N.; Craig, A.; Struve, J.; Luo, N. L.; Banine, F.; Liu, Y.; Chang, A.; et al. Hyaluronan accumulates in demyelinated lesions and inhibits oligodendrocyte progenitor maturation. *Nat Med* **2005**, *11* (9), 966-972. DOI: 10.1038/nm1279.

(174) Cargill, R.; Kohama, S. G.; Struve, J.; Su, W.; Banine, F.; Witkowski, E.; Back, S. A.; Sherman, L. S. Astrocytes in aged nonhuman primate brain gray matter synthesize excess hyaluronan. *Neurobiol Aging* **2012**, *33* (4), 830.e813-824. DOI: 10.1016/j.neurobiolaging.2011.07.006.

(175) Tran, S. H.; Wilson, C. G.; Seib, F. P. A Review of the Emerging Role of Silk for the Treatment of the Eye. *Pharm Res* **2018**, *35* (12), 248. DOI: 10.1007/s11095-018-2534-y.

(176) Johari, N.; Moroni, L.; Samadikuchaksaraei, A. Tuning the conformation and mechanical properties of silk fibroin hydrogels. *European Polymer Journal* **2020**, *134*, 109842.

(177) Kambe, Y.; Yamaoka, T. Biodegradation of injectable silk fibroin hydrogel prevents negative left ventricular remodeling after myocardial infarction. *Biomater Sci* **2019**, *7* (10), 4153-4165. DOI: 10.1039/c9bm00556k.

(178) Diab, T.; Pritchard, E. M.; Uhrig, B. A.; Boerckel, J. D.; Kaplan, D. L.; Guldberg, R. E. A silk hydrogel-based delivery system of bone morphogenetic protein for the treatment of large bone defects. *J Mech Behav Biomed Mater* **2012**, *11*, 123-131. DOI: 10.1016/j.jmbbm.2011.11.007.

(179) Leng, X.; Liu, B.; Su, B.; Liang, M.; Shi, L.; Li, S.; Qu, S.; Fu, X.; Liu, Y.; Yao, M.; et al. In situ ultrasound imaging of silk hydrogel degradation and neovascularization. *J Tissue Eng Regen Med* **2017**, *11* (3), 822-830. DOI: 10.1002/term.1981.

(180) Li, S.; Yu, D.; Ji, H.; Zhao, B.; Ji, L.; Leng, X. In vivo degradation and neovascularization of silk fibroin implants monitored by multiple modes ultrasound for surgical applications. *Biomed Eng Online* **2018**, *17* (1), 87. DOI: 10.1186/s12938-018-0478-4.

(181) Jin, K.; Wang, X.; Xie, L.; Mao, X. O.; Zhu, W.; Wang, Y.; Shen, J.; Mao, Y.; Banwait, S.; Greenberg, D. A. Evidence for stroke-induced neurogenesis in the human brain. *Proc Natl Acad Sci U S A* **2006**, *103* (35), 13198-13202. DOI: 10.1073/pnas.0603512103.

(182) Kazanis, I.; Gorenkova, N.; Zhao, J. W.; Franklin, R. J.; Modo, M.; Ffrench-Constant, C. The late response of rat subependymal zone stem and progenitor cells to stroke is restricted to directly affected areas of their niche. *Exp Neurol* **2013**, *248*, 387-397. DOI: 10.1016/j.expneurol.2013.06.025.

(183) Rouleau, N.; Cantley, W. L.; Liaudanskaya, V.; Berk, A.; Du, C.; Rusk, W.; Peirent, E.; Koester, C.; Nieland, T. J. F.; Kaplan, D. L. A Long-Living Bioengineered Neural Tissue Platform to Study Neurodegeneration. *Macromol Biosci* **2020**, *20* (3), e2000004. DOI: 10.1002/mabi.202000004.

(184) Chaudhuri, O.; Cooper-White, J.; Janmey, P. A.; Mooney, D. J.; Shenoy, V. B. Effects of extracellular matrix viscoelasticity on cellular behaviour. *Nature* **2020**, *584* (7822), 535-546. DOI: 10.1038/s41586-020-2612-2.

(185) Chaudhuri, O. Viscoelastic hydrogels for 3D cell culture. *Biomater Sci* **2017**, *5* (8), 1480-1490. DOI: 10.1039/c7bm00261k.

(186) Zheng, H.; Zuo, B. Functional silk fibroin hydrogels: preparation, properties and applications. *J Mater Chem B* **2021**, *9* (5), 1238-1258. DOI: 10.1039/d0tb02099k.

(187) Allam, M.; Hu, T.; Cai, S.; Laxminarayanan, K.; Hughley, R. B.; Coskun, A. F. Spatially visualized single-cell pathology of highly multiplexed protein profiles in health and disease. *Commun Biol* **2021**, *4* (1), 632. DOI: 10.1038/s42003-021-02166-2.

(188) Ganesh, S.; Hu, T.; Woods, E.; Allam, M.; Cai, S.; Henderson, W.; Coskun, A. F. Spatially resolved 3D metabolomic profiling in tissues. *Sci Adv* **2021**, *7* (5). DOI: 10.1126/sciadv.abd0957.

(189) Nakano, S.; Yokoyama, Y.; Aoyagi, S.; Himi, N.; Fletcher, J. S.; Lockyer, N. P.; Henderson, A.; Vickerman, J. C. Evaluation of biomolecular distributions in rat brain tissues by means of ToF-SIMS using a continuous beam of Ar clusters. *Biointerphases* **2016**, *11* (2), 02A307. DOI: 10.1116/1.4939251.

APPENDIX

Conference contributions:

(i) **Phuagkhaopong S.**, Gorenkova N., Carswell V.O. H., and Seib F. P. Histological evaluation of engineered self-assembling silk fibroin hydrogel biodegradation in a MCAO stroke rat models. 2nd Virtual Doctoral School Multidisciplinary Symposium (DSMS2020), University of Strathclyde, Glasgow, UK. May 26–28, 2020. **Oral presentation.**

(ii) **Phuagkhaopong S.**, Gorenkova N., Carswell V. O. H. and Seib F. P. Biodegradation of engineered self-assembling silk fibroin hydrogels after intracerebral injection in a rat model of chronic ischemic stroke. 11th Virtual World Biomaterial Congress (WBC2020). December 11–15, 2020. **Poster presentation.**

Peer-reviewed publications:

(i) **Phuagkhaopong S.**, Mendes L., Muller K., Wobus M., Bornhauser M., Carswell V.O. H., Duarte F. I., Seib F. P. Silk Hydrogel Substrate Stress Relaxation Primes Mesenchymal Stem Cell Behavior in 2D. ACS Appl. Mater. Interfaces. 2021;13(26): 30420–30433.

(ii) Matthew S.A.L., Totten J.D., **Phuagkhaopong S.**, Egan G., Witte K., Perrie Y., Seib F.P. Silk Nanoparticle Manufacture in Semi-Batch Format. ACS Biomater. Sci. Eng. 2020;6(12): 6748–6759.

My contributions included training of Matthew in silk processing, manufacture and characterization of silk nanoparticles, and also giving her an advice on experimental design and data interpretation .

Papers in preparation/review:

(i) **Phuagkhaopong S.**, Gorenkova N., Aruvornlop P., Carswell V.O. H., Seib F.P. 'Impact of the chronic ischemic stroke microenvironment on silk fibroin hydrogel biodegradation and de novo tissue formation'. (In preparation, see Chapter 3)